UNDERSTANDING THE IMPACT OF POLYMER SELF-ORGANIZATION ON THE MICROSTRUCTURE AND CHARGE TRANSPORT IN POLY(3-HEXYLTHIOPHENE)

A Thesis
Presented to
The Academic Faculty

by

Avishek R. Aiyar

In Partial Fulfillment
of the Requirements for the Degree
Doctor of Philosophy in the
School of Chemical and Biomolecular Engineering

Georgia Institute of Technology
May 2012

UNDERSTANDING THE IMPACT OF POLYMER SELF-ORGANIZATION ON THE MICROSTRUCTURE AND CHARGE TRANSPORT IN POLY(3-HEXYLTHIOPHENE)

Approved by:

Professor Elsa Reichmanis, Advisor
School of Chemical and Biomolecular Engineering
Georgia Institute of Technology

Professor David Collard
School of Chemistry and Biochemistry
Georgia Institute of Technology

Professor Dennis Hess
School of Chemical and Biomolecular Engineering
Georgia Institute of Technology

Professor Bernard Kippelen
School of Electrical and Computer Engineering
Georgia Institute of Technology

Professor Carson Meredith
School of Chemical and Biomolecular Engineering
Georgia Institute of Technology

Date Approved: 23rd December 2011

Life bustles under the bridge, energy unabated.

The waters smile, wavering in sympathy,

At the face harbored on its lap,

Treasuring every drop that departed,

To give to grandma, sleeping beneath.

-To my grandmother who never said goodbye

ACKNOWLEDGEMENTS

I cannot imagine spending six years in graduate school without an external support system like the kind I have had the pleasure and privilege of enjoying.

First and foremost, I would like to thank my PhD adviser, Elsa, for all the support she has given me over the past three years or so that I have been with her. I joined her at a time where I was at the cross-roads: forced to decide between an "escape route" from graduate school in the form of a job offer from Intel and a position as a PhD student in her group. It was a decision between a comfortable life with a healthy pay packet at an international company of the stature of Intel or one with myriad question marks that at that time were leading me into the unknown. In the end I decided to turn down my lucrative offer and join Elsa's group instead and it is a decision that has vindicated my ambition to pursue a doctorate. Having worked on engineering problems during my years as a Master's student, I was moving onto a "sciency" field, and I can proudly say that I have experienced the emotional highs that I strongly believe only science can provide. For that, and for simply being a great adviser and wonderful person, I would like to thank Elsa.

Thanks are also due to my committee, Profs. Dennis Hess, Carson Meredith, Bernard Kippelen and David Collard. I am proud to be associated with such luminaries in their respective fields. I will always remember Prof. Hess, who I have enjoyed wonderful conversations with over the years, especially at 6 in the morning when Bala and I dropped into his office to submit our report on a course project that we had worked all night on, or during my diurnal visits to the second floor water fountain. He was always an email away and a constant source of support and encouragement. Dr. Collard was like a second adviser to me, especially during the

period when I was writing a journal article that his student, Rakesh Nambiar, and I had worked together on. I learned immensely from him, and was touched by his constant appreciation of my inclination towards science. Dr. Kippelen's course, where I learned so much about organic optoelectronics, was inspirational, not to mention his careful scrutiny of my work, which has taught me to be more professional. Thanks also to Prof. Meredith for his helpful comments during my proposal and my review and for simply being a very nice person.

I bow down to the Reichmanis group members who put up with my idiosyncrasies over the past three years. I would like to sincerely thank Byoungnam Park, who patiently taught me the nuances of organic semiconductors and is simply the most thorough and professional researcher I have come across. Thanks also to Zhaokang Hu, Mincheol Chang, Boyi Fu and Ji-Hwan Kang for being amazing office-mates. Many thanks to Daniel Acevedo, an REU student who joined our lab during the summer of 2010. I had the privilege of mentoring him and I have rarely come across someone who is as motivated as Daniel. Nothing makes me more proud than to mention that the summer experience had a huge impact on him and he is now a graduate student at the University of Massachusetts, Amherst. I finally get why professors enjoy teaching so much.

Over the years I have got opportunities to collaborate with some amazing researchers. Prof. Mohan Srinivasarao is very much part of my PhD committee without actually being a part of it. We have worked together a lot and it has been a pleasure bouncing ideas off him and gaining a vast amount of knowledge in return. I especially enjoyed participating in the numerous proposals we wrote together, even at the cost of "thesis-time"! I have worked with his student, Min Sang Park for the best part of the last three years and it was fantastic working with someone as motivated as him. That is what makes science so much fun. Karthik Nayani in the Mohan group is another bright young graduate student who I have had interesting conversations

with that I have thoroughly enjoyed. Rakesh Nambiar in the Collard group deserves huge credit for some of the work we carried out in collaboration. Jung-Il Hong was extremely helpful running the XRD scans on the tons of samples that I kept giving him! Mariacristina Rumi in the Marder group was ever so helpful and patient in explaining photophysics to me. I like to believe that I collaborated with Prof. Jean-Luc Bredas as well, although my association with him is represented by a solitary presentation that I made to his group. I am proud that I got to interact with him and that I get to mention his name in my thesis!

I would be remiss if I did not mention the help and support I received from my Master's adviser, Prof. Mark G. Allen. My foundations in research lay in the Microsensors and Microactuators (MSMA) group and I shall forever remember him for his kindness and infinite understanding when I decided to transfer into Elsa's group. Working with such people has made my six years at GT a pleasurable experience. I would also like to thank all MSMA members for their support. Special thanks are reserved for Dr. Nisarga Naik, sister, lunch-time buddy and one of my best friends. I doubt I could have made it through grad school without her.

To ChBE and Prof. Amyn Teja in particular, I owe a lot. I would especially like to thank the department for finding my work worthy of the Ziegler Award and the Center for Organic Photonics and Electronics (COPE) for not only funding me through the years, but also awarding me the prestigious COPE Fellowship. These recognitions meant a lot to me and were hugely motivational.

Thanks also to all the friends I made in ChBE, with whom I shared both my successes and my failures as a grad student. Dr. Edward Park and Dr. Samirkumar Patel remain special friends. My gratitude to the amazing group of friends outside of work: Shankar Narayanan, Rohan Rao, Ananda Nagavarapu, Vivek Sahu, Siddharth Gupta, Subrahmanyam Kalyanasundaram, Balaji Ganapathy, Sumit Mishra, Ashish Sinha and Varun Rai. The friendships I formed with them shall remain with me

forever. I will never forget my "racquetball quartet" of Mark Elton, Ian Yang, Shankar Narayanan and myself as we won the 2011 School Championships. Thanks also to Greg Book for all our racquetball sessions.

Finally and most importantly, I thank my family. To my mother and father, who have been nothing but supportive of every event in my life, carefully overseeing my transition from the family brat to the family geek. To my brother Arvind and sister-in-law, Sukanya, I owe more than what words can express. I love you guys to death. To my grandmother, I dedicate this thesis. She was and is the shining light of my life.

TABLE OF CONTENTS

LIST OF TABLES

LIST OF FIGURES

SUMMARY

Conjugated polymers represent the next generation of conducting materials that will enable technological devices incorporating thin film transistors, photovoltaic (PV) cells etc. in a cost effective roll-to-roll manner. The charge carrier mobility, which characterizes the ease with which charges can be transported through the material, is the key metric by which these materials are gaged and is also a decisive factor that limits device performance. Given the impact of microstructure on charge transport, ordered self-assembly in polymeric semiconductors assumes paramount relevance. This thesis outlines a fundamental investigation of the correlations between the morphology and microstructure of a model conjugated polymer, poly(3-hexylthiophene) (P3HT), and its corresponding charge transport properties in an organic field effect transistor (OFET) geometry. Moreover, the *evolution* of the structural and electrical properties are mapped, which provide new insights into the self-assembly process.

The variation in the electrical properties is studied as film formation evolves as a function of solvent evaporation from a sessile P3HT solution droplet. The channel formation process is mapped using four contact field effect measurements. The channel formation study is complimented by interrogating the evolution of the polymer chain conformations using *in situ* Raman spectroscopy, which reveals the presence of an intermediate lyotropic liquid crystalline phase before film crystallization. The manifestation of the liquid crystalline phase offers a potential rationale to the mobility profiles recorded by the *in situ* electrical measurements. A joint investigation of both measurements reveals that the onset of channel current occurs well before polymer crystallization and that the subtle structural changes in the P3HT film continue to

evolve even after crystallization, which further impact the observed drain current.

The large impact of polymer chain conformations on the drain current revealed in the above study provided substantial impetus to understand the role of single chain effects on macroscopic charge transport in P3HT. We report that differences in regioregularity of side chain attachment in poly(3-hexylthiophene) (P3HT) as small as ca. 4% are sufficient to induce dramatic changes in the electronic and morphological properties of the material. Casting the electronic absorption spectra in the framework of Spano's model reveals that the conjugation length of the polymer chain is surprisingly sensitive to regioregularity. This observation correlates well with the field effect mobilities that are attenuated by one to two orders of magnitude in the lower regioregularity polymer film. We suggest that the increased intrachain order coupled with a reduced fraction of grain boundaries in the higher RR film is responsible for the reported differences. These studies serve as important pieces in the microstructure-charge transport puzzle.

A greater insight into the correlation is obtained by devising a technique to tune the crystallinity of the P3HT films and correlating that with the field effect mobility. We shown the formation of ordered supramolecular precursors in P3HT solutions through the application of low intensity ultrasound. These precursors survive the casting process, resulting in a dramatic increase in the degree of crystallinity of the thin films obtained by spin coating. The crystallinity of the films is *tunable*, with a continuous evolution of meso-scale structures observed as a function of ultrasonic irradiation time. A multiphase solid state morphology is obtained that in turn results in a percolation type charge transport mechanism. This investigation is then extended to understand the role of process conditions, the solvent used and molecular parameters such as regioregularity.

CHAPTER I

INTRODUCTION

1.1 Micro vs Macro-electronics

The modern world, primarily driven by electronics, has an almost relentless demand for better technology. This is evident in our efforts to understand charge transport in materials, which dates back to as early as 1727, when Stephen Gray, an English scientist, discovered electrical conduction.[1] The now widely applicable Ohm's Law, which for the first time established a relationship between the applied voltage and subsequent current flowing in a conductor, followed in 1827. Arguably the most important breakthrough was achieved in 1906, when Whittier Pickard filed a patent for the silicon crystal detector or the "cat's whisker diode" that demonstrated the semiconductor effect-a major breakthrough in electronics.[2] This was quickly followed by the drive towards miniaturization, marked by the invention of the "point contact transistor" by Bardeen, Brattain and Shockley in 1947 at Bell Laboratories. Sixty years on and the metal-oxide semiconductor field effect transistor (MOSFET), which incorporates semiconducting silicon as the active material, is ubiquitous. The MOSFET is especially known for its incorporation in modern computer chips and as an active element in modern digital circuitry.

In recent years, the drive towards miniaturization has been accompanied by a simultaneous emergence of "macroelectronics," where the primary metric is not the minimum feature size of the circuitry, but the area over which the circuits can be constructed. Macroelectronics find wide-spread use in display technology, forming an integral part of the backplane circuitry in flat-screen displays. Applications of

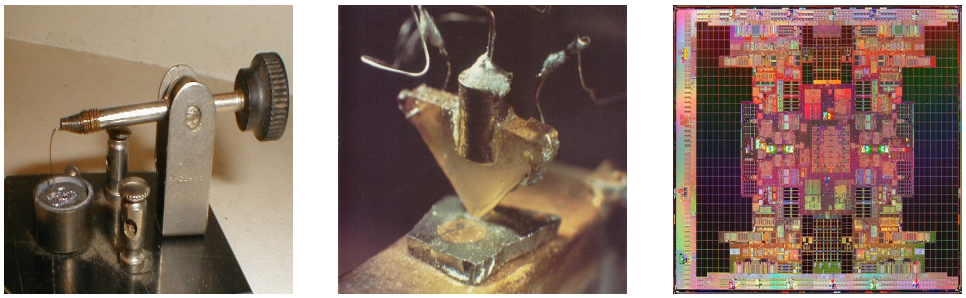

(a) (b) (c)

Figure 1: The evolution of electronics from the (a) Cat's whisker diode[2] to (b) the point contact transistor and (c) the modern day Intel processor with 2 billion transistors.

this technology have also expanded to other arenas such as radio-frequency identification tags, smart cards etc., where the essential requirement is not necessarily the performance of the device but the cost of production. Importantly, macroelectronics technology can be easily transferred to the manufacture of light emitting diodes (LEDs), solar cells, thin film transistors etc. on large scales, which can make light emission and harvesting extremely economical. Moreover, this raises, for the first time, the possibility of truly "flexible" electronics and thus an entirely new array of applications.[3,4] It is important to remember that the performance of materials envisaged for macroelectronics probably cannot compete with single crystal silicon (c-Si) and in fact, it is not meant to.

Amorphous silicon (a-Si) has been an excellent candidate for the above described macroelectronic applications. Films of a-Si can be deposited from the vapor phase using conventional deposition techniques such as chemical vapor deposition. As shown in Figure 2, mobilities as high as 1 $cm^2V^{-1}s^{-1}$ have been obtained from films of a-Si. However, this does not represent the current state-of-the-art as significant progress in both deposition procedures as well development of new inorganic materials has been made that has enabled even higher mobilities.[4] In spite of the significant progress

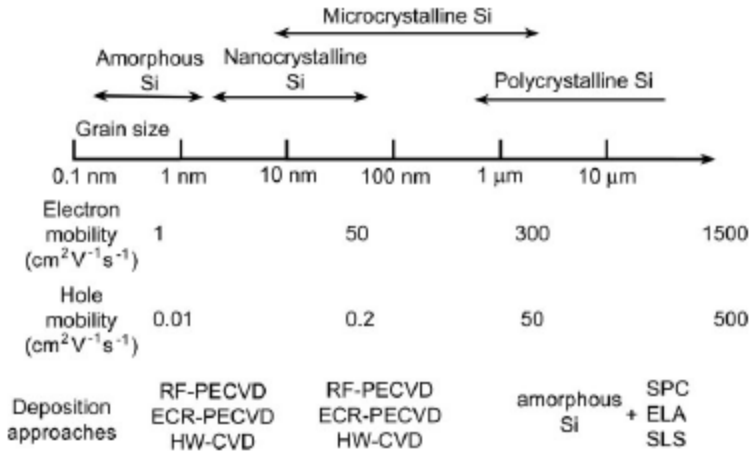

Figure 2: Carrier mobilities of various forms of silicon. From Rogers et.al. [3]

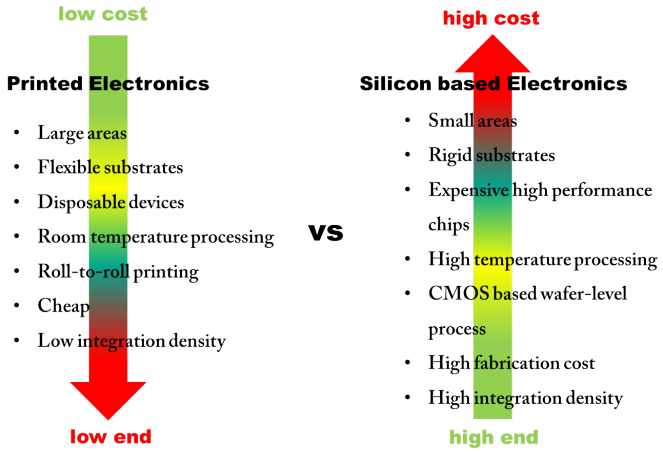

Figure 3: Comparison of printed vs conventional electronics. [5]

made in inorganic macroelectronics, in order to fully justify large scale, high throughput production of flexible circuitry, deposition processes need to be further simplified.

Organic materials, especially *conjugated polymers*, offer distinct processing advantages, while simultaneously keeping the technology extremely cost-effective (See Figure 3). This has has paved the way for organic semiconductors (OSCs) to be a strong potential competitor to a-Si technology. [6] Moreover, using novel synthetic strategies a vast array of organic conjugated molecules can be synthesized with tunable functionality designed to suit a given application. Such control over material properties is not available using a-Si technology. [7] As mentioned earlier, the goal of organic electronics

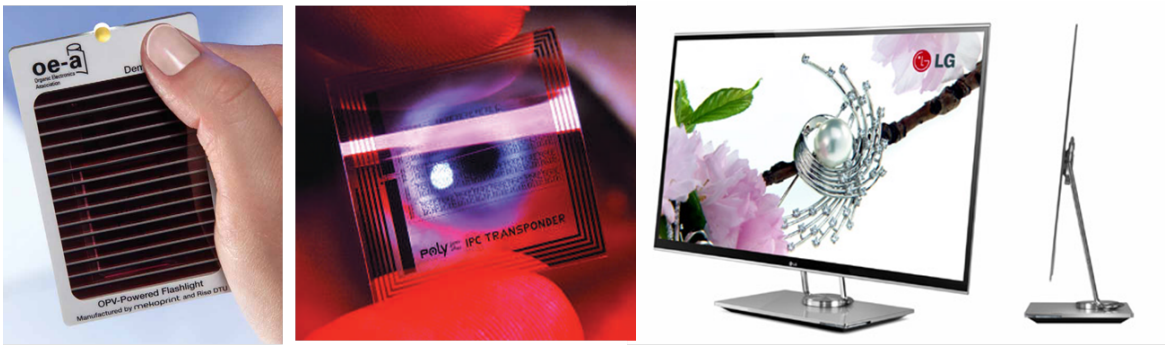

Figure 4: Examples of devices based on organic semiconductors (a) a flashlight based on organic photovoltaics[13] (b) RFID tags[14] and (c) the first commercial OLED based display from LG Electronics[15]

is not to displace c-Si but to enable applications that would benefit from the unique combination of electronic properties of conjugated materials with the versatility of plastics. Figure 4 shows some examples of devices constructed with organic semiconductors as the active materials. Molecular semiconductors have been successfully applied as photoconductive elements in xerography.[8] However, with improvement in charge carrier mobility and processeability, the applicability of organic semiconductors has expanded tremendously. Typical applications in which OSCs are commonly employed include light emitters (organic light emitting diodes or OLEDs),[9] light harvesters (organic solar cells)[10] and purely electronic devices (organic field effects transistors or OFETs and memory devices).[11,12] The primary advantage of organic semiconductors lies in their ease of processability which makes them an attractive replacement for inorganic materials. As will be discussed in the following sections, conjugated materials can be rendered soluble in common solvents and thus printed using commercial gravure and offset printers, allowing for "roll to roll" printing of "inks" of the material over large areas. This offers the potential to reduce the cost per device and hence is an attractive feature. This thesis is going to primarily focus on materials for organic macroelectronics.

1.2 Charge transport in organic semiconductors

1.2.1 Conjugation and the consequences of conjugation

[8,16,17]

The discovery of conductivity in organic materials represented a remarkable breakthrough that may be considered on par with the invention of the point contact transistor. Whilst the latter ushered in the age of microelectronics, the former served to significantly expand the repertoire of a class of materials whose only contribution to the electronics industry until that time was to provide insulators. Hence, the demonstration of semiconducting behavior in crystals of anthracene in 1960,[18] effectively ushered in the age of organic electronics. The discovery of electrical conductivity in polymeric materials by Alan Heeger, Alan McDiarmind and Hideki Shirakawa, who demonstrated high conductivity in oxidized iodine doped polyacetylene, followed in 1976.[19] The magnitude of their accomplishment became apparent as they went on to receive the Nobel Prize in Chemistry for the year 2000.

In order to understand the evolution of conductivity in organic semiconductors, we must revisit the electronic structure of carbon and the bonding pattern between carbon atoms in extended chains. Carbon has the electronic structure $1s^2 2s^2 2p^2$, and thus four valence electrons. The electronic architecture of conventional saturated polymers such polyethylene (PE), in which all four valence electrons in the sp^3 hybridized carbon atom are utilized in covalent sigma (σ) bonds, is fundamentally different from that of conjugated polymers. The latter consists of a system of carbon atoms with alternating single and double bonds, with the carbon atoms now carrying an sp^2+p_Z character-the so called π *conjugated system*. The implications of such a bonding scheme are enormous. The unpaired electron in the p_Z orbital (the π electron) is now free to delocalize (with certain restrictions which will become apparent later in the text) along the backbone because of the orbital overlap between successive carbon atoms that leads to extended π states. It is this electronic delocalization

that provides the "highway" for charge carriers to move along the backbone of the polymer chain leading to a conducting system. In addition, these π states also result in a significant reduction of the band-gap, such that $E_g(\pi)<E_g(\sigma)$, where E_g is the electronic band-gap (the use of π and σ indicates conjugated and non-conjugated systems respectively), which explains why many conjugated polymers absorb light in the visible region of the spectrum. The effect of a π conjugated system is apparent from a comparison of the optical band-gap of a typical σ bonded polymer like PE (ca. 8 eV) vs a π bonded conjugated systems (ca. 1-4 eV). Figure 14(b) depicts some typical conjugated polymers that are often encountered in the literature.

Conjugated systems, unlike inorganic semiconductors like silicon, are quasi one-dimensional in nature since the covalent bonding is restricted *within* a chain, while interchain interactions are significantly weaker and of the Van Der Waals type (in contrast to c-Si which has a three dimensional covalently bonded lattice). As a consequence, charge carriers observed in OSCs are not conventional free electrons or holes, such as those found in c-Si, but they are actually "self-localized quasi-particles", or polarons or bipolarons in condensed matter physics terminology.[16] These can be envisaged as charge carriers that are dressed by a cloud of polarization that constantly travels with the charge, Figure 5, whose presence leads to local changes in the geometry of the lattice.[20] Polarons and bipolarons are the manifestation of *electron-phonon* coupling which are invariably present in conjugated materials and are critical in explaining the properties of such systems. Figure 6 shows an example of the strong coupling between the lattice structure and the electronic structure. Although the example is shown for butadiene, it is a universal feature in all π conjugated systems. Addition of π electrons to the existing σ framework (which provides structural integrity to the molecule), leads to changes in bond lengths which are dictated by the π electron densities which in turn are reshuffled due to electron-electron interactions. The π electrons in conjugated systems are highly polarizable and easily delocalized.

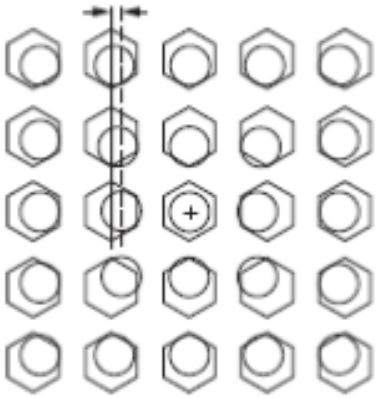

Figure 5: The polarization effects induced by the presence of an extra charge on the central benzene atom. This "cloud" of polarization always travels with the charge. Obtained from[20].

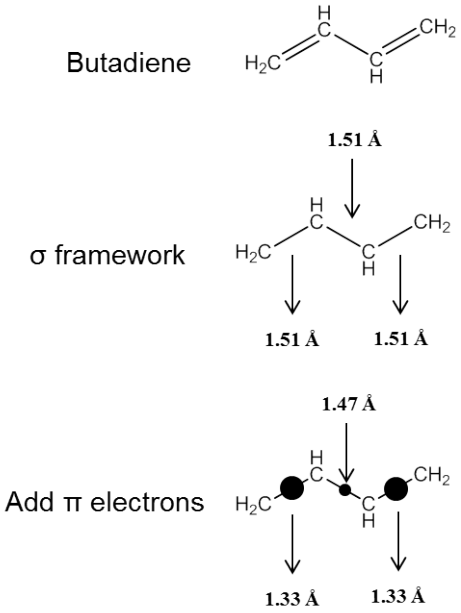

Figure 6: The strong coupling between the geometrical (lattice) structure and the electronic structure in butadiene. The black circles indicate the π electron densities.[21]

Since the geometry of the molecules is closely linked with its electronic structure, it can expected that the presence of the quasi-particles will influence the electronic states of the conjugated system. This is indeed the case as can be seen from Figure 7, where new localized energy states appear within the "forbidden gap" of the polymer. A hole polaron thus consists of a radical cation and a free radical and a

bipolaron consists of two electrons or two holes.[17] These species can appear in organic semiconductors through a multitude of processes such as optical absorption in neutral systems, charge transfer doping or even charge injection. Such phenomena have important consequences for charge transport and are ultimately responsible for the hopping transport regime that is predominantly observed in disordered semiconductors. This phenomenon will be discussed in more detail in the next section.

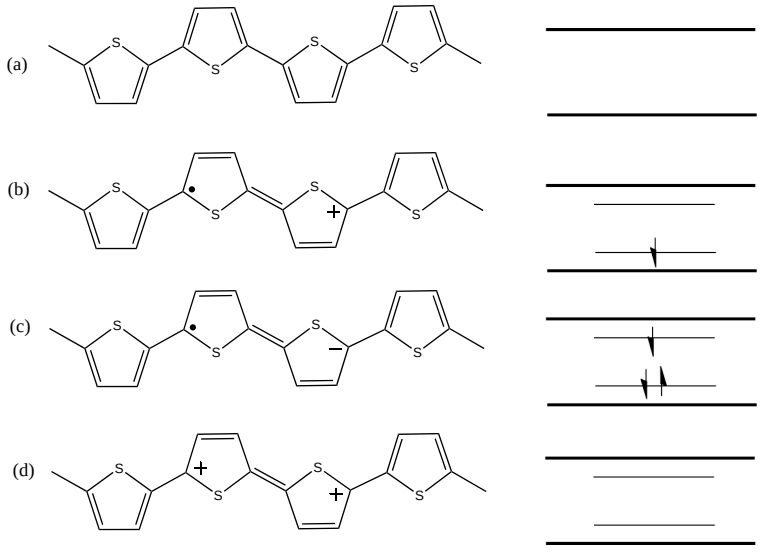

Figure 7: Schematic and band structures of (a) neutral species, (b) hole polaron (c) electron polaron and (d) hole bipolaron. Note: polarons are actually delocalized over greater distances in reality

1.2.2 Understanding charge transport in conjugated materials

[22,23]

As will be seen in the subsequent sections, the performance of any device employing organic semiconductors depends critically on the *charge carrier mobility*. In this section, a basic introduction to the theory of charge transport in OSCs will be provided which will be useful for understanding some of the results presented in this thesis.

The key characteristic that quantifies charge transport in a material is the charge carrier mobility. In the absence of any external applied potential difference, carriers

diffuse via a random walk process that can be described by Equation 1, where $< x^2 >$ denotes the mean square displacement of the charges, D is the diffusion coefficient, t is the time and n=2,4,6 for one, two and three dimensional systems respectively.

$$< x^2 >= nDt \tag{1}$$

The quantity of interest, mobility or μ, can then be correlated with the diffusion coefficient and the temperature at which the diffusion process is taking place by the well known Einstein relation, Equation 2, where k_B is the Boltzmann constant, T is the temperature and e is the electronic charge.

$$\mu = \frac{eD}{k_B T} \tag{2}$$

However, in all practical devices based on OSCs, an electric field is typically present across the semiconductors and thus causes the charge carriers to drift in response. In such real world scenarios, the mobility is now defined as the ratio of the average drift velocity of charges, ¡v¿, in response to an applied electric field E, as depicted in Equation 3. It is a measure of the ease with which charge carriers can drift within a material in the presence of an electric field.

$$\mu = \frac{< v >}{E} \tag{3}$$

Unlike three dimensionally bonded inorganic semiconductors where room temperature mobilities typically range from 10^2-10^4 $\mathrm{cm^2V^{-1}s^{-1}}$, charge transport in organic semiconductors is limited by hopping between conjugated segments, as a result of which mobilities are usually orders of magnitude lower. This is a typical characteristic of all "disordered" semiconductors, with the actual mobility closely related to the morphological condition of the films (crystalline, polycrystalline, amorphous). For example, even within organic semiconductors, single crystals of rubrene have been

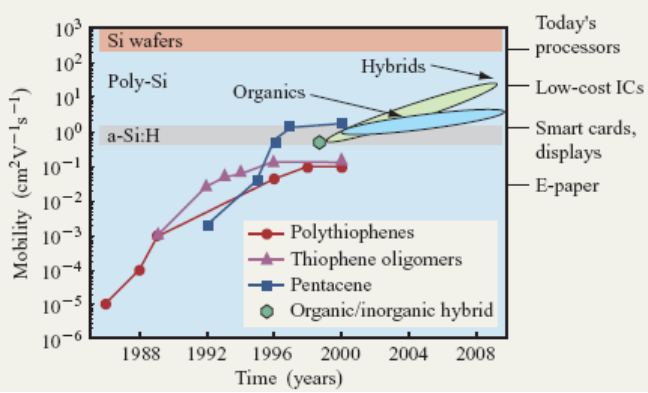

Figure 8: Performance of typical organic semiconductors. From Shaw et.al.[25]

known to support hole mobilities as high as 20 $cm^2V^{-1}s^{-1}$ [24], whilst the mobility in amorphous/semi-crystalline films of most conjugated polymers are well within 1 $cm^2V^{-1}s^{-1}$. Figure 8 shows the mobility of a representative set of organic semiconductors relative to that of c-Si.[25] The significant difference in mobility between organic semiconductors and c-Si can be understood by analyzing the fundamental processes that govern charge transport in conjugated systems.

The presence of disorder or the absence of three dimensional periodicity, like that found in c-Si, in most organic semiconductors, especially polymeric ones, implies that band theory cannot be applied to model the transport of charges. In addition, in order to observe band-like transport, the bandwidths of the respective transport bands (valence and conduction bands) must at least be of the order of 0.1 eV.[26] The bandwidths in organic semiconductors are clearly determined by the splitting of the highest and lowest occupied molecular orbitals or the HOMO and the LUMO respectively, when going from isolated chains to interacting segments. A higher bandwidth would not only drive the system towards band-like transport, but it would also imply a high degree of interchain interactions that can only be sustained in a highly *ordered* system. In fact, in a hypothetical infinitely long polymer chain with no conjugation defects, theoretical bandwidths of several electron volts have been calculated.[27] However, in reality, this is clearly not the case in most organic semiconductors (barring

some organic single crystals mentioned earlier), especially those obtained by solution processing of polymers. Disorder induced breaks in the conjugation pathway, along with electron-phonon coupling that is invariantly observed in such systems, causes the injected charges to interact with certain molecular vibrations, thus localizing the carriers. This localization of charge carriers in such disordered systems can also be understood by considering Equation 4, where τ is the carrier residence time, $\hbar$ is the Planck's constant divided by 2π and W is the bandwidth.

$$\tau \approx \frac{\hbar}{W} \tag{4}$$

Inorganic semiconductors have fairly large bandwidths and thus the electron and holes move so fast that carriers are not localized on any one segment of the solid and thus no polarization cloud can be formed (refer to Figure 5). In sharp contrast, given the low bandwidths in typical organic semiconductors, the residence time scales are of the order of typical vibrational frequencies found in the molecule. This in turn would imply that the molecules on which the carriers reside have enough time to geometrically relax and thus trap the charge, leading to the formation of the polaron. The "trapped" carriers now have to "hop" from chain to chain through a thermally activated process. This is a major reason why mobilities in disordered conjugated semiconductors are typically orders of magnitude lower than in c-Si.

The events that lead up to the localization of charge carriers on individual conjugated segments are important in calculating the hopping rates. At the molecular level, this process can be cast in the framework of the semi-classical Marcus-Hush electron transfer theory,[28,29] given by Equation 5,where k_{hole} is the hopping rate of holes, k_B is the Bolztmann constant, T is the temperature, $\hbar$ is Planck's constant divided by 2π. V and λ are *electronic coupling matrix element* or the *transfer integral* and the *reorganization energy* respectively and are the primary factors that govern the hopping rate. Figure 9 illustrates this process of charge hopping, which in essence

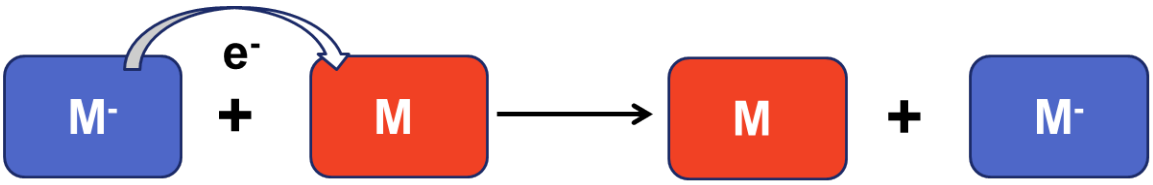

Figure 9: The process of charge hopping

is a self-exchange redox reaction explaining why it can be cast in the framework of the Marcus theory.

$$k_{hole} = (\frac{\pi}{\lambda k_B T})^{1/2} \frac{V^2}{\hbar} exp(-\frac{\lambda}{4 k_B T}) \tag{5}$$

Hopping essentially involves the transfer of a charge carrier (an electron in Figure 9) from an ionized molecule M^- to a neutral molecule M. The optimized geometries in the ionized and neutral states are different and thus the process of charge transfer also results in intra-molecular relaxation as the geometries switch between the two states of the molecule involved in the redox reaction. The energy required to bring about these geometry modifications is known as the *reorganization energy*. The *transfer integral* is a measure of the degree of electronic communication between the molecules involved in the self-exchange reaction. Based on Equation 5, it is evident that in order to maximize the hopping rate of charge carriers, two primary conditions must be satisfied: (i) The electronic coupling must be maximized and (ii) the reorganization energy must be minimized. A combination of these factors not only determines the mobility of charge carriers, but it also provides an insight into the transport mechanism operating within the semiconductor. The transport mechanism (band vs hopping) results from a balance between the energy gained by delocalization of electrons within the electronic band versus the energy gained by carrier localization on a conjugated segment, with the latter resulting in geometry relaxations around the charge and the subsequent formation of a polaron. At the same time, the conformation of the polymer chain and the microstructure of the final film are critical factors

that influence V and λ.

On the macroscopic scale, charge transport in disordered semiconductors is often cast in the framwork of the disorder formalism, developed by Bassler and coworkers.[30] According to the formalism, the loss of long-range order results in a hopping type charge transport mechanism through a manifold of localized states with energetical and positional disorder. The hopping rate then takes on a Miller-Abrahams form that predicts an increase in mobility with increasing temperature, consistent with a thermally activated hopping mechanism.[31] A detailed description of macroscopic charge transport models is, however, beyond the scope of this thesis.

The goal of this thesis is to extract the mobility of charge carriers and correlate these mobilities with the various structural aspects of the thin film. A detailed understanding of this correlation is of paramount significance given the strong dependence of the hopping rate on the *intra* and *inter*-molecular order, which in turn are determined by the microstructural quality of the thin films. Moreover, existing reports on polymeric semiconductors, though crucial in furthering the state of the art, remain anomalous and abound with contradictory results. These anomalies are partly due to the diverse effects that are simultaneously manifest in disordered polymeric systems. This thesis also attempts to isolate individual microstructural effects in order to better clarify their role in dictating macroscopic charge transport. Since the mobility inherently carries information about V and λ, this study can also provide some insight into intra (λ) and inter(V)-chain effects. Section 1.3 discusses the various methods that can be used to extract the mobility and section 1.4 briefly discusses typical organic semiconductors encountered in the literature.

1.3 Experimental techniques for determination of charge carrier mobility

As seen in section 1.2, the mobility of charge carriers is not only an index of performance of devices utlizing an organic semiconductor, but because of its sensitivity to

the microstructure of the thin film, it can also be used to understand microstructure-charge transport correlations. A variety of techniques have been developed that can be used to characterize the mobility of charge carriers spanning distances from the nanoscale to the macroscale.[22] A combination of such techniques would thus be required to gain a complete understanding of charge transport.

1.3.1 Time of Flight (TOF)

The TOF technique relies on the photo-generation of charge carriers when the material in question is irradiated with light. The geometry of a typical TOF measurement setup is shown in Figure 10. A thick organic layer (a few microns) is sandwiched between two electrodes. The material is then irradiated with a light pulse in close proximity to one of the electrodes, which leads to generation of photo-carriers. A potential difference applied across the two electrodes then causes the carriers to migrate from one electrode to the other, leading to a current being generated in the circuit. The photo-current measured at the collecting electrode as a function of time is then indicative of the mobility of carriers. In highly ordered materials, a sharp photo-current vs time profile is observed, while the profile is significantly broadened for disordered conductors due a dispersion of arrival times of the photo-generated carriers. The mobility can be calculated from Equation 6, where μ is the TOF mobility, v is the drift velocity of the photo-generated carriers under the influence of the applied electric field, E is the electric field, L is the sample thickness or the distance between the two electrodes and t is the averaged transient time.

$$\mu = \frac{v}{E} = \frac{L^2}{Vt} \tag{6}$$

1.3.2 Diode Configuration

The diode configuration utilizes space-charge limited current (SCLC) effects to extract the mobility of charge carriers. This technique is especially useful in scenarios where

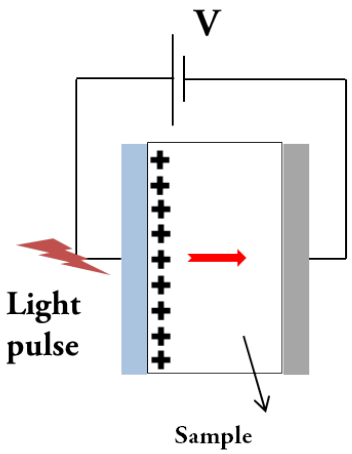

Figure 10: Measurement of mobility using the TOF technique

charge injection/collection from electrodes is required. Like the TOF method, SCLC based methods also involve a sandwich structure with the film sandwiched between two electrodes. The equations derived for estimating mobility require that the charge transport be limited by the bulk properties of the film and that it is not contact limited. This condition is satisfied by choosing contacts that preferentially allow for favorable injection of either electrons or holes but not both. This technique allows for an independent estimation of both the electron as well as hole mobilities. For an ohmic contact between the semiconductor and the metal, the injected charge carriers form a space charge region in close proximity to the injecting electrode. In the absence of charge traps and at sufficiently low electric field, the current density through the semiconductor scales quadratically as a function of the applied bias and is obtained from Child's Law, Equation 7, where J is the current density, ε_0 and ε_r is the permitivitty of free space and the semiconductor respectively, V is the applied voltage and L is the film thickness. The *field independent mobility* can then be extracted from the J-V characteristics of the SCLC diode. In scenarios where there is a functional dependence of the mobility on the applied electric field, such as disordered semiconductors, the mobility is then substituted by a modified expression given by Equation 8, where μ_0 is the zero field mobility and γ is a constant. The

SCLC expression can then be modified as shown in Equantion 9.[32]

$$J = \frac{9}{8}\varepsilon_0\varepsilon_r\mu\frac{V^2}{L^3} \tag{7}$$

$$\mu = \mu_0 exp(\gamma\sqrt{E}) \tag{8}$$

$$J = \frac{9}{8}\varepsilon_0\varepsilon_r\mu_0 \exp(0.891\gamma\sqrt{\frac{V}{L}})\frac{V^2}{L^3} \tag{9}$$

1.3.3 Pulse Radiolysis Time-Resolved Microwave Conductivity (PR-TRMC)

Unlike SCLC, PR-TRMC is a contact-free technique that can be used to estimate carrier mobilities of both bulk films as well as on highly localized scales such as single polymer chains. The sample is irradiated with a pulse of highly energetic electrons that create a low density of free charge carriers. These free carriers then result in a change in the conductivity of the sample, which is estimated by measuring the change in the microwave power reflected by the sample, making the measurement frequency dependent. The change in conductivity, $\delta\sigma$, is then given by Equation 10, where N_{e-h} is the number of electron-hole pairs generated and can estimated from the total energy dose divided by the energy required to create one e-h pair.

$$\Delta\sigma = e\Sigma\mu_{TRMC}N_{e-p} \tag{10}$$

The elegance of this technique lies in the fact that the spatial extent over which the mobility is being average can be tuned by simply changing the frequency of the microwave radiation, thus enabling estimations of mobility spanning multiple length scales. This technique can thus be particularly useful when understanding intra-chain and inter-chain transport in conjugated polymers.

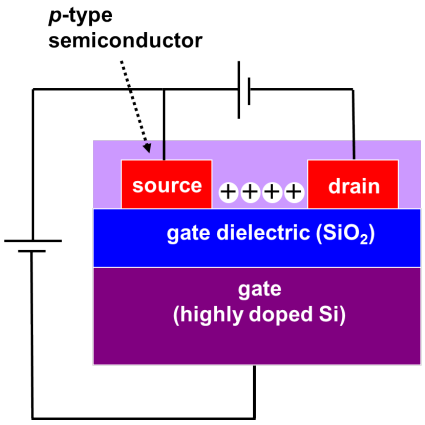

Figure 11: Schematic diagram of the bottom contact, bottom gate OFET geometry

1.3.4 Field-Effect Transistor Geometry (OFET)

The field effect transistor is ubiquitous in modern computer processors, more popularly known as the Metal Oxide Semiconductor Field Effect Transistor or the MOSFET. OFETs are the organic equivalents of the MOSFET and represent a very convenient way of extracting the mobility (known as the field effect mobility for reasons that will become apparent). Moreover, in addition to being a measurement technique, OFETs find direct application in the active matrix circuitry of liquid crystal displays, where they are employed as thin film transistors or TFTs.[33] The OFET is also the primary device that is fabricated and tested in this thesis as a means to access the charge transport properties in the conjugated polymer thin films and hence it will be discussed in greater detail in this section.

1.3.4.1 Device operation

[34]

The structure of an OFET is shown in Figure 11. This particular geometry is referred to as the bottom contact bottom gate geometry given the placement of the electrodes as well as the gate relative to the semiconductor thin film. Several geometries can be constructed,[35] but the bottom contact configuration was chosen because of the ease of device fabrication.

The equations that describe the flow of current in an OFET are essentially derived from MOSFET theory with one important distinction: MOSFETs operate in the *inversion mode*, whereas OFETs operate in the *accumulation mode* as will be discussed.

As can be seen from the geometry of the OFET, Figure 11, the gate dielectric separates the gate electrode from the organic semiconductor, forming a metal-insulator-semiconductor (MIS) capacitor. The application of a gate voltage (V_G) causes accumulation of charge carriers at the semiconductor-dielectric interface, which subsequently flow upon the application of a potential difference between the source and drain electrodes ($V_D - V_S$). The source is typically grounded. In p-channel operation of the OFET, application of a negative gate voltage causes the accumulation of holes in the channel region of the transistor which flow under the influence of a negative drain voltage. The density of accumulated charges is determined by the total capacitance of the dielectric and thus its thickness and dielectric constant. It is important to note that in such a *field-effect* device, the charges accumulate in a 1-2 nm thick region in the semiconductor away from the interface with the gate dielectric, known as the accumulation region.[36] In essence, the charge carrier mobility in an OFET configuration would thus be dictated by the microstructural order within the first few monolayers of the organic film in contact with the gate dielectric. This also justifies our use of the OFET as a device to interrogate the effects of polymer microstructure on macroscopic charge transport, given that subtle changes in ordering between the polymer changes would induce large changes in the field effect mobility.

The current-voltage characteristics of the OFET are calculated with the gradual channel or Shockley approximation, which is based on the assumption that the lateral electric field between the source and the drain is significantly smaller than the vertical field across the thickness of the film. Under normal circumstances, this condition is satisfied since typically channel lengths of the transistor, L, are orders of magnitude

higher than the thickness of films, which are typically a few tens of nanometers. Transistors can be operated in two regimes, the linear regime and the saturation regime of operation, depending on the magnitude of the drain voltage relative to the gate voltage. In the linear region of operation, as the name suggests, the drain current increases linearly with the applied drain voltage. This is characterized by Equation 11. As the drain voltage is further increased, at some point it equals the applied gate voltage, which results in the depletion of charge carriers near the drain contact: the so called *pinch point*. C_{ox} is the capacitance of the gate dielectric, W and L are the channel width and length respectively and V_T is the threshold voltage. The threshold voltage is defined as the voltage required to induce *mobile* charge carriers in the channel. The drain current in the saturation region is given by Equation 12. Figure 12 shows typical output and transfer characteristics of an OFET.

$$I_{D,linear} = \frac{W}{L}\mu C_{ox}(V_G - V_T)V_D \tag{11}$$

$$I_{D,sat} = \frac{W}{2L}\mu C_{ox}(V_G - V_T)^2 \tag{12}$$

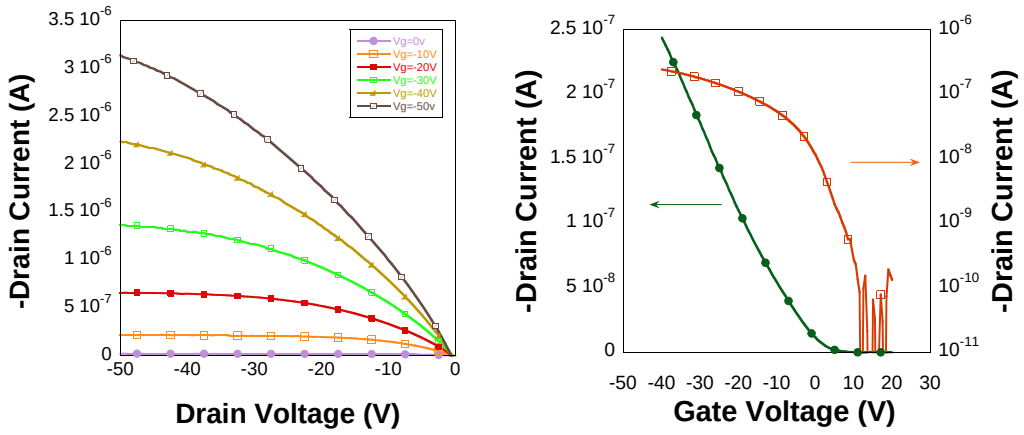

(a) (b)

Figure 12: (a) Output and (b) transfer characteristics of a typical p-channel organic transistor. Results obtained by Aiyar et.al. in the Reichmanis lab

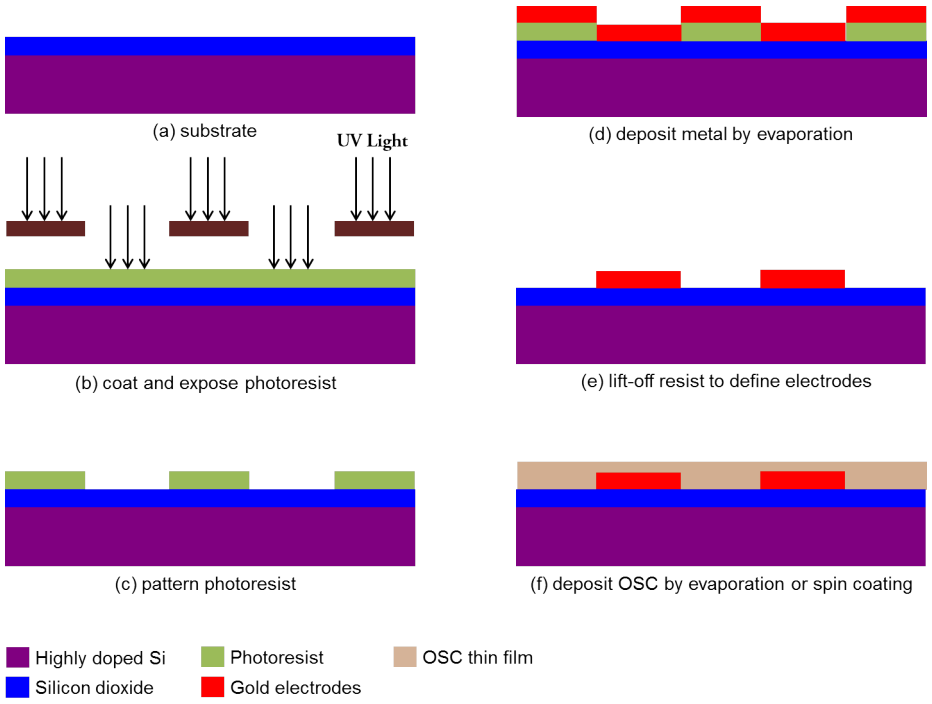

Figure 13: Fabrication of a bottom gate OFET device

It must be noted that the above equations assume that the mobility is independent of the gate voltage, which may not be universally true for OFETs.[37] Although a gate voltage dependence of mobility has been predicted by the multiple trapping and release model, the mobility calculations in this work are performed without incorporating this dependence and Equations 11 and 12 are used without any modifications.

1.3.4.2 Fabrication of OFETs

Figure 13 shows the sequence of steps required for the microfabrication of the OFET. The device is typically constructed on a highly doped silicon substrate, which also serves as the bottom gate contact. Dry thermal oxide is grown on top of the silicon to a thickness of 200-300 nm (Figure 13(a)), and this serves as the gate dielectric. Photoresist (Shipley 1827) is then spin coated on top of the oxidized wafer at 3000 RPM for 40 secs and soft-baked at 115°C for 2-3 minutes on a contact hot plate to remove residual solvents (Figure 13(b)). The resist is then exposed using 405 nm UV light (Karl Suss MA6 mask aligner) with a total dose of 400 mWcm^{-2} and developed

in MF-319 developer (Rohm and Haas) for ca. 2 mins in order to define the electrode patterns in the resist (Figure 13(c)). The metal electrodes (5 nm of chromium as the adhesion layer, followed by 50 nm of gold) are then deposited on the patterned substrates using Electron-Beam Evaporation (CVC Inc.) ((Figure 13(d)). The final step of the substrate fabrication is resist lift-off, which ensures that any metal outside of the electrode pattern is removed along with the underlying photoresist (Figure 13(e)). This process is achieved by soaking the wafers in acetone over-night. The OFET is fabricated by simply spin coating or thermal evaporation of the organic semiconductor on the substrate (Figure 13(f)).

1.4 Materials

[8,16,17]

Although organic electronics began with the discovery of conductivity in anthracene[18] and later polyacetylene[19], it has rapidly expanded to include a vast array of materials. Organic semiconductors that are widely reported in the literature and currently being investigated can be classified into two different groups: (i) Molecular semiconductors such as anthracene, which was responsible for the advent of organic electronics, and a number of new materials such as a pentacene and rubrene. Molecular semiconductors also encompass oligomeric materials such as those belonging to the thiophene and acene family and finally (ii) polymeric semiconductors or conjugated polymers which are going to be the primary focus of this thesis. Some representative organic semiconductors are shown in Figure 14.

Although significant strides towards development of both single crystal arrays[38] as well as solution processed small molecules[39] have been made, polymeric semiconductors may be more amenable for large-area applications envisaged for flexible printed electronics in light of their better mechanical and rheological properties.[40] Poly(3-hexylthiophene) (P3HT), which is also the subject of investigation in this thesis, is one of the first high mobility soluble conjugated polymers to be developed.[41]

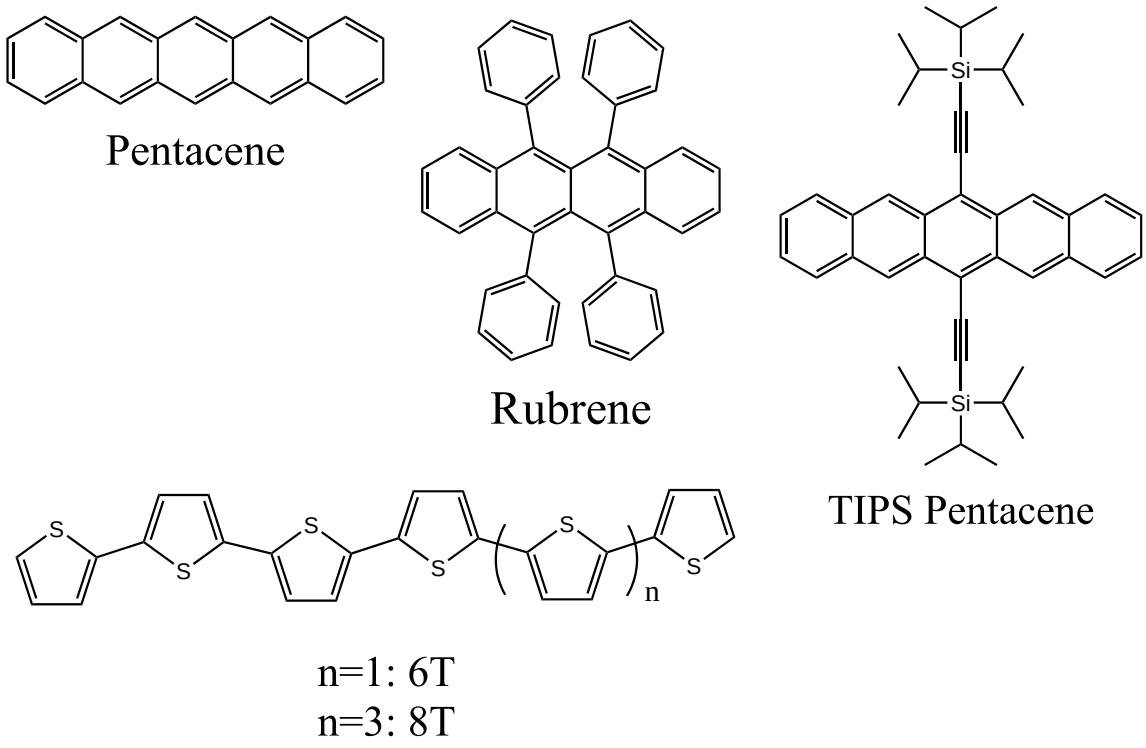

(a) Molecular Semiconductors

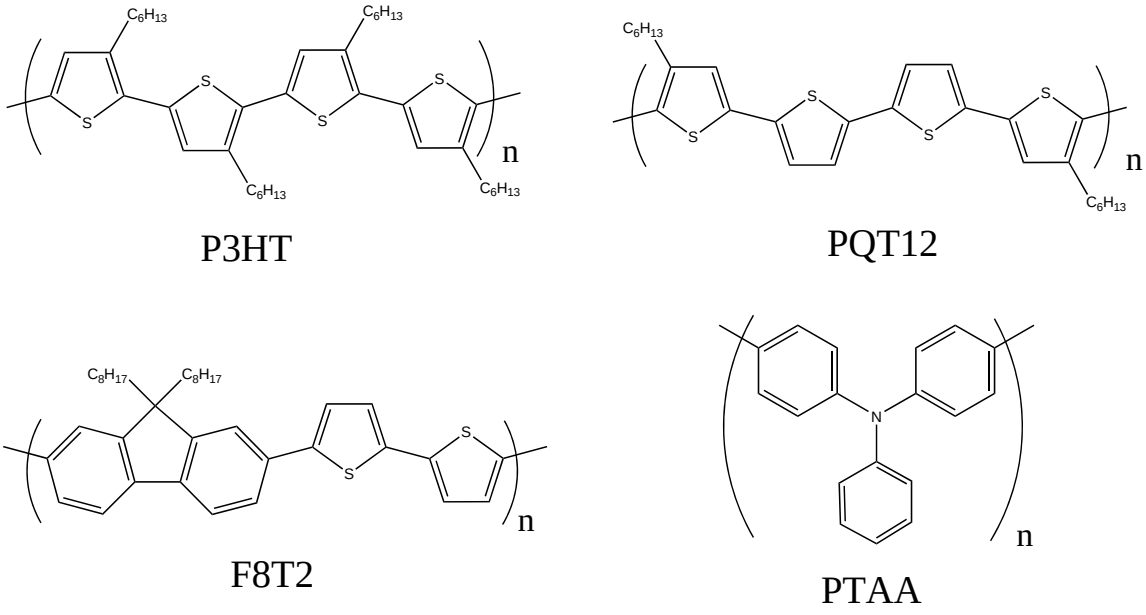

(b) Conjugated polymers

Figure 14: Representative examples organic semiconductors

It has also served as an excellent model system to establish transport mechanisms that typically operate in disordered organic thin films and have served as an excellent starting point for improved molecular design. The following section discusses the properties of P3HT in greater detail.

1.4.1 Poly(3-hexylthiophene)

Polythiophenes are one of the earliest conjugated materials that have served as excellent model materials to understand the nature of charge transport in disordered organic semiconductors. Tsumura et.al. fabricated the first OFET, as early as 1986, composed of an electrochemically synthesized polythiophene film which demonstrated a field effect mobility of 10^{-5} $cm^2V^{-1}s^{-1}$.[42] However, polythiophenes by themselves are intractable and cannot be solution processed. This problem was overcome by Elsenbaumer et.al., who functionalized the insoluble backbone with alkyl side chains that imparted solubility to the polymer system, without affecting its ability to conduct charge.[43] Ever since, a consistent improvement in the performance of poly(alkylthiophene)(PAT) based OFETs have been obtained, by continuously improving the molecular design[7,44,45] and identifying the importance of processing conditions on the final film microstructure.[41,46,47].

The material used in this study, P3HT, represents a compromise between solubility and mobility.[48] The molecular structure of P3HT is shown in Figure 15. It consists of the conjugated aromatic core, which also represents the direction of delocalization of the π electrons, and the solubilizing alkyl side chains. This combination of conjugated aromatic and insulating aliphatic moieties has interesting repercussions for both structural ordering as well as charge transport. Poly(3-alkylthiophenes)(P3ATs) in general can be ordered along three dimensions: conformational ordering along the direction of conjugation or backbone, π stacking between linear polymer chains and finally lamellar stacking between chains, as shown in Figure 15.

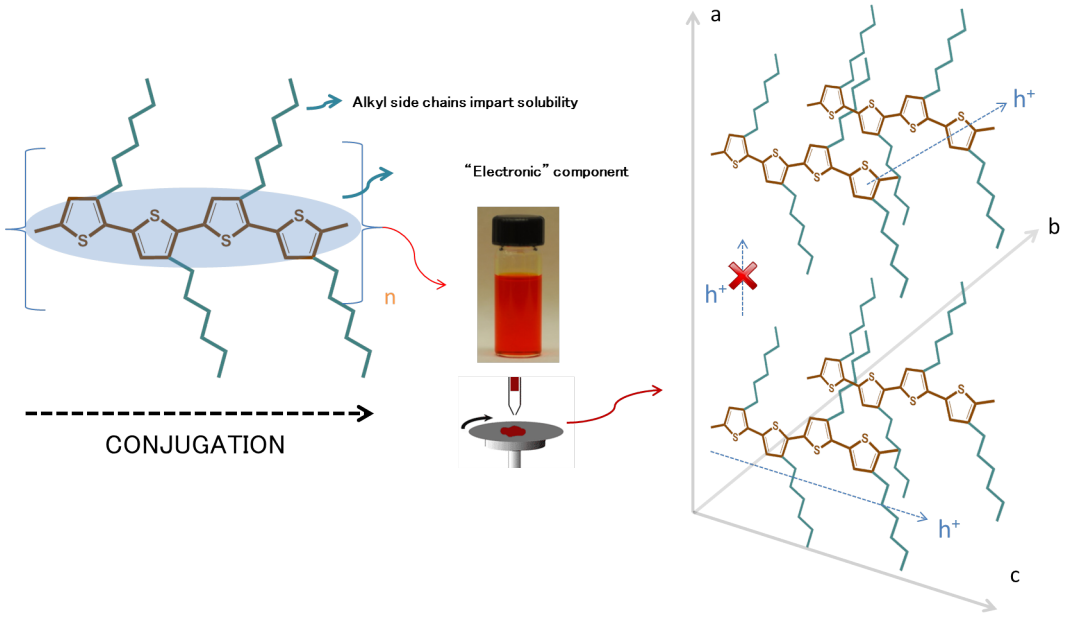

Figure 15: The molecular structure of P3HT and the packing of P3HT polymer chains in a thin film.

Looking at the packing motif adopted by the polymer chains in the solid state, three possible modes of charge carrier transport can be envisaged: along the conjugated polymer backbone (the c-axis), between polymer chains through the direction of $\pi - \pi$ stacking (the b-axis) and finally along the direction of the side chains (the a-axis). The degree of electronic wave-function overlap is expected to the highest along the polymer backbone and hence it is not unreasonable to expect that charges would prefer to delocalize in that direction. In terms of rates, the π stacking direction also represents a favorable pathway for the carriers to move (albeit not as easily as along the direction of conjugation), and finally by the direction along the side chains, where carriers move primarily by quantum mechanical tunneling and hence is an unlikely direction of charge transport. This transport scheme could also suggest why P3HT with hexyl side chains represents the optimal design, where side chains shorter than hexyl impart insufficient solubility while those any longer begin to impede the packing of the polymer chains inducing structural disorder. Field effect mobility measurements confirm the effect of the alkyl side chains, as shown in Figure 16.

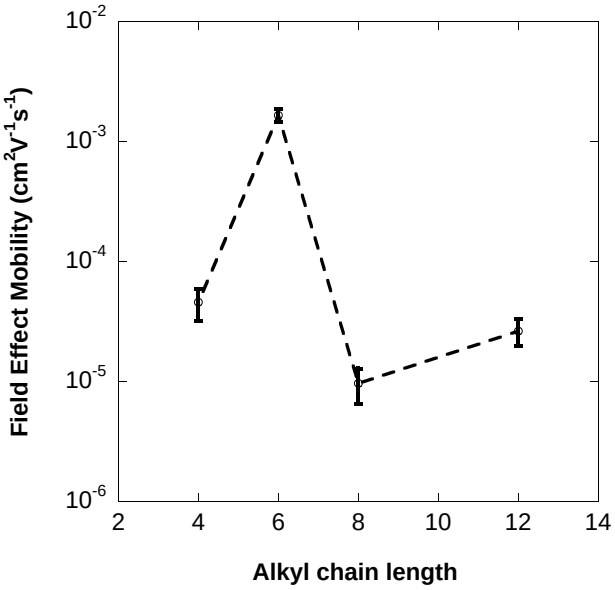

Figure 16: Dependence of mobility on the alkyl side chain length. Results obtained by Aiyar et.al. in the Reichmanis lab (unpublished).

P3HTs can be designed with different molecular architectures, which are dictated by the details of the placement of the alkyl side chains along the conjugated backbone, known as the *regioregularity* of the polymer, which is depicted in Figure 17. The regioregularity has a dominating influence on the microstructure of the films and thus the charge transport properties as will be discussed in greater detail in subsequent chapters of this thesis. Specifically, Sirringhaus et.al. reported that the HT side chain content of the polymer can strongly influence the thin film texture, with 81% and 96% regioregular samples yielding films that have the polymer backbone stacked in a *face-on* and *edge-on* orientation respectively.[49] An edge-on conformation of the polymer stacks, where the π-stacking axis coincides with the direction of planar charge transport in OFETs provides for films which exhibit a mobility as high as 0.1 $cm^2V^{-1}s^{-1}$ and two orders of magnitude higher than that obtained from films with a face-on conformation of the lamellae. The high mobility in the regioregular polymer could be sustained by enhanced delocalization of the polaron, which was detected by charge modulation spectroscopy, and was not observed in the reegiorandom

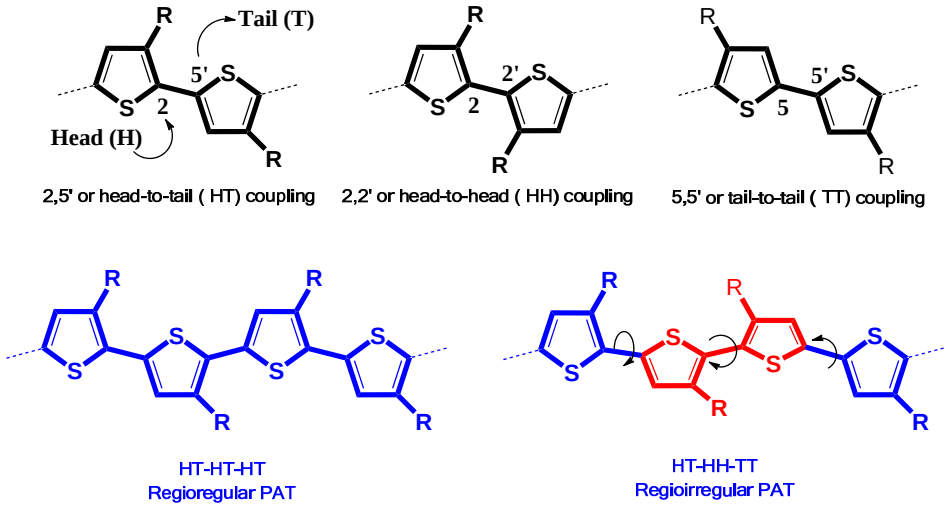

Figure 17: Regiospecificity of side chain arrangement in polythiophenes (top). Regioregular and regioirregular P3AT (bottom). Obtained from Osaka et.al. [50]

polymer. [49]

Along with the regioregularity, the molecular weight of P3HT has also been identified as a key molecular parameter that controls the morphology of the film, [51,52] although the mechanism of the effect is still under debate. But in effect, both the regioregularity and the molecular weight directly affect single chain properties and hence the effects are manifest in supramolecular assemblies as well. Some attention has also been paid to the processing conditions before, during and after the film formation process. Kim et.al. have shown that the use of self-assembled monolayers (SAMs) to change the chemical nature of the gate dielectric surface can have a significant impact on the texture of the polymer film, resulting in concurrent differences in field effect mobility, [53] consistent with the charge transport being limited by an ultrathin accumulation layer at the critical semiconductor-dielectric interface, as discussed in Section 1.3.4.1. Post-deposition thermal annealing of the films has also been reported to improve the performance of OFETs based on P3HT. [54,55] By using different film deposition techniques such as dip coating, drop casting and spin casting, Surin et.al. have demonstrated a close correlation between the microscopic

morphology with the charge transport in the conjugated polymer films.[47]

These results clearly demonstrate that in polymeric systems in general and P3HT in particular, the microstructure-charge transport correlation is a multi-dimensional problem and not easily reduced to isolated effects.

1.5 Motivation and outline of thesis

Although organic semiconductors in general, and conjugated polymers in particular offer distinct advantages over their inorganic counterparts for large area electronics, they also pose serious challenges that must surmounted to enable their commercialization in real world applications. Performance wise, even though marked improvements are reported on almost a daily basis, inorganic technologies based on a-Si, copper indium gallium arsenide etc. remain the industrial benchmark. This inferior performance is primarily because polymeric semiconductors suffer from relatively poor charge carrier mobility:a key index of performance for OSCs. Improvement of charge carrier transport in polymer thin films remains a challenge, in part because polymers, especially high molecular weight variants, present a significant barrier to crystallization[56] and also because we have yet to completely understand the physics of charge transport in such disordered systems.

Unraveling the complex correlations between the microstructure of the polymer thin films and their corresponding charge transport properties is thus of paramount significance in furthering the state-of-the-art in organic semiconductors. Moreover, fundamental questions still remain regarding the contribution of individual factors towards the macroscopic charge transport that need to be addressed, Figure 20, and this thesis attempts to identify, if not suggest, correlations.

Revisiting Marcus theory that relates the hopping rate of charge carriers with two key parameters, V, the *transfer integral* and λ, the *reorganization energy*. As shown in Figure19, both V and λ are intricately linked to the state of the ordering

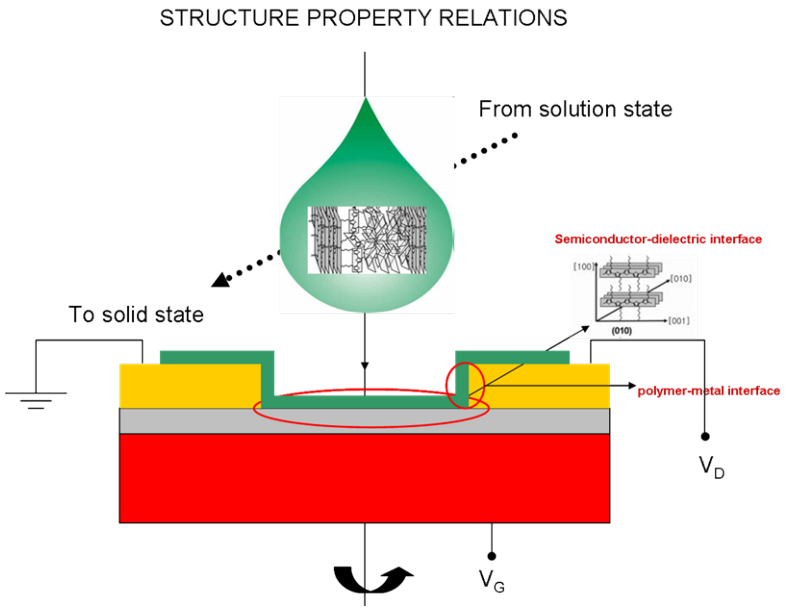

Figure 18: Research outline

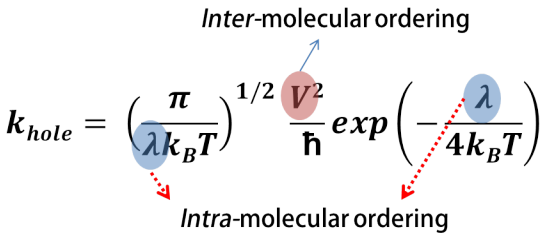

Figure 19: Structural ordering and transport at the micro-scale

of the system, *intra*-chain for λ and *inter*-chain for V. Thus, answering key questions about the microstructure-charge transport correlation requires addressing the roles of structural order and disorder. Here, we thus focuses on elucidating the following key questions:

- How does microstructure evolve?
- How does the evolution of structural properties correlate with that of electrical properties?
- Can microstructure be controlled?

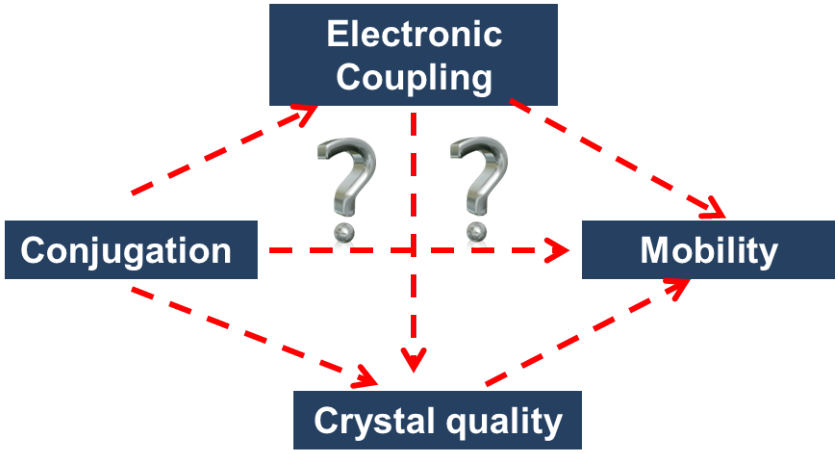

Figure 20: The role of microscopic factors in macroscopic charge transport

- If so, what is the role of crystallinity in controlling macroscopic charge transport?
- What is the role of *intra* vs *inter*-chain effects?

These points are also summarized in Figure 20.

This thesis thus focuses on a fundamental study of such correlations in the first high mobility solution processable semiconducting polymer, poly(3-hexylthiophene) (P3HT). P3HT is a model system and hence is especially amenable to a study such as this which attempts to elucidate correlations identified above. Using a commercially available polymer that is known, readily available and has been the subject of previous fundamental molecular scale investigations may provide some continuity and perhaps build a more sound foundation to our results. Moreover, the issues raised above are key to really understanding *any* polymer based system and to developing not only improved materials, but also the requisite processes that must also be developed to extract the maximum performance from the material. Note that the objective of this work is not to optimize the performance of organic transistor, but more to use the OFET as a tool to characterize the mobility, which in turn is an important performance index that is critically dependent on the polymer film microstructure.

As mentioned above, although the results are obtained using P3HT as the organic semiconductor, they can be extrapolated to other polymeric semiconductors as well since the physics of charge transport remains unchanged. Figure 18 shows the overall outline of the research conducted towards completion of this thesis. We focus on two different yet equally important aspects of polymer self-organization. In chapter 2, an attempt is made to understand the *process* of channel formation starting from the solution state leading up to the solid state, using a combination of *in-situ* spectroscopic techniques as well channel current measurements. Not only are the dynamics of film formation studied, but also the channel and contact properties are mapped as a function of polymer film thickness. Such a study is believed to be critical to optimization of morphologies conducive to facile charge transport. Chapter 3 explores the role of regioregularity of side chain attachment on the self-assembled nanostructure. A subtle effect of the regioregularity is discovered which can bring out dramatic differences in the field effect mobility. Chapter 4 details a novel technique for generating ordered precursors that translate into highly ordered films in the solid state, but more importantly, it provides an important insight into the correlation between the degree of crystallinity in polymer based materials and charge transport. Chapter 5 extends the work in Chapter 4 to understand the role of different deposition methods in controlling the morphology of P3HT films and their effect on field effect mobilities. Chapter 6 summarizes our findings by connecting the results in Chapters 2 through 5.

Critical morphological parameters that control macroscopic charge transport in conjugated polymers are identified. Overall, our understanding of charge transport in organic semiconductors is a continuously evolving process and we aim to elucidate the role of one of many important factors that control macroscopic charge transport in polymeric semiconductors, namely *microstructure*.

CHAPTER II

HOW DOES THE CONDUCTING CHANNEL FORM IN P3HT?

The most critical step in fabricating solution-processed OFETs is the solidification process of the polymer solution at the polymer/gate dielectric interface where the charge transport properties of the resultant thin film are determined by the structural organization of the polymer molecules. In this section, the conducting channel formation process in poly(3-hexylthiophene) (P3HT) FETs is described via *in situ* sheet conductance measurements using four-contact geometry field effect devices. The variation in the electrical properties is studied as film formation evolves as a function of solvent evaporation time measured from the point the solution droplet is deposited on the device. In the *in situ* measurements, the onset of the drain current is achieved by percolation between P3HT chains resulting from the increase in P3HT concentration in solution during solvent evaporation. The P3HT channel sheet conductance and P3HT/Au contact resistance extracted from the gated four-contact measurements varies during channel formation. After percolation, the four contact mobility increased up to a peak value of 0.17 $cm^2V^{-1}s^{-1}$ after which it continuously decreases. This is an important result that suggests a competition between the evolution of P3HT microstructure involving potential phase transitions between isotropic, liquid crystalline and polycrystalline phases and atmospheric degradation, both of which are critical factors that should be considered in optimizing device performance. The phase transitions are explored in more detail in Section 2.3.

2.1 Conducting Channel Formation in Poly(3-hexylthiophene) Field Effect Transistors: Bulk to Interface[1]

2.1.1 Introduction

P3HT has been widely used in OFETs due to its high mobility and good solubility which allow formation of a functional interface at which charge transfer and transport occur.[57] Electrical and structural properties of P3HT near both, the gate dielectric and metal electrode are of significant interest since they govern performance of OFETs and organic sensors by controlling charge transport in the conducting channel and the charge injection barrier.[54,57]

A number of strategies have been applied to manipulate the electrical and structural properties of P3HT at the semiconductor/gate dielectric interface. For instance, enhancement of the carrier mobility through choice of solvent and deposition method has been achieved by altering the evaporation rate of the solvent from the P3HT solution, which in turn impacts thin film crystallinity,[58] prompting device optimization through the use of a variety of deposition processes.[47,59] For example, P3HT FETs fabricated with high boiling point solvents showed higher mobilities than those prepared using low boiling point solvents due to enhanced crystallinity of the resulting P3HT films.[46,59] The observed structural differences are believed to result from subtle differences in the self-organization of the polymer chains in solution during film formation.[47] In a spin-cast film obtained from volatile solvents, polymer chains are kinetically limited from assembling into ordered structures due to rapid solvent evaporation, which results in a film that exhibits a relatively low carrier mobility compared with a film prepared by drop-casting where polymer chains are allowed to form large crystalline domains desirable for charge transport.[60] The conformation of the conjugated polymers in solvents is reflected in the final microstructure of the films formed from a given solution, and thus critical in determining the charge transport

[1] ***J. Phys. Chem. C 2011, 115, 11719***

properties of the thin films.[61] Thus, an understanding of how conjugated polymer chain conformations evolve with solvent evaporation is crucial in manipulating thin film properties. This is especially important since the continuous removal of solvent from the polymer solution leads to successive phase transitions eventually leading to the observed, final microstructure.[62] However, our current understanding of the microstructure-charge transport correlation does not extend to these intermediate phases, control of which will be critical to controlling the final semiconductor film architecture. Further, selected intermediate phases might provide a more favorable orientation for charge transport than the final microstructure itself.[62] In addition, a coherent description of the evolution of electrical properties associated with electrical channel formation in solution processed FETs is not available, in contrast to FETs prepared from vacuum-deposited organic semiconductors where the onset of current between source and drain electrodes is believed to occur by geometric percolation between organic semiconductor islands grown on gate dielectric substrates.[63] Therefore, interrogating the evolution of structure in conjugated polymer systems, rather than simply the final state assumed by the polymer chains, in concert with the evolution of electrical current enables one to not only establish a more comprehensive correlation between the structural changes and electrical properties, but also raises the possibility of quenching the self-assembly process in states that are more favorable to charge transport. Such an understanding could open routes for manipulation of polymer chain conformations into favorable packing motifs that are conducive to facile charge transport, thus leading to new opportunities for device optimization.

2.1.2 Experimental Methods

2.1.2.1 Materials

The P3HT used for this study was purchased from Sigma Aldrich and used without further purification. This material had a M_n of 24 kD and M_w of 47.7 kD (from GPC in tetrahydrofuran calibrated with polystyrene standards using a Waters 1515

Isocratic HPLC system with a Waters 2489 UV/Vis detector, using a Styragel HR 5E column) and a head to tail regioregularity of 92-94% (as estimated from the ^{1}H NMR spectrum obtained from a solution of the polymer in deuterated chloroform at 293 K recorded using a Bruker DSX 300 NMR spectrometer). P3HT solutions with a concentration of 3 mg/mL were prepared using 1,2,4 trichlorobenzene (TCB) (B.P. 218-219 C) as the solvent.

2.1.2.2 Fabrication of P3HT field effect devices

We fabricated two and four-contact devices in which P3HT films are formed on 200 nm thick SiO_2 gate dielectrics via drop-casting. A highly doped silicon wafer served as a gate electrode, and source and drain electrodes (Au (50 nm)/Cr (2 nm)) were patterned using photolithography with the channel length of 15 to 165 μm and the width of up to 2 mm. In the four-contact devices, two sharp voltage probes separated by 90 μm were patterned between the source and drain electrodes with a spacing of 165 μm to measure the sheet conductance of P3HT films. P3HT solutions with a concentration of 5 mg/mL were prepared using a series of solvents with different boiling points, including chloroform (B.P. = 60.5-61.5 °C), thiophene (B.P. = 84 °C), and 1,2,4 trichlorobenzene (TCB) (B.P. = 218-219 °C).

2.1.2.3 In situ electrical and structural characterization of P3HT films

: The two- and four-contact devices were put into a small box equipped with electrical feed-throughs connected to a semiconductor parameter analyzer (Agilent 4155C), and a 2 μL droplet of the P3HT solution was deposited onto the devices through a hole in the box for *in situ* source-drain current measurements at a particular gate voltage during solvent evaporation. The volume of a droplet of solution was controlled using a micro-pipette. All the electrical measurements were carried out in air. Tapping mode AFM measurements were performed using a Veeco Digital Instruments Dimension

3100 scanning probe microscope in tapping mode with a silicon tip (NSC 14, Mikromasch), on fully dried films obtained on bare silicon dioxide substrates prepared under the same conditions as the bottom contact substrates for electrical measurements.

2.1.3 Results and Discussions

2.1.4 *in situ* electrical characterization of channel formation

The FET device configuration used in this study is shown in Figure 21. For *in situ* electrical measurements, we adopted the bottom contact FET configuration with two voltage probes between the source and drain electrodes, allowing for measurements of the channel and contact resistances. Four-contact geometry devices were employed to record the variation of the channel sheet conductance, allowing measurement of the four-contact mobility and threshold voltage independent of the P3HT/Au contact properties. In the measurement, two voltage probes between the source and drain electrodes monitored the potential along the conducting channel under application of a given gate voltage above the threshold voltage, inducing mobile charge carriers in the channel. The sheet conductance σ_{sq} was calculated using Equation 13, where d_{12} and V_{12} are the distance and potential difference between two voltage probes (V_1 and V_2), respectively, as illustrated in Figure 21. Here, W is the channel width, and I_D is the drain current.

$$\sigma_{sq} = \frac{d_{12}}{W} . \frac{I_D}{V_{12}} \tag{13}$$

The values of the four-contact mobility and threshold voltage are determined from the plot of sheet conductance as a function of gate voltage, as described in Equation 14, where C_{ox} is the capacitance of the gate dielectric per unit area:

$$\mu = \frac{1}{C_{ox}} . \frac{d\sigma_{sq}}{dV_G} \tag{14}$$

The relation in Equation 14 is valid when the charge carriers induced in the linear

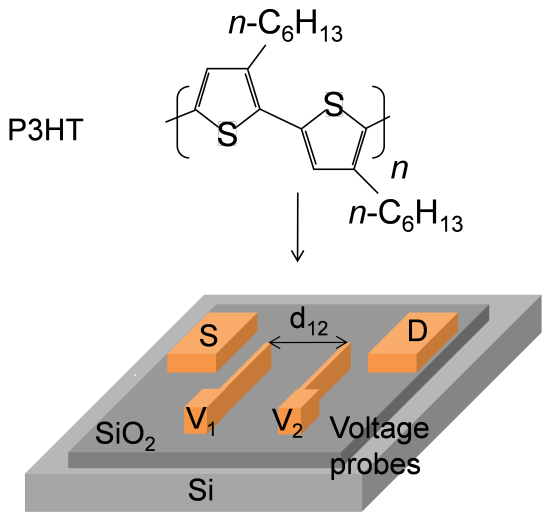

Figure 21: Schematic diagram of the bottom contact FET used in this study

regime of transistor operation are mobile.

The formation of the P3HT conducting channel during solvent evaporation from a solution of P3HT in chloroform was confirmed by the current onset in the *in situ* current-voltage measurements, as shown in Figure 22. The current measured in Figure 22, I_{D}, consists of the bulk current, I_{B}, and the interface current, I_{I}, that flows in the two dimensional conducting channel close to the SiO_2 gate dielectric, as given by the Equation 15, where σ_{Bulk} represents the bulk conductivity, C_{ox} , the capacitance of the gate dielectric per unit area, L, the channel length, t, the film thickness and W, the width. The magnitude of the interface current in the linear regime of transistor operation is determined by the applied drain voltage V_{D}, the FET mobility μ, and the two dimensional charge carrier concentration $C_{\mathrm{ox}}(V_{\mathrm{G}}\text{-}V_{\mathrm{T}})$, where V_{T} is the threshold voltage. Figure 22(b) shows the equivalent circuit diagram in which the channel resistance (R_{B}+R_{I}) and the contact resistance (R_{S}+R_{D}) comprise the total resistance.

Upon deposition of a 2 μl droplet of P3HT solution in chloroform, the current onset was observed with a sharp increase of the drain current to a peak current of 120 μA within a few seconds as shown in Figure 22(a). The first peak after current onset was followed by a second peak, after which the current continuously

decreased. Prior to dropping the P3HT solution onto the device, the observed current was limited to the leakage current through the silicon dioxide gate dielectric, which was at the level of hundreds of picoamps (pAs). The onset of an observable current in Figure 22(a) is suggested to arise from percolation of the polymer chains forming the conducting pathways. During solvent evaporation from the free surface, the local concentration of polymer at the free surface sharply increases. This creates a spatial conductance gradient in which the sheet conductance of the film near the free surface is the highest right after current onset.[64–66] After percolation of the polymer chains, the occurrence of the two drain current peaks can be attributed to rearrangement of the P3HT polymer chains due to evaporation of chloroform. After drying, the P3HT film morphology was interrogated by AFM (Figure 22(c)). As seen from Figure 22(c), the P3HT polymer chains self-assemble into a nanofibrillar morphology with nanofibers of relatively uniform widths that constitute crystalline-like domains.

$$I_D = I_B + I_I = \sigma_{bulk}\frac{Wt}{L} + \frac{W}{L}\mu C_{ox}(V_G - V_T) \tag{15}$$

2.1.5 Dynamics of film formation: Role of solvent boiling point and bulk and interface effects

The time required for formation of the conducting channel scales with the evaporation rate of the solvent used, as shown in Figures 23. The higher boiling solvents, thiophene and TCB, were used to elucidate the origin of the current variation under scenarios where the solvent evaporation time is extended due to the higher boiling points compared with chloroform. Upon deposition of a P3HT/thiophene solution, current onset was observed within about 10 seconds, while for the TCB solutions the onset occurred at approximately 20 seconds. This result supports the principle that the observed current onset originates from percolation between polymer chains due to an increase in polymer concentration. Higher evaporation rates accelerate the time associated with the solution reaching a critical concentration at which a conducting

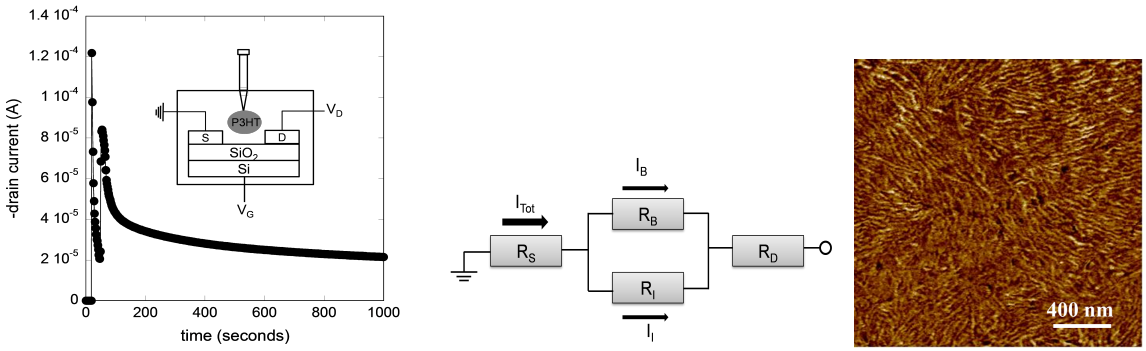

(a) (b) (c)

Figure 22: (a) Plot of drain current vs. time for a FET formed with a drop deposition of a P3HT solution with chloroform. The channel length and width were 15 μm and 2 mm, respectively. The inset shows a schematic diagram of the *in situ* current measurement. Gate and drain voltages were maintained at -15 and -3 V, respectively. (b) A circuit diagram of a FET. R_{S}: contact resistance at source electrode, R_{D}: contact resistance at drain electrode, R_{B}: channel resistance in the bulk and R_{I}: channel resistance at the conjugated polymer/gate dielectric interface. (c) AFM phase image taken from a P3HT drop-cast film (3 mg/1 mL chloroform) on SiO_2.

path is formed through percolation between polymer chains. After current onset, the drain current increased rapidly, by over two orders of magnitude, ranging from tens of pAs to several nAs in tens of seconds for both devices. A sharp increase of the drain current immediately before its saturation is clearly seen in the devices. We surmise that the sharp increase of the drain current is due to formation of a P3HT conducting channel close to the SiO_2 gate dielectric. As solvent evaporates, solvent loss begins at the top surface defined by the solution/air interface and ends at the polymer/substrate interface.[64] In other words, the P3HT/air interface approaches the P3HT/SiO_2 interface with continued solvent evaporation. Near the end of the solvent evaporation process, the degree of relaxation of the individual polymer chains at the P3HT/SiO_2 interface is minimized with a maximum density of the polymer chains. The significant current increase before saturation, thus, arises from the contribution of the interface current which is proportional to the FET mobility μ and the charge carrier density $C_{ox}(V_G\text{-}V_T)$ in Equation 15 finalizing the formation of the conducting channel(vide infra).

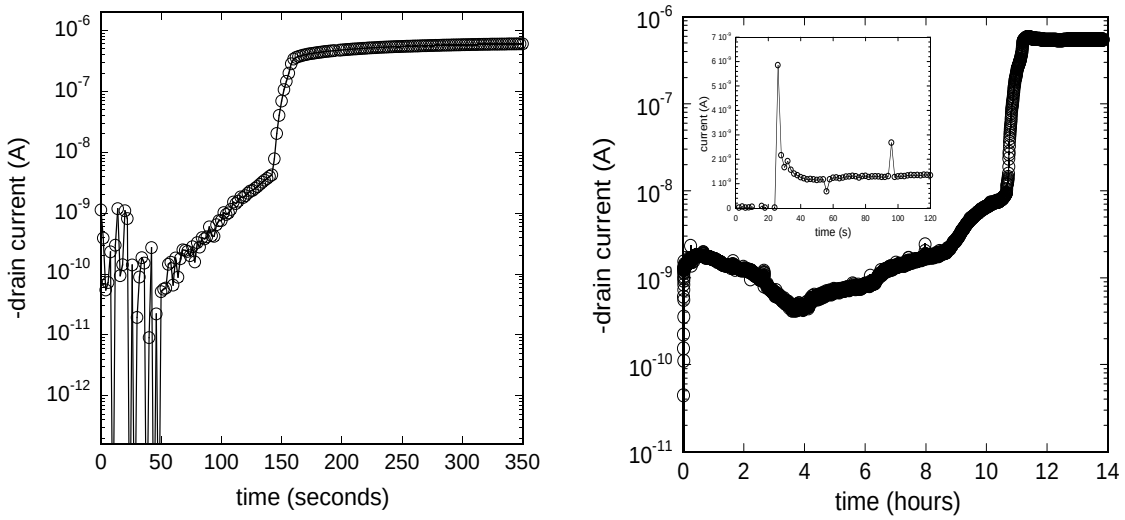

(a) (b)

Figure 23: Variations of the drain current of P3HT FETs, during solvent evaporation, prepared from the drop deposition using different solvents of (a) thiophene and (b) TCB. The inset shows the magnified view near current onset. For all the FET devices, gate and drain voltages were fixed at -10 and -5 V, respectively. The thicknesses of the samples ranged between 2 and 3 μm

2.1.6 Isolating interfacial effects at the semiconductor-dielectric interface

To focus on the conducting channel formation close to the gate dielectric, it is necessary to reduce the bulk current by decreasing the film thickness and thereby increasing the contribution of the interface current to the total current, as described in Equation 15. A relatively thin semiconductor film was prepared from chloroform solution by tilting an FET device during drop deposition, allowing the solution to flow downwards; a process which is similar to a dip-coating process. A schematic of the methodology is shown in the inset of Figure 24. A maximum drain current was obtained about 3 seconds after P3HT solution deposition which was followed by the gradual current decay as shown in Figure 24. These results suggest that the motions associated with the polymer chains quickly become limited by the rapid evaporation of chloroform. Interestingly, the abrupt current variations after current onset were not observed here, contrary to results for devices prepared from substrates which were

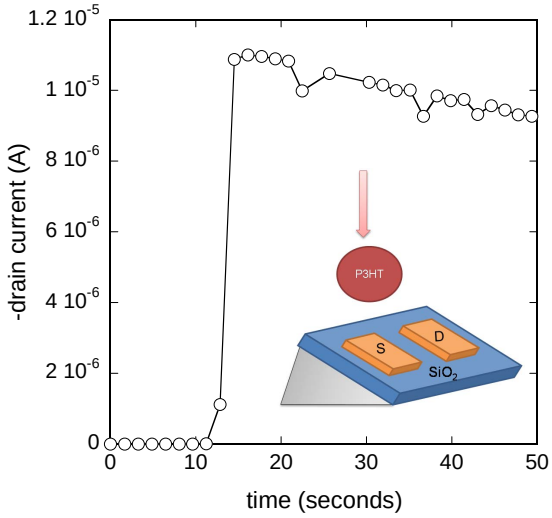

Figure 24: Plot of drain current as a function of time in a P3HT FET during chloroform evaporation. The inset shows the schematic of a modified drop deposition in which a FET device was tilted with a certain angle. Gate and drain voltages were fixed at -10 and -5 V, respectively. The thickness of the sample was 21020 nm

kept horizontal during deposition of the droplet (Figure 22(a)). This observation is direct evidence that the current variations resulted from reorganization of the semiconducting polymer chains in the presence of solvent. With the tilted device, the almost instantaneous volume change combined with the fast evaporation of chloroform suppressed the movement of the polymer chains in the channel region and thus possibly explains the absence of the significant current variations that are observed in Figure 22(a).

To measure the change in the electrical properties of P3HT close to the SiO_2 gate dielectric during channel formation, the modified drop deposition method used in Figure 24 was combined with an *in situ*, gated four-contact sheet conductance measurement. For this measurement, two different gate voltages (-40 and 0 V) were applied alternately for a period of tens of seconds. Upon switching the gate voltage from -40 (blue circles) to 0 V (red circles), the sheet conductance drops abruptly because of the reduced charge carrier density. The inset of Figure 25(a) shows the change in sheet conductance when the current onset is first observed, in which the

sheet conductance soared to 6.0×10^{-7} S $\square^{-1}$. To evaluate both, the four contact mobility and threshold voltage with respect to time, the sheet conductance values at the time when the gate voltage is switched from -40 to 0 V was used to measure the value of $d\sigma_{\square}/dV_G$. The error in extracting the four contact mobility and threshold voltage was unavoidable because of the time interval of several seconds associated with switching the gate voltage. Figure 25(b) shows the plot of the sheet conductance vs. time at two gate voltages (0 and -40 V), estimated from the data obtained in Figure 25(a). Figure 25(c) depicts the plot of gate voltage versus sheet conductance as a function of time, from which the four contact mobility and threshold voltage can be extracted from the slope and gate voltage intercept, respectively. The four-contact mobility and threshold voltage derived from the values of the sheet conductance were plotted as a function of time during chloroform evaporation in Figure 25(d). The four contact mobility initially increased from 0.10 to 0.17 $cm^2V^{-1}s^{-1}$, which was followed by a decrease of up to 0.02 $cm^2V^{-1}s^{-1}$ in several hours. This was accompanied by a simultaneous sharp drop in the threshold voltage from 182 to 46 V, stabilizing near a value of 22 V at the end of the measurement period. The trend observed for the variations of the hole mobility and threshold voltage was confirmed through experiments on multiple FET samples. In the experiments performed here, the presence of the peak mobility was observed reproducibly with its value spanning an order of magnitude ranging between 0.03 and 0.17 $cm^2V^{-1}s^{-1}$. The large variation in the magnitude of the peak mobility can be attributed to variations in deposition conditions, i.e. differences in substrate tilting angle prior to solution deposition and/or quantity of P3HT solution, which affect the time available for self-organization of the conjugated P3HT polymer chains at the P3HT/SiO_2 interface.

The observed change in four contact mobility seen in Figure 25(d) is closely related to the structural changes in the P3HT film that is in contact with the SiO_2 gate dielectric. Given that only a few molecular layers close to the gate dielectric govern

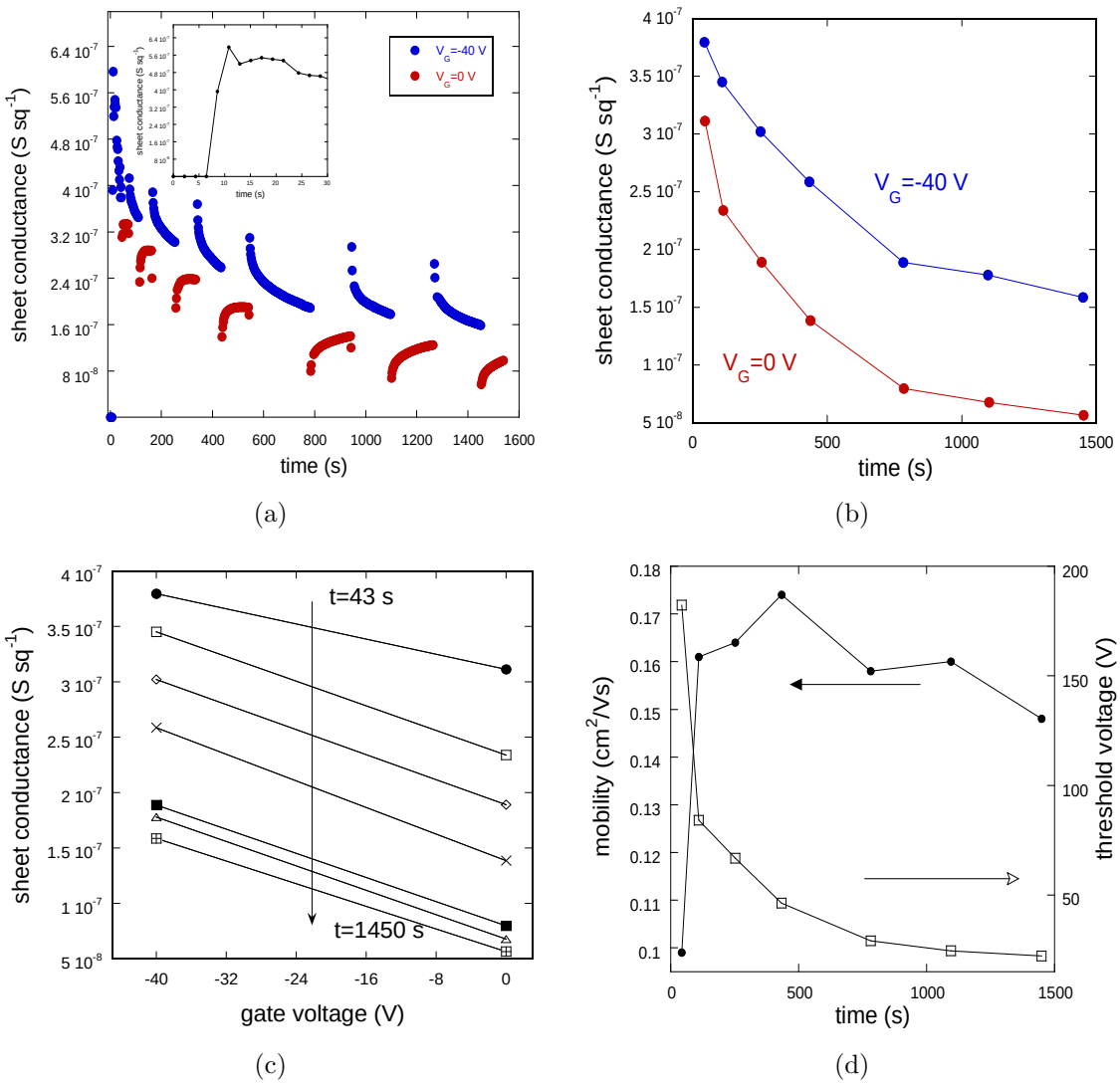

Figure 25: (a) Plot of sheet conductance as a function of time for a four contact device with d_{12}=90 μm, w=1.2 mm, and L=165 μm. The drain voltage was kept at -5 V, and two gate voltages of -40 (blue circles) and 0 V (red circles) were switched periodically. The inset is a magnified view of the plot near the current onset.(b) Plot of sheet conductance as a function of time at V_G=0 and -40 V. (c) Plot of sheet conductance as a function of gate voltage with time. (d) Plot of four contact mobility and threshold voltage as a function of time.

charge transport in the P3HT film, it is necessary to address retention of chloroform at the P3HT/SiO_2 interface over the entire time range in Figure 25(d), since the presence of solvent in a polymer film will enhance the movement of the polymer chains which in turn will affect the molecular ordering within the P3HT film.[67,68] While

information relating to the presence of chloroform at the P3HT/SiO_2 interface during the *in situ* measurement is not readily available, the amount of chloroform retained in the film after spin-coating can be roughly estimated from previous studies.[64,69] In these reports, the mass of toluene in a polystyrene film obtained by spin coating, was monitored as a function of time at 115°C using gas chromatography. It was found that toluene was retained in the spin-coated polymer film for more than 6 hours producing a desorption rate in the range 1-5 $\times$ $10^{-5}s^{-1}$. The vapor pressure of toluene at 115°C is higher than that of chloroform at room temperature by a factor of 5 and hence the desorption rate of toluene determined in these experiments is predicted to be larger than that of chloroform in our experiments. This difference leads to the expectation that some chloroform would be retained at the P3HT/SiO_2 interface for a significant time period after polymer solution deposition.

From these considerations, we hypothesize that the observed variation in P3HT four contact mobility is associated with relaxation of P3HT polymer chains in the film assisted by solvent retained close to the SiO_2 substrate. Using polarized Raman spectroscopy, we demonstrated in a separate study (this is detailed in Chapter 2.3) that the continuous removal of TCB from a drop-cast P3HT solution on a silicon dioxide substrate leads to the formation of an intermediate lyotropic liquid crystalline phase that is characterized by anisotropic ordering of P3HT chains over a macroscopic area. This intermediate phase was found to last for several hours before transitioning into a solid state consisting of nano-scale crystalline domains associated with a concurrent loss of long range order.[62] Thus, it may be possible that the increase in four contact mobility leading to the peak mobility observed in Figure 25(d) is due to the presence of an intermediate anisotropic phase which is followed by loss of macroscopic ordering and concomitant decrease in mobility. This will be discussed in greater detail in the next section.

In elucidating the origin of the variation in four contact mobility during chloroform

evaporation, the possibility of degradation of P3HT in air must also be considered. In particular, molecular oxygen and/or water have been accepted as major dopants for polythiophenes.[70] Molecular oxygen has been known to form a charge transfer complex in P3HT enhancing the bulk conductivity. In those experiments, the increase of current in P3HT-based FETs in air was explained by formation of electron acceptor states associated with molecular oxygen.[71] Further, Chabinyc et al.[72] pointed out that water degrades polythiophene devices by trapping charge carriers that flow in the channel, thereby reducing the FET mobility. The current decay in the presence of water, whose rate depends on relative humidity, is consistent with our observation that the channel sheet conductance decreased with time after first reaching a peak FET mobility, as seen in Figure 25(a).

To summarize, electrical properties of P3HT films during solvent evaporation, as measured using FET structures, continuously evolve with time, with two dominant mechanisms dictating this evolution. The first involves ordered self-organization of the conjugated polymer chains (specifically P3HT) in solution, possibly mediated through the formation of a lyotropic liquid crystalline phase, that improves molecular ordering of the P3HT layers close to the SiO_2 gate dielectric, which accounts for the observed enhancement in FET hole mobility. The second relates to degradation of the P3HT based device in air, resulting in a decrease in FET hole mobility and threshold voltage. The appearance of the peak mobility represents a crossover between the two dominant operating mechanisms. Once current onset is achieved, the polymer chains continue to self-organize into ordered structures resulting in the increase in mobility as a function of time up to the point where it is thought that atmospheric degradation becomes the dominant mechanism. Importantly however, as suggested by Raman spectroscopic evidence, structural changes resulting in the complete loss of anisotropic ordering within P3HT films cannot be neglected as a source of the presence of the peak mobility. To clarify the mechanism, additional, controlled environment

experiments are required.

2.1.7 Conclusion

In conclusion, we found that a significant structural change in the P3HT film at the P3HT/SiO_2 interface occurs during channel formation. It should be possible to maximize the magnitude of the peak mobility by enhancing chain alignment and orientation and/or retarding chemical degradation. Understanding of the change in the electrical properties of conjugated polymers during solvent evaporation can provide insights into the time scale of channel formation, which would benefit the design of optimized processes for the development of high performance flexible electronic devices. Within this framework, a comprehensive study of the effects of solvent and fabrication conditions on the electrical properties of conjugated, semiconducting polymers should be performed.

2.2 Solvent Evaporation Induced Liquid Crystalline Phase in Poly(3-hexyl thiophene)[2]

2.2.1 Introduction

In Chapter 2.1, we studied the evolution of the channel current as a function of solvent evaporation time. The evolution of the field effect mobility as a function of solvent evaporation time is especially interesting since it is well documented that the mobility mirrors the structural properties in the thin film (see Chapter 1, Introduction). So, a question that naturally arises from the *in situ* electrical study reported earlier, is how do polymer chain conformations and microstructur evolve concurrently. It has been reported that structural changes result from the behavior of polymer chains in the solvent during film formation,[47] and resulting conformations of conjugated polymers in solvents play a crucial role in determining electrical properties. Nevertheless, a coherent picture of the formation of the conducting channel in organic FETs and the role of polymer relaxation in the solution process is incomplete.[61] In this section, we report an *in situ* structural characterization using polarized Raman spectroscopy, wherein we identify a lyotropic liquid crystalline phase during the solvent evaporation process, which is otherwise absent in the fully dried film. This could form a potential explanation for the sharp rise of the field effect mobility which will be explored in detail in Section 2.3.

2.2.2 Experimental

2.2.2.1 Materials

The P3HT used for this study was purchased from Sigma Aldrich and used without further purification. This material had a M_n of 24 kD and M_w of 47.7 kD (from GPC in tetrahydrofuran calibrated with polystyrene standards using a Waters 1515 Isocratic HPLC system with a Waters 2489 UV/Vis detector, using a Styragel HR

[2] ***Raman experiments conducted by M.S. Park and M. Srinivasarao; J. Am. Chem. Soc. 2011, 133, 7244.***

5E column) and a head to tail regioregularity of 92-94% (as estimated from the ^{1}H NMR spectrum obtained from a solution of the polymer in deuterated chloroform at 293 K recorded using a Bruker DSX 300 NMR spectrometer). P3HT solutions with a concentration of 3 mg/mL were prepared using 1,2,4 trichlorobenzene (TCB) (B.P. 218-219 C) as the solvent.

2.2.2.2 UV-Visible Spectroscopy

Absorption spectra were recorded in trasmission mode using a UV-visible spectrophotometer with a 10 × objective (N.A. 0.25) (Olympus BX 60). The P3HT solution was dropped onto a pre-cleaned glass slide and the spectra were recorded as a function of solvent evaporation time.

2.2.2.3 in situ Drain Current and Raman Measurement

We fabricated two-contact devices for the *in situ* current measurements. Source and drain electrodes (Au (50 nm)/Cr (2 nm)) were patterned using photolithography with the channel length of 50 m and the width of 2 mm. Two contact measurements were performed using a semiconductor parameter analyzer (Agilent 4155C). A 2 umL droplet of the P3HT solution was deposited onto the devices for *in situ* current measurements during solvent evaporation. The volume of a droplet of solution was controlled using a micropipette.

For the correlation between structural changes and electrical properties, the Raman spectra were recorded simultaneously along with the *in situ* drain current measurements by focusing the excitation laser (15 μm spot size) on the conducting channel, as shown in Figure 26. Raman spectra were recorded using a spectrometer (RXN 1, Kaiser) with a thermoelectrically cooled CCD detector and coupled with a Leica optical microscope (50 × objective, N.A. 0.75). A 785 nm laser diode was used and the irradiation levels were kept below 0.1 mW/cm^2. No sample degradation induced

by the irradiation was observed during the acquisition of spectra. In order to monitor spectral change as a function of solvent evaporation time, Raman spectra were continuously recorded in 15 second time intervals, starting from the deposition of the solution droplet onto the device (t=0) until a fully dried film was obtained. All the electrical and Raman measurements were carried out in air. Peak fitting and analysis was conducted using the Spectracalc software package, GRAMS (Galactic Industries Corp., USA).

All the Raman experiments were performed in collaboration with Min Sang Park in the group of Prof. Mohan Srinivasarao.

2.2.3 Angular Dependence of Raman Intensity from an Evaporating Sessile P3HT Droplet

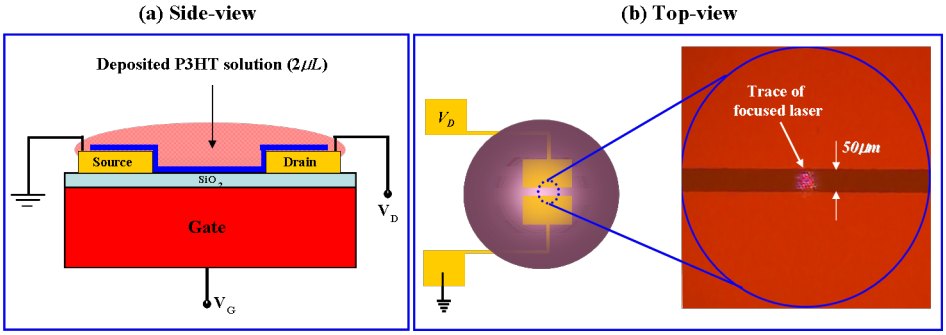

Figure 26: Experimental setup for *in-situ* current and Raman measurements: (a) A schematic of two-contact device used for the electrical measurements. (b) Optical microscopic image after depositing the solution onto the channel region of the two contact device. The central spot is the image of the focused laser spot used for the Raman measurements.

Figure 26 shows the experimental setup used for the Raman measurements. Initial measurements were conducted on bare SiO_2 substrates without electrical measurements, whilst later experiments involved a simultaneous measurement of both. Figure 27 is shows the Raman spectra for P3HT as a function of angle θ obtained 660 minutes after we deposited the solution on to the substrate. It is easy to detect the angular dependence of the peak intensities at 1443cm^{-1} and 1378cm^{-1} which are

attributed to the stretching of the C=C and C-C vibrations in the thiophene ring, respectively.[73–75] It is clear from the angular dependence of the Raman peak intensities that P3HT chains have anisotropic ordering. Other evidence of the anisotropic nature of the P3HT chains comes from the observation that the fluorescence background of the Raman spectra also displays a strong angular dependence.

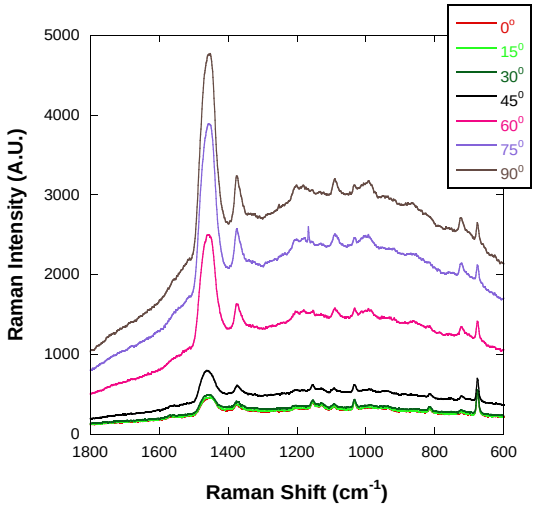

Figure 27: Polarized Raman spectra measured 660 minutes after deposition of the P3HT/TCB solution at room temperature. Spectra were consecutively taken as a function of angle between the incoming polarization direction and arbitrary direction of the conjugated backbone 15°intervals. Peaks at 677cm^{-1} are attributed to the C-Cl stretching mode of 1,2,4-TCB.

Interestingly, the angular dependence was observed only in the time period between approximately 630 to 720 minutes after solution deposition, with measurements proceeding from 0-1200 minutes. It is noteworthy that in all of the spectra showing angular dependence, we can detect characteristic peaks of pure solvent that are distinct from those of pure P3HT. In particular, the peak at 667cm^{-1} attributed to the C-Cl stretching mode in 1,2,4-TCB[76] is clearly shown in those spectra, which implies that a non-negligible amount of solvent still remains. No angular dependence was discernable before this time period noted above, which is evidence of considerable mobility of polymer chains in solution up until this time. At longer times, it is thought that continued solvent evaporation produces polycrystalline states consisting

of nano-scale domains where a large distribution of crystal orientation arises among domains.[77] Because the Raman intensities obtained from the sample are averaged across the spot size of the laser used in this study (15 μm, which far exceeds typical domains sizes in a polycrystalline film), no angular dependence was observed outside of the time window mentioned above. Representative spectra from outside this period (630 720 minutes) are shown in the Figure 28. Judging from the evolution of the anisotropic nature of polarized Raman spectra connoting long-range orientation of P3HT chains and considerable residual quantity of solvent as judged by the characteristic peaks of 1,2,4-TCB, we propose the possibility of a phase transition from an isotropic solution state to a liquid crystalline phase, followed by evolution of the solid state consisting of nano-scale crystalline domains as solvent further evaporates.

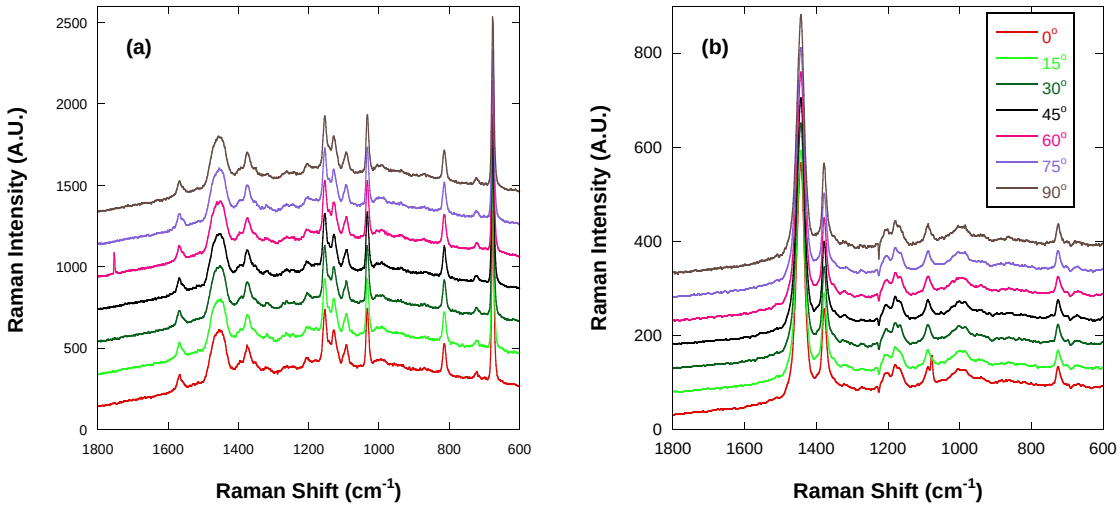

(a) (b)

Figure 28: Plots of polarized Raman spectra consecutively measured by rotating the sample stage at: a) 30 minutes (isotropic solution state) and b) 800 minutes (fully dried film) after deposition respectively.

2.2.4 Raman Peak Analysis: Further Evidence of a Liquid Crystalline Phase

The existence of a liquid crystalline phase during solvent evaporation is supported by P3HT backbone peak analysis. It has been reported that the vibrational frequency

of C=C stretching mode of the thiophene ring is the principal feature that reflects the state of extended conjugation in thiophene based conjugated materials.[74,75] In this respect, the variation in peak frequency of the C=C stretching mode is an effective indicator of changes to the conformation of the P3HT polymer chain. Figure 29 shows the time evolution of C=C vibrational frequency, showing that the peak frequency of this vibration gradually decreases by 15cm^{-1} during the transition from the isotropic solution state (1458cm^{-1}) to the fully dried film state (1443cm^{-1}). Such a frequency shift can be interpreted as the extension of conjugation upon solvent evaporation.[75,78] The variation in conjugation length arises from strong interactions between neighboring chains as they begin to order into a closely packed structure. The damping effect that tends to reduce the oscillations due to strong interactions between neighboring chains is likely responsible for the shift to lower frequency. It should be noted that the time duration for a significant change of frequencies to occur is in agreement with the time scale for detecting the anisotropy in polarization intensities of Raman scattering.

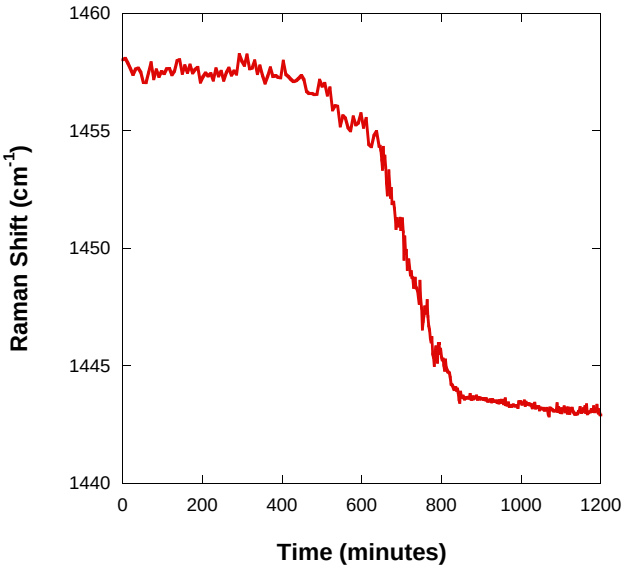

Figure 29: The variation of frequencies assigned to C=C stretching in thiophene ring as a function of evaporation time.

The time evolution of full width half maximum (FWHM) in a discontinuous fashion during the same time frame, as depicted in Figure 30, is additional evidence of a possible phase transition. A significant increase in peak width in polymeric system occurs when the chain conformation changes from a well-defined ordered state to a random state. It is because the structure of disordered chains encompasses a broad distribution of chain conformations and thus their vibrational transitions have a broad bandwidth. Therefore, the gradual decrease in FWHM as evaporation proceeds can be rationalized by the fact that the P3HT backbone is forced to planarize as packing density increases because of solvent evaporation. By contrast, in the dilute solution state, internal twisting about ring-to-ring bonds may induce a deviation from coplanarity, thereby producing conformational disorder of the polymer chain resulting in loss of conjugation. Therefore we suggest that the time dependant behavior (Figures 29 and 30) characterizes a transition into a phase that is distinct from either an isotropic solution or crystalline state: that of a *liquid crystal*.

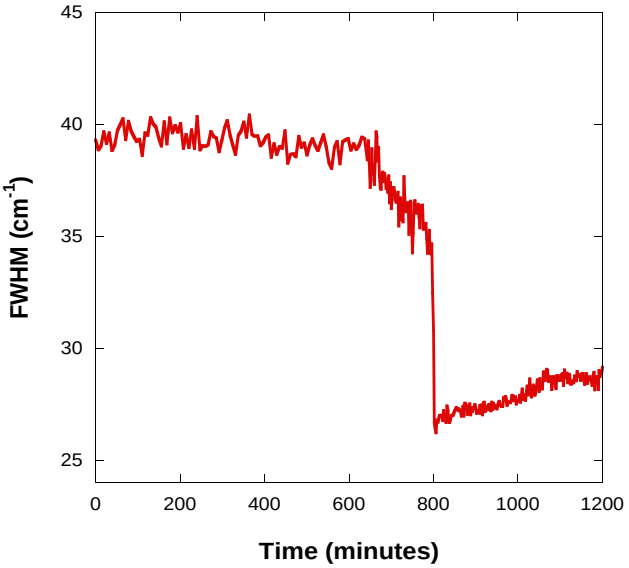

Figure 30: Time evolution of FWHM of Raman peak assigned to C=C stretching in thiophene ring.

These peak analyses, combined with the anisotropic nature of the peak intensity,

provide evidence for a possible phase transition from isotropic solution to a crystalline phase via an intermediate liquid crystalline phase. In order to confirm our theory, we observed the perimeter of droplet where we were able to detect the anisotropy in polarized Raman spectra under a polarized optical microscope. It is well known that when solvent evaporates from a sessile solution droplet, the solute molecules are driven to the edge of the three-phase contact line where the concentration of the solute increases.[79,80] At a critical concentration, the solutes can form a liquid crystalline phase.[81] Under crossed polarizers, we observed regions that display optical anisotropy, Figure 31 which may result from preferential P3HT chain alignment along one direction, justifying our assertion of a possible liquid crystalline phase in P3HT. It should be noted that experimental factors such as evaporation rates and initial concentration of solute in a given droplet may result in different time scales for the phase transition from one sample to the next. For instance, in the case of a faster evaporation rate under high air circulation rates, the isotropic solution undergoes a phase transition to liquid crystal earlier than 630 minutes and the time duration when the sample exhibits a liquid crystalline phase may be shorter. In an effort to better understand these dynamic phenomena, systematic studies of the film formation mechanism must be performed with greater control over relevant experimental factors.

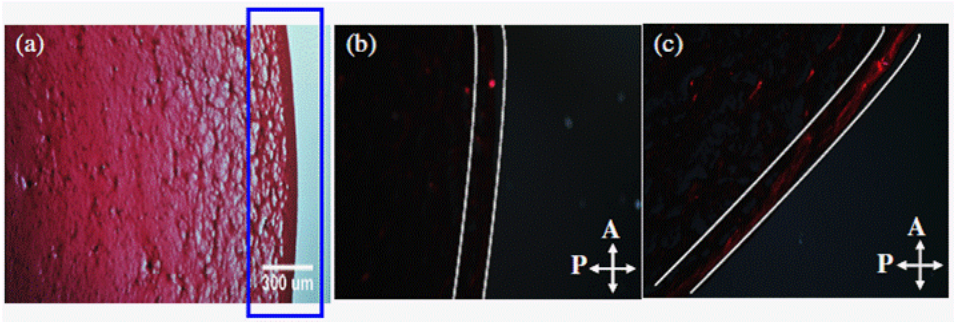

Figure 31: (a) Optical microscopic image (10×) of the fully dried P3HT film. The diameter of drop is approximately 5 mm. (b) and (c) The images of the same film (20×) in the vicinity of perimeter under crossed polarization, when the direction of outward flow of solvent is parallel (b) and 45°tilted with respect to (c) to the polarizer.

2.2.5 Conclusion

In summary, using polarized Raman spectroscopy we have demonstrated that P3HT can possess a lyotropic liquid crystalline phase beyond a critical concentration. Liquid crystalline ordering of P3HT chains during film formation may enable us to design improved materials for high charge mobility, since the liquid crystalline phase possesses long range orientational order and the capacity for *self-healing*, i.e., repairing of the structural defects, in contrast to the crystalline phase.[82] Solvent-evaporation induced self assembly is thus a simple, controllable, and cost-effective method of achieving long range order in thin films of conjugated polymers.

2.3 A Joint in situ Structural and Electrical Characterization of the Film Formation Process in P3HT[3]

2.3.1 Introduction

In the previous section, we demonstrated the possibility of a liquid crystalline phase being manifest (under certain conditions) during the process of solvent evaporation and film formation in P3HT. The coincident times scales at which the liquid crystalline phase, Figure 27 and the sharp current onset, Figure 23(b) are observed raise the possibility that current onset could have a structural origin, where the long range orientational order in the liquid crystalline P3HT films leads to a dramatic increase in the drain current. Moreover, this would also support the sharp mobility increase observed in Figure 25(d). However, as noted in Section 2.2, the observation of liquid crystallinity is strongly dependent on several parameters and is not universally observed across the films. In this section, we report the time dependence of the microstructure formation of P3HT film via solution casting by the *in situ* monitoring of the structural changes using spectroscopic techniques. This is coupled with a simultaneous measurement of the drain current, which provides a fundamental insight into how the evolution of microstructure correlates with that of the charge transport.

2.3.2 Experimental Methods

The experimental techniques and materials used are identical to that reported in Section 2.2. The experimental setup used to conduct the joint investigations is shown in Figure 26.

2.3.3 Results

2.3.3.1 in situ Drain Current and Raman Scattering Measurements

The experimental apparatus used is shown in Figure 26. The method used to measure the current is identical to that described in Section 2.1. Only P3HT solutions in TCB,

[3] ***Raman experiments conducted by M.S. Park and M. Srinivasarao***

a slow evaporating solvent, are investigated. The use of high boiling point solvents is suitable for such an experiment because not only does it provide enough time to track changes in the Raman spectra, but it also reduces the dynamic effects in an evaporating solution, such as flow of solvent and temperature gradients, which can complicate the analysis. The evolution of the drain current as a function of time was already discussed in Section 2.1. Instead, we are going to focus especially on the region where the sharp onset of the drain current is observed, leading upto its eventual saturation.

We reported earlier that the evolution of the drain current of P3HT films deposited from solutions with various solvents presents an interesting result: it was found that the drain current increases sharply at a specific time after the deposition of the solution onto a two contact device before eventually leveling off, Figure 32(a). We have labeled key points on the current vs time curve that correspond to significant transitions observed in the Raman spectra, Figure 32(b). The changes observed in the Raman spectra are especially interesting since the spectra corresponding to points B and C in Figure 32(c) closely resemble those obtained from regiorandom (50% head-tail content of side chains) and regioregular (ca. 92% head-tail content of side chains) P3HT respectively, Figure 33. Given the extent of molecular disorder (because of a steric hindrance motivated backbone torsions) in the regiorandom variant, it is expected that it would form a highly amorphous film in contrast to the regioregular variant, which is expected to yield a polycrystalline/semi-crystalline film. Moreover, these differences in the state of order in the sample is also manifest in the Raman spectra, as shown in Figure 33. Thus, we suggest that the Raman spectrum consisting of relatively strong and sharp peaks (regioregular/ordered P3HT sample) result from the collective vibrations in the crystalline domains of P3HT, whereas the weak and poorly developed peaks are attributed to the vibration modes emanating from disordered regions of the film. In addition, we suggest that in the absence of

resonance Raman effects (energy of the excitation (∼1.58 eV, 785 nm, is significantly lower than the energy required for electronic transitions in P3HT (>1.91 eV, <650 nm)), the substantial changes of peak intensity are a result of phase transitions.

As shown in Figure 32(c), the change in Raman spectra between points B and C are abrupt (within ca. 2 minutes of each other) relative to the duration over which the measurements are conducted (1200 minutes). Interestingly, the sharp increase of the drain current (point A) is observed well before the transition in the Raman spectra between B and C:the point at which we suggest the film starts to crystallize. This is especially surprising given the strong correlation between the structural order in the film and its charge transport properties (see Introduction). In fact the Raman spectra composed of weak and blurry peaks exist for a considerable period of time *after* the drain current increases sharply. It should be noted that we repeated the experiments multiple times and although, as mentioned previously, the time scales for observation of the transitions varied between experiments, the qualitative trend remained the same. We also tracked the intensity change of the Raman peak associated with the solvent, TCB (at 677 cm^{-1} assigned to C-Cl stretching), so that the evolution of drain current can be related to the residual amount of solvent in the film. Figure 32(a) shows the residual solvent in the evaporating droplet as a function of time (obtained from the normalized Raman intensity of the solvent peak), which shows that solvent remains in the film even when the drain current starts to increase sharply (point A).

As mentioned in Section 2.2, the Raman peak at ca. 1445 cm^{-1} attributed to C=C symmetric stretching in thiophene rings is strongly affected by not only the conformation of P3HT chains, but also by interactions between neighboring chains,[74,75,78] and hence is an indicator of the state of ordering between P3HT chains in the evaporating droplet. Figure 34 shows the variation of the normalized intensity of the C=C stretching mode ($I_{C=C}$) measured after point B (the peak intensities are normalized with respect to the the intensity at point D). The normalized intensity increases very

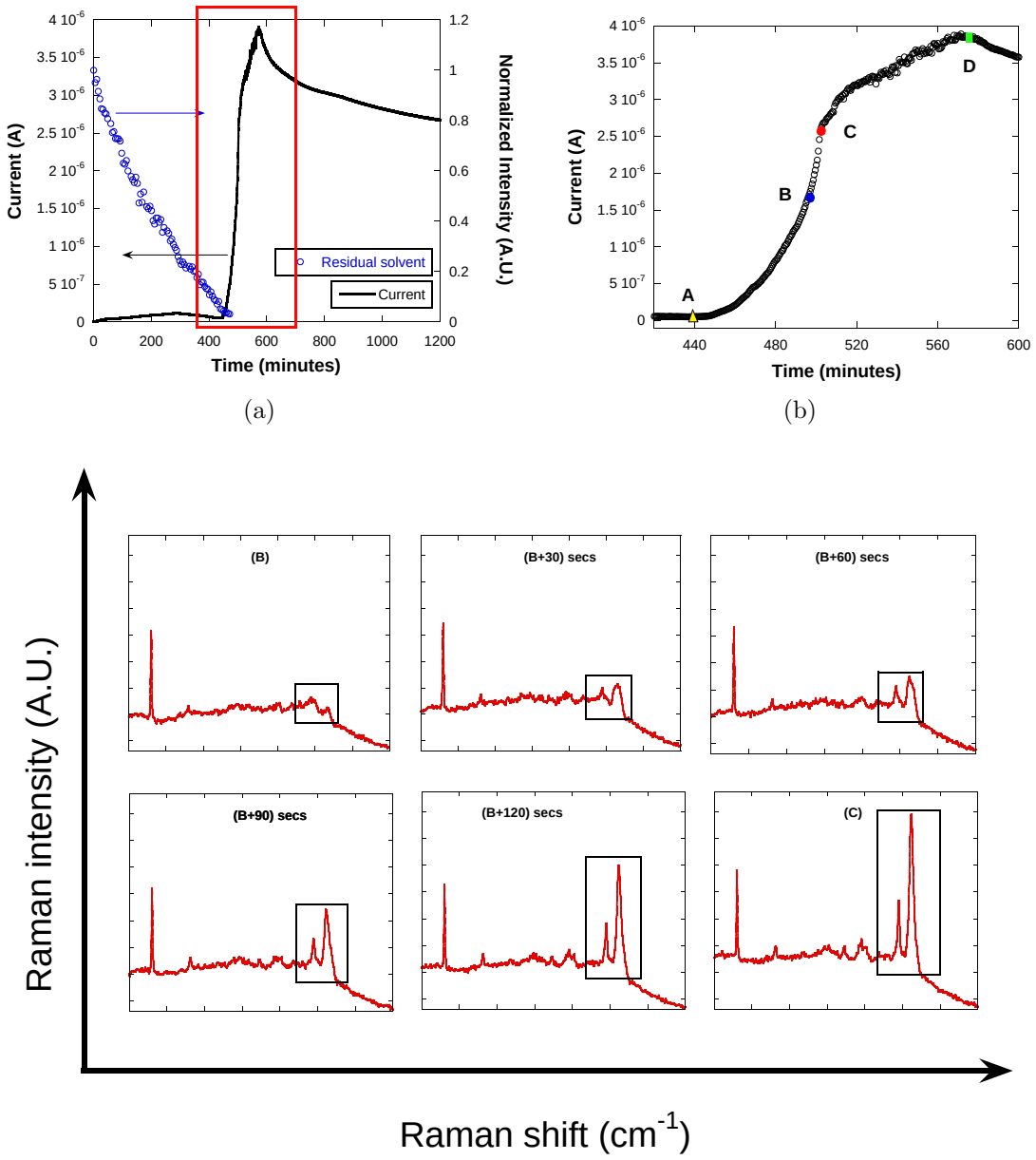

Figure 32: (a) Time evolution of the intensity of Raman peak attributed to C-Cl stretching in TCB (blue points) and drain current (black points).(b) Figure (a) magnified to highlight the region of interest where the sharp increase in current is observed; A: time at which the drain current sharply increases, B: the moment after which weak and blurry peaks disappear, C: the moment at which Raman spectra consists of strong and sharp peaks similar to those of crystalline domain, and D: the moment at which drain current shows its maximum.(c) The variation of Raman spectra between points B and C.

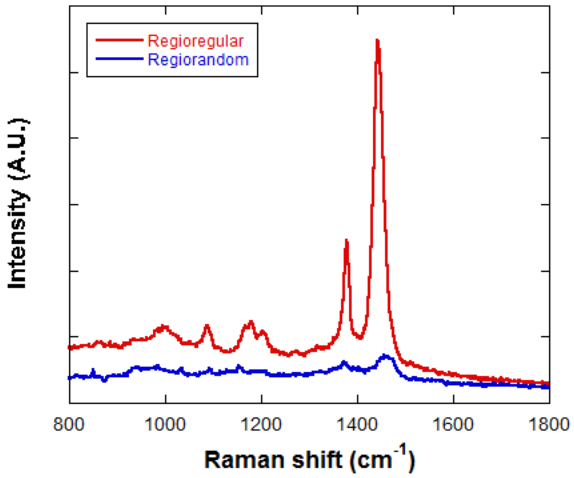

Figure 33: Raman spectra obtained from regiorandom (black line) and regioregular P3HT (red line)

sharply until point C, slowly increasing up to point D, beyond which it eventually saturates.

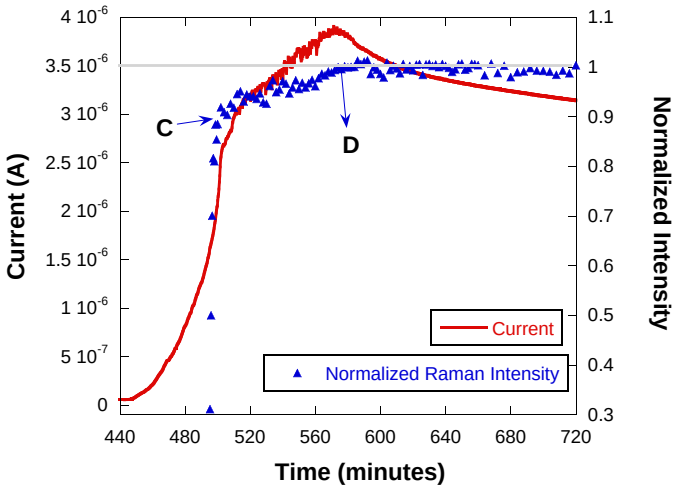

Figure 34: Correlation between the intensity variation of Raman peak assigned to C=C stretching in crystalline phase and drain current with time. Intensity was normalized by its maximum.

In addition, substantial variations of the position and bandwidth of C=C stretching are observed in the non-crystalline phase (between moments B and C) and in crystalline phase (after moment C). The time evolution of the position and full width at half maximum (FWHM) of the principle Raman band for P3HT is shown in Figure

35. The peak position continuously red-shifts to lower wave-numbers from ca. 1446.5 cm^{-1} and settles at about 1445.0 cm^{-1} ca. 1050 minutes after the deposition. The FWHM also continuously changes with time, from ca. 25 cm^{-1} at point C and rising up to ca. 27 cm^{-1} as time goes.

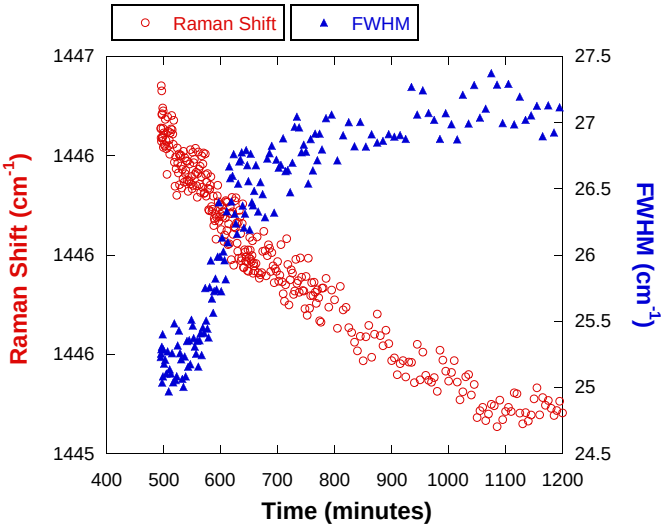

Figure 35: The time evolution of the position and FWHM of the Raman band assigned to C=C stretching of P3HT

The Raman spectra are indicative of phase transitions that may contain evidence for the source of the sharp current onset. We supplement the joint Raman and drain current experiments with *in situ* absorption spectroscopy that also contains evidence of a continuous phase transition as will be discussed in detail in the next section.

2.3.3.2 Optical Absorption Spectra

As will be demonstrated in subsequent sections, the absorption spectra reflect the microstructure of the thin films and thus is an invaluable tool in studying the evolution of the microstructure as well. For the *in situ* experiments reported here, we deposited the P3HT solution in TCB onto a transparent glass slide and recorded the absorption spectra in transmission mode. The absorption spectra as a function of time are shown in Figure 36(a). The expected bathochromic shift of the absorption maximum, λ_{max}

corresponding to the $\pi - \pi^*$ when going from the initial solution state to the final solid state is clearly observed in Figure 36(a). In addition to the λ_{max} of 520 nm in the solid state, two low energy vibronic peaks at ca. 560 nm and ca. 610 nm, which have been previously attributed to increased molecular order in the P3HT film[83] are also observed. Thus the evolution of the three principle peaks reported above are expected to throw light on the evolution of the film microstructure as solvent evaporates from the sessile droplet.

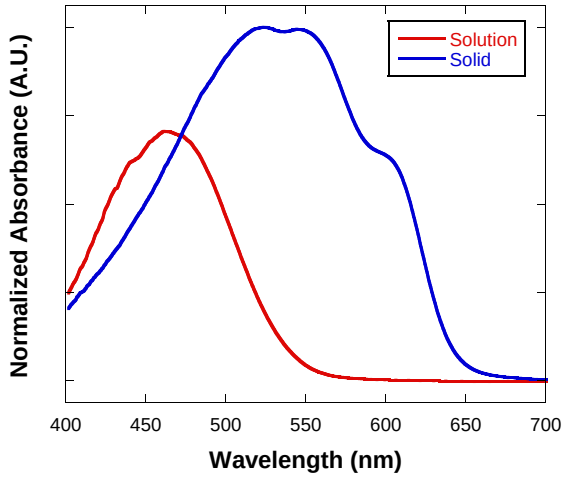

(a)

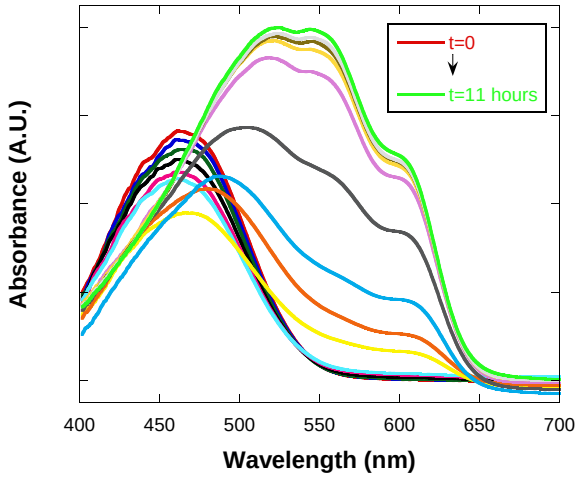

(b)

Figure 36: (a) Optical absorption spectra immediately after depositing the regioregular P3HT solution and the fully dried P3HT film (b) the time evolution of absorption spectra after the deposition. The spectra were measured every 30 minutes.

As mentioned earlier, the presence of the vibronic features is indicative of enhanced crystallinity and thus we can use that as index of the evolving crystallinity. Notably, from Figure 36(b) the intensity of the absorption band with the maximum at ca. 460 nm continuously decreases until 5 hours after deposition of the solution. In addition, the vibronic side band at 610 nm is first noticeable ca. 5.5 hours after the deposition and thus possibly represents a nascent stage of the development of molecular order within the network of the P3HT chains. Interestingly, while the λ_{max} continuously red shifts to higher wavelengths with solvent evaporation, the feature at 610 nm is invariant in position from the instance of its first appearance, Figure 36(b). A concomitant increase in the vibronic peak at 560 nm is also observed. Overall, the absorption spectra keep evolving even after the appearance of the *signatures of crystallinity* noted above (i.e., ca. 7-11 hours after the deposition), with the intensity of all absorption bands increasing gradually and red-shifting with respect to the original absorption spectrum at time t=0. The intensity and the peak positions appear to stabilize roughly 7 hours after depositing the solution. It should be noted here that the absorption spectra were recorded independent of both the *in situ* Raman as well as the drain current measurements. Thus, although we expect the qualitative trend of phase transitions (derived from absorption spectra) to prevail, we cannnot correlate the time scales at which they occur with similar deductions from Raman spectroscopy.

2.3.4 Discussion

2.3.4.1 Phase transitions in the evaporating sessile P3HT droplet

In section 2.2, we already demonstrated that the continuous removal of solvent from an evaporating P3HT droplet leads to successive phase transitions.[62] This can be rationalized by the fact that the P3HT chains undergo continuous conformational changes as the evaporating solvent forces isolated chains into supramolecular assemblies where inter-chain interactions begin to compete with intra-chain ordering (i.e. conjugation).

The absorption spectra in Figures 36(a),36(b) show a clear bathochromic shift of the $\pi - \pi^*$ transition indicative of an *evolving* extension of the main chain conjugation.[84] Moreover, the continuous decrease of the frequency (red-shift) of the C=C vibration in Figure 35 suggests that the conjugation is continuously extended with time until ca. 1050 min after the deposition. We have already demonstrated the presence of a lyotropic liquid crystalline phase in the course of solvent evaporation. Thus, it is feasible to expect the evolution of the absorption spectra to reflect the presence of an intermediate ordered phase before the formation of the fully dried polycrystalline film. This is also supported by the the absence of a distinct isosbestic point in the absorption spectra, implying the presence of a multiphase morphology which is consistent with the intermediate phase we have suggested.[85]

A closer examination of the absorption spectra reveals the time scales at which phase transitions possibly occur. For example, the absorption maximum decreases continuously after deposition of the solution for a period of 5 hours with no associated changes in either the peak position (ca. 460 nm) or the peak width, ruling out any conformational changes within that time period. Instead, we suggest that the initial intensity decrease is purely due to a drop in concentration of the solute due to the outward flow of the solution. It is well known that when a solution droplet is deposited onto a solid surface, solvent evaporation is highest at the very edge of the droplet thus creating a concentration gradient that drives solution from the center to replenish the evaporating solvent at the edge.[65] This picture is consistent with the observation of decreasing intensity of the absorption maximum in the absorption spectra. On the other hand, the advent and the increase in intensity of vibronic transitions at 610 nm (5.5-6.5 hours after the deposition) indicate that considerable inter-chain interactions exist and the extent of these interactions grow as solvent evaporates before the formation of crystalline domains in P3HT film.[83]

It is interesting to note that the evolution of UV-visible spectra via solvent evaporation is analogous to thermochromic transitions observed in poly(3-alkylthiophene)s (P3ATs). Yang et al. interpreted the continuous blue-shift of the absorption maximum as a result of conversion of the crystalline phase into a disordered phase via a quasi-ordered intermediate phase.[85] A similar quasi-ordered phase has also been reported by Zerbi et al.[86] and Tashiro et al.[87], in which the inter-annular bond on the individual conjugated segments that form the phase, experience partial twisting of adjacent thienyls, but the degree of twist is insufficient to completely disrupt the intra-molecular ordering into a coiled conformation. As the name suggests, the degree of ordering within a qausi-ordered phase is lower than in an ordered phase, where the degree of intra-molecular disorder is minimized. The continuous evolution of the absorption maximum indicative of evolving conjugation lengths is consistent with a transition from a disordered (isotropic solution) to the ordered phase (fully dried film) through an intermediate quasi-ordered phase. This is further validated by the absence of a distinct isosbestic point, which would be present in the absence of a multi-phase morphology.[85]

The analysis of the absorption spectra provides a strong foundation to further our understanding of the phase transitions that are clearly active in an evaporating droplet. A detailed analysis of the Raman spectra is expected to augment the picture we have already formed using absorption spectroscopy. In following section, we will integrate our analysis of the spectral analyses (Raman as well as UV-Vis) and discuss the correlation between the evolution of the drain current and the microstructural changes of P3HT before and after the formation of crystalline domains (as determined by Raman spectroscopy, Figure 32(c)).

2.3.4.2 Evolution of structure and the evolution of the drain current: is there a correlation?

It is conceivable that the solvent would play a crucial role in dictating the evolution of the polymer chain conformations, especially given reports that the presence of the solvent can lower the glass transition temperature of the polymer,[67,68] allowing for sufficient mobility of the chains with the capacity to influence the microstructure. In fact, Figure 32(a) shows the presence of solvent (evidenced by the non-zero relative intensity of the Raman peak for the solvent) in the film at the instant when the drain current starts to increase sharply (moment A in Figure 32(b)). The sufficient mobility of the polymer chains (due to the presence of the solvent) also possibly explains why the Raman spectrum exhibits characteristic features for non-crystalline state of P3HT (weak and blurry peaks) at moment A. The non-crystalline state prevails up to moment B, beyond which we could not distinguish the solvent peaks from that of the background noise. It is surprising that the increase in drain current (moment A to moment B) occurs even though the Raman detects no signs of a crystalline phase, especially given the intimate correlation between microstructure and charge transport in organic semiconductors. However, given the high P3HT solution concentration at point A (very low amount of solvent detected by Raman), it is possible that the threshold concentration required to form a highly conductive pathway has been achieved, while at the same time the evolving inter-chain distances (because of increasing number of P3HT chains in a given area/volume) may not have reached the the threshold to induce sufficient crystallinity that can be detected by the Raman technique.

As discussed above, we have established that the sharp onset of the drain current cannot be ascribed to to the development of crystallinity since that takes place at a much later stage in the evaporation process (from point B to C in Figures 32(a) and 32(c)). This result supports the premise that the abrupt increase in drain current

is associated with a non-crystalline state. It is noteworthy that this non-crystalline state can either be a high-concentration isotropic solution state or a lyotropic liquid crystalline (LC) phase. Failure to detect evidence for a LC phase in the simultaneous measurements of the evolution of the Raman spectra and drain current is because P3HT in solution undergoes a phase transition from an isotropic solution state to a LC phase at a critical concentration, and experimentally, it was not possible to match the area of droplet which is beyond a critical concentration in the solution state with the channel area of the two-contact device.

Interestingly, even beyond crystallization of the film (point C), further changes are detected by Raman. Judging by the rapidly increasing Raman intensity (see Figures 34 and 35) from moment B to moment C, we suggest that P3HT chains nucleate, resulting in formation of well-defined crystalline domains around point C. This is supported by a careful examination of the evolving Raman peaks between points B and C. Figure 37 shows peak shape analysis for the Raman spectrum obtained at (B+30) secs and at the moment C. Interestingly, the shape of the C=C stretching mode at point (B+30) (at ca. 1450 cm^{-1}) appears asymmetric and in fact can be decomposed into two peaks (Figure 37, whereas the peak at and after moment C exhibits a relatively symmetric shape. Both bands decomposed in Figure 37, one at ca. 1463 cm^{-1} and the other at ca. 1446 cm^{-1}, are attributed to C=C stretching mode in thiophene ring, but result from C=C stretching in different ordered phases. The Raman peak at ca. 1463 cm^{-1} can be attributed to C=C stretching mode in a less ordered phase and that from more ordered crystalline-like domains is located at a lower wave number (ca. 1446 cm^{-1}), as verified by other researchers using resonance Raman spectroscopy.[74,88,89] The asymmetric peak shape prior to crystallization at point C can be rationalized by the presence of a near equal contribution to the Raman peak from both the nucleated crystallites (at ca. 1446 cm^{-1}) and non-crystalline regions of the film (at ca. 1460 cm^{-1}). However, with further evaporation time, the

asymmetry is lost as the peak at 1446 cm^{-1} intensifies, probably due to an increase in nucleation density of P3HT crystallites. Even beyond point C, the C=C peak intensity keeps increasing gradually up to the maximum (around point D), which may be a consequence of slow increase of structural order as well as the increase of domain size due to a rapidly diminishing residual solvent content in the film. Although most solvent is lost by evaporation when crystallization occurs, there must be a small quantity of solvent that is retained in the P3HT film, which imparts limited mobility for the P3HT chains to slowly reorganize. Revisiting Figure 32(b), we can see that although the drain current increases from point A onwards in a continuous fashion, we can bifurcate the current evolution into three regions, i.e, A-B, B-C, and C-D, based on that fact that each region is associated with a different current-time slope. Especially, the rate of increase in drain current is the highest between B and C. This observation is possibly a result of the phase transitions described above.

All in all, we suggest that there exists a strong correlation between the evolution of the polymer chain conformation as well as the nucleation and formation of crystalline assemblies and the drain current. The disorder to order transition proceeds through an intermediate quasi-ordered phase beyond which the conjugation length continues to increase promoting the formation of an increased number of crystallites. The behavior can also in part account for the mobility vs time data reported in Section 2.1, Figure 25(d). We hypothesize that the observed variation in P3HT four contact mobility is associated with relaxation of P3HT polymer chains in the film assisted by solvent retained close to the SiO_2 substrate. It is possible that the formation of an intermediate lyotropic liquid crystalline phase that is characterized by anisotropic ordering of P3HT chains over a macroscopic area is responsible for this mobility profile. This intermediate phase was found to last for several hours before transitioning into a solid state consisting of nano-scale crystalline domains associated with a concurrent loss of long range order. Thus, it may be possible that the increase in four contact

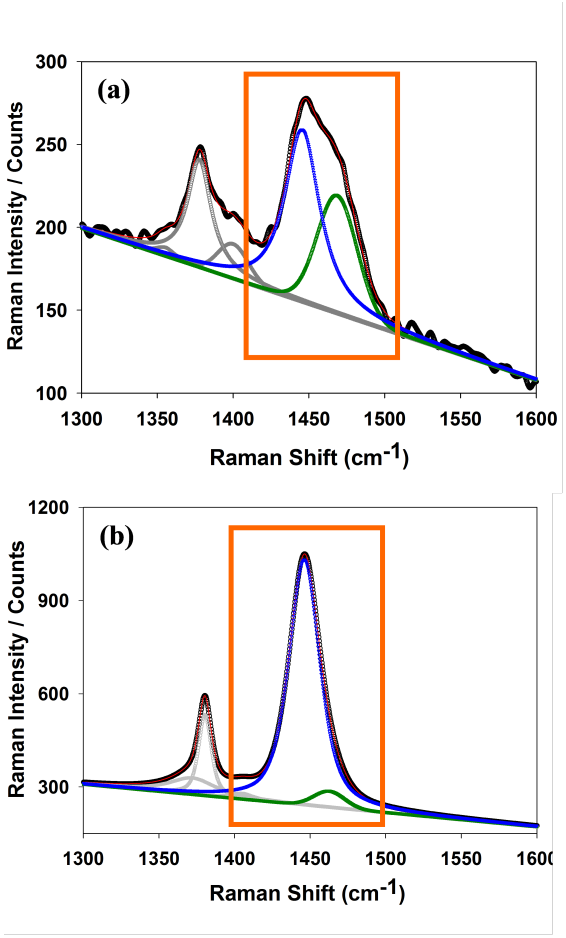

Figure 37: Fitting results for peaks around 1300-1550 cm^{-1} in Raman spectra measured (a) at the moment of B+30 seconds and (b) at the moment of C. The blue and green plots are attributed to C=C stretching mode of P3HT in less ordered and highly ordered states respectively.

mobility leading to the peak mobility observed in Figure 25(d) is due to the presence of an intermediate anisotropic phase which is followed by loss of macroscopic ordering and concomitant decrease in mobility. Although not measured for P3HT/chloroform, we suggest that similar transitions, although significantly accelerated due to rapid solvent evaporation, occur in those cases as well, resulting in a peak mobility being reproducibly observed.

2.3.5 Conclusion

We elucidated how the P3HT chains behave and structural order evolves in a sessile evaporating droplet of P3HT in solution. We believe that clarification of the mechanism of conducting channel formation will open new avenues for tailoring the chain conformation and degree of $\pi - \pi$ interactions for various applications. Our observations also point directly to advantages that will emanate from the incorporation of LC characteristics into π-conjugated semiconducting polymers. Liquid crystallinity may emerge as a necessary design feature for solution processed semiconducting polymers and related processes where the as deposited thin polymer films have the requisite morphology for efficient charge transfer and high mobility. imperative for the development of viable flexible electronic device fabrication methodologies is the need to elucidate the relevance of drying kinetics to the structural changes for association of conducting polymers with each other, which critically affects the conformation of polymer chains, the stacking geometry, and electronic performance.

CHAPTER III

A DRAMATIC EFFECT OF REGIOREGULARITY ON THE NANOSTRUCTURE AND CHARGE TRANSPORT IN P3HT

3.1 Introduction

Although a strong correlation exists between charge transport and microstructure and the degree of crystallinity in OSC thin films, the presence of disorder leads to a very complex correlation between the two. Moreover, the roles of order across length scales ranging from the nano-scale to the macro-scale remains vague. Clarification of the roles of *intra* and *inter*-chain effects is expected to a lead to a significantly improved understanding of how structural order controls macroscopic charge transport that operates in OFETs. In this chapter we explore how single chain effects can induce changes in intra as well as inter-chain ordering.

It is known that the attractive properties of conjugated polymers are somewhat offset by their relatively poor charge transport properties, since large free energy barriers to crystallization[56] inevitably lead to a structurally inhomogeneous system. Conjugated polymer thin films are thus typically composed of ordered crystallites embedded in a largely amorphous matrix,[90] and charge hopping between transport sites is significantly impeded by disorder.[22,30] In such variegated systems, identifying the exact individual roles of intra-chain, inter-chain and inter-grain charge transport in determining the macroscopic field effect mobility becomes a substantial challenge.[90,91] Much of the research in the area of conjugated polymers has thus focused on understanding and suppressing the effects of structural disorder on charge transport

through "controlled" supramolecular self-assembly, either through improved molecular design[45,92] or by exploiting solvent-solute-substrate interactions.[47,53,93] Specifically, the molecular weight (MW)[51,52,94] and regioregularity (RR),[49,95] defined as the percentage of head-tail (H-T) attachment of side chains in regiochemical diads (see Figure 17 in Chapter 1), have been identified as key molecular parameters that control thin film microstructure and thus charge delocalization in P3HT. In essence, both parameters are intricately linked, in that they both directly influence single chain properties and hence multi-chain assemblies.

An understanding of the effects of MW forms a useful platform to elucidate the role of RR. Although a multitude of theories, all unified by the observation of a significant increase in field effect mobility with MW, have been reported to explain the effects of increasing chain length on macroscopic charge transport in P3HT films,[51,52,94,96] questions remain regarding the etiology of this phenomenon. Kline et.al.[52,97] proposed two plausible explanations for the observed increase in mobility: longer chains in high MW P3HT (i) facilitate a net reduction in inter-chain hopping events as intramolecular charge transport through longer conjugated segments becomes facile[98] and (ii) act as charge transport conduits connecting crystalline domains separated by low conductivity amorphous grain boundaries.[90] Alternatively, Zen et.al.[51] and Chang et.al.[94] have ascribed the mobility increase to improved intermolecular transport, resulting from either reduced distortion of the conjugated backbone or fewer chain defects within individual grains. Early work of Bredas et.al. shows that deviations from backbone co-planarity can have detrimental consequences for the electronic properties in conjugated systems leading to the limiting case of near vanishing bandwidths (BWs) for bithiophene having a 90 dihedral angle.[99] The presence of alkyl substituents, required to solubilize the intractable main chain, only serve to amplify the effect.[100,101] Such effects are also manifest through the reduction of the RR of the polymer.[49,95] A higher percentage of sterically demanding head-head (H-H)

substituents result in significant loss of backbone planarity through the formation of conformational defects or "twistons"[102]- kinks in the delocalization pathway of charge carriers that lead to loss of conjugation.[98] Although the effect of RR on the microstructure and charge transport in P3HT films is documented,[49] the subtlety of the effect remains open to question. While Sirringhaus et.al. showed that a ca. 15% difference in RR can lead to a hundred fold increase in field effect mobility,[49] Kim et.al. demonstrated that even a mere 5% difference is sufficient to significantly alter the performance of bulk heterojunction solar cells.[95] However, a precise evaluation of the relationship between mobility and RR has not been presented, and an exploration of the impact of this relationship in the context of P3HT film microstructure and in-plane charge transport using a field effect transistor (FET) geometry is still missing. Developing an understanding of the level of significance RR plays in allowing polymer chains to assemble into nano- and micro-structures is essential for identification of design rules for high performance polymer based semiconductors.

In this chapter, we seek to understand how subtle differences in RR of the hexyl side chains in P3HT can influence the supramolecular assembly of polymer chains when deposited from the solution state, and subsequent thin film properties. We demonstrate that differences in RR as small as ca. 4% can, surprisingly, result in dramatic variations in field effect mobilities by as much as two orders of magnitude. The differences in the electronic absorption spectra, which are analyzed in light of Spano's model,[103] are consistent with the spectral signatures of enhanced intrachain order in higher RR P3HT. The observed morphological differences are in agreement with the photophysical changes, and also point to an increase in the conjugation length of the polymer chain, resulting in nanofibrillar structures that are consistently wider for the higher RR variant. Moreover, the difference in mobility between the two P3HT samples persist even when comparing the results obtained from films that are spin coated from solvents that differ by as much as ca. 120 in their boiling point

(BP), suggesting that RR has an overriding influence on charge transport. These data provide clear evidence that RR must be considered with great care when optimizing charge transport in solution processed conjugated polymer films. Furthermore, the results of this study highlight the importance of intra-chain vs inter-chain effects.

3.2 Experimental Procedures

3.2.1 Materials

Regioregular P3HT (P100 and P200 Sepiolid: referred to as HT94 and HT98 P3HT from here on) used for the study was purchased from Rieke Metals, Inc. and used without further purification. The molecular weight and regioregularity of both samples are summarized in Table 1. All the solvents used in the study were anhydrous (except for benzyl chloride) and purchased from Sigma Aldrich and used without any further purification.

Table 1: Molecular weight and regioregularity of the P3HT samples used

P3HT Sample	**Molecular Weight (kDa)**		**Regioregularity**
	M_N	M_W	%H-T
P100 (HT94)	19.7	42	92-94
P200 (HT98)	12.7	23	98

The MW data were obtained through gel permeation chromatography (GPC) of the polymer samples in tetrahydrofuran solution. A Waters 1515 Isocratic high performance liquid chromatography system with a Waters 2489 UV/Vis detector, fitted with a Styragel HR 5E column was used. MW data were determined using polystyrene standards. Polymer regioregularity was estimated from the ^{1}H NMR spectra obtained from deuterated chloroform solution at 293 K using a Bruker DSX 300.

3.2.2 Organic FET (OFET) fabrication and characterization

The FET devices used for electrical characterization consisted of two contact devices where P3HT films were prepared via spin coating the relevant polymer solution onto

a 300 nm thick SiO2 gate dielectric. The highly doped silicon wafer served as the gate electrode while Au/Cr was used for the source and drain contacts. The source and drain contacts were fabricated using a standard photolithography based lift-off process, followed by E-beam evaporation (CVC Inc.) of 50 nm Au contacts with 5 nm of Cr as the adhesion layer. Before spin coating P3HT solutions, all devices were cleaned for 15 minutes in a UV-Ozone cleaner (Novascan PSD-UV) to ensure complete removal of any residual photoresist and other organic contaminants. At the end of the cleaning process, the substrates were hydrophilic. The solutions used for fabricating the OFETs were prepared in a nitrogen glove-box (<1 ppm of moisture and oxygen) by dissolving P3HT in either chloroform (CHCl3), p-xylene, chlorobenzene (MCB) or benzyl chloride (BCl) as solvent at ca. 50°-160°C (depending on the boiling point of the solvent) with stirring. The solution concentrations were between 4-6 mg/mL. Solutions in BCl, a very poor solvent for P3HT at room temperature, were prepared at a lower concentration (ca. 2.5 mg/mL) in order to prevent precipitation during spin coating. In addition, because of the tendency of P3HT to aggregate in poor solvent systems, solutions of P100 and P200 in both p-xylene and BCl were spin coated from hot solution (ca. 110°C and ca. 160°C, respectively) onto room temperature substrates. It should be noted that the solubility of P100 in all solvents examined here was higher compared to that of P200 because of its lower regioregularity. P3HT film thickness varied between ca. 8 nm to ca. 30 nm for films obtained from BCl and CHCl3 solutions, respectively.

OFETs were prepared by spin coating the solutions onto pre-cleaned substrates at a spin speed of 1500 rpm and were tested in a nitrogen environment without any further treatment. An Agilent 4155C semiconductor parameter analyzer was used for the measurements. Although thermal annealing was not performed, the devices were stored in the glove-box for several hours prior to testing to minimize the effect of residual solvent on the electrical properties. The field effect mobility was calculated

in the linear region of transistor operation (V_{D}=-3 V) by plotting the drain current (I_{D}) versus gate voltage (V_{G}) and fitting the data to the following equation[104]:

$$I_D = \mu C_{ox} \frac{W}{L} (V_G - V_T) V_D \tag{16}$$

Where V_{T} is the threshold voltage, W and L are the transistor channel width and length respectively and C_{ox} is the capacitance per unit area of the silicon dioxide gate dielectric=$1.15 \times 10^{-8} F\mathrm{cm}^{-2}$.

3.2.3 UV-Vis spectra of P3HT

The solution and solid state UV-Vis spectra were obtained using an Agilent 8510 Spectrophotometer. Films for solid state studies were spin coated onto pre-cleaned glass slides.

3.2.4 Grazing Incidence X-Ray diffraction (GIXD)

Out-of-plane grazing incidence X-ray diffraction data were obtained using a Panalytical X'Pert Pro system equipped with a Cu X-ray source operating at 45 kV and 40 mA. Grazing incidence angle was fixed at 1°and the detector was scanned from 3°to 20°. Peak positions were obtained from the measured profiles by fitting the peaks using the analysis software (MDI JADE). Samples for GIXD measurements were prepared by spin coating P3HT/$CHCl_3$ solutions (with and without ultrasonic irradiation) on hydrophilic silicon substrates with native oxide that were cleaned using the same procedure used for bottom contact FET substrates.

3.2.5 Atomic Force Microscopy (AFM) studies of P3HT

The AFM measurements were performed on films spin coated on bare silicon dioxide substrates, with a Veeco Digital Instruments Dimension 3100 scanning probe microscope in tapping mode with a silicon tip (NSC 14, Mikromasch).

3.3 Field-Effect Mobility

That subtle differences in regioregularity have a dramatic effect on the charge transport properties of P3HT OFETs is apparent from Figure 38(a), which shows the field effect mobility for HT94 and HT98 films spin coated from various solvents onto bottom contact substrates (see experimental procedures). The transfer and output characteristics are typical of p-channel OFET operation in the accumulation mode, Figures 38(b) and 38(c). The high turn-on voltages (V_{ON}) obtained, as seen from the semi-log plot in Figure 38(b), are attributed to the effects of residual doping and/or acceptor-like traps at the P3HT-oxide interface.[105,106] This is especially likely given the absence of both thermal annealing which is believed to "de-dope" the semiconductor film,[55] as well as passivation of hydroxyl groups (generated due to the UV-ozone treatment of the substrates) that can act as charge traps.[107] Additional experiments show that there is indeed a large reduction in V_{ON} when using a combination of thermal annealing and semiconductor-dielectric modification, Figure 38(d). However, both treatments were avoided in the current analysis in order not to obscure the effect of RR. The mobility values are calculated from the linear region of transistor operation (V_D =-3V) by fitting the slope of the drain current (I_D) versus gate voltage (V_G) curve, as shown in Figure 38(b), with each data point corresponding to the average mobility value extracted from at least three transistors.

Different solvents are employed, both to investigate the effects of solvent-solute interactions on the final microstructure of the polymer film, as well as to confirm that the effect of RR is not particular to any one solution system. In all cases, a significant difference in the field effect mobility between HT94 and HT98 films is observed reproducibly, ranging from $3.3\pm2.3 \times 10^{-3}$ $cm^2V^{-1}s^{-1}$ to $1.6\pm0.48 \times 10^{-2}$ $cm^2V^{-1}s^{-1}$ and $5.2\pm1.79 \times 10^{-4}$ $cm^2V^{-1}s^{-1}$ to $2.3\pm1.4 \times 10^{-2}$ $cm^2V^{-1}s^{-1}$ for films obtained from spin coated polymer solutions in $CHCl_3$ and MCB respectively. These variations are consistent with the results of Sirringhaus et.al., who reported a two order

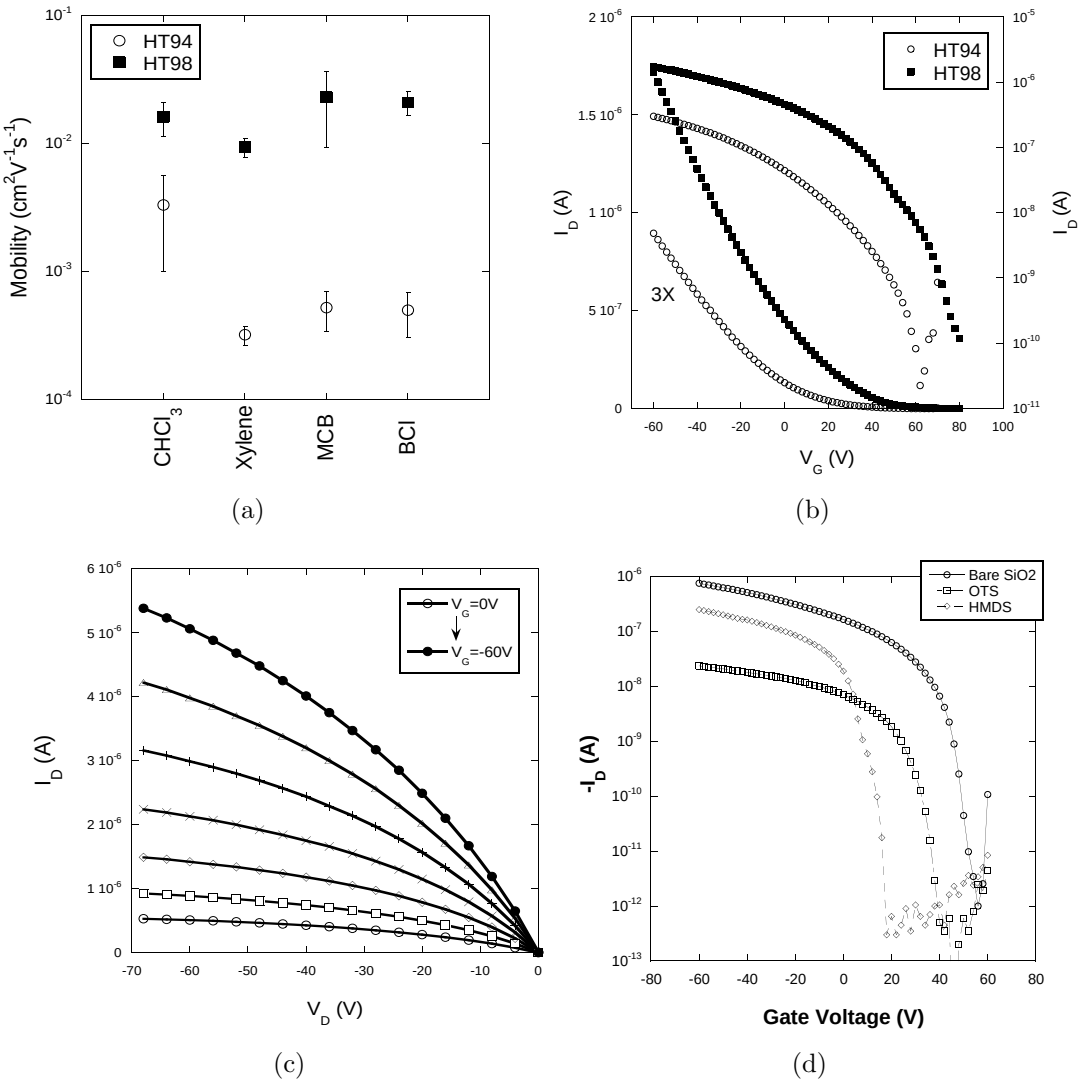

Figure 38: (a) Average field effect mobilities obtained from ca. 92% (open circles) and 96% (filled squares) regioregular P3HT from various solvents. Mobilities were calculated in the linear region of operation with V_D = -3V. (b) Transfer characteristics of P3HT OFETs spin coated from chloroform solutions. The transfer curve for HT94 P3HT has been magnified for clarity. (c) Typical output characteristics obtained from 92% regioregular P3HT OFET spin coated from chloroform solution. All measurements were performed in a nitrogen glove-box. (d) Transfer characteristics of HT98 OFETs obtained by spin coating from solutions in chloroform on substrates with (i) no modification and (ii) modified with OTS and HMDS. All the devices were annealed at 100°C in a nitrogen glove-box for a period of ca. 10 hrs.

of magnitude difference in field effect mobility in P3HT OFETs, albeit for a significantly higher difference (ca. 15%) in RR.[49] For a given RR, only minor variations are observed upon changing the solvent environment, except for the anomalous case

of HT94 in $CHCl_3$, which routinely exhibits a mobility that is an order of magnitude higher than that obtained from the three other solvents and significantly, is relatively close to that of HT98 obtained from $CHCl_3$ solution ($3.3\pm2.3 \times 10^{-3}$ $cm^2V^{-1}s^{-1}$ in HT94 vs $1.6\pm0.48 \times 10^{-2}$ $cm^2V^{-1}s^{-1}$ in HT98). Contrary to earlier reports, a strict correlation between mobility and solvent BP is not observed,[46] evidenced by the fact that the highest mobility for HT94 OFETs is observed for films obtained from CHCl3, in spite of BCl having a boiling point that is higher by ca. 120. It must be noted that although significant thickness variations (ca. 8 nm to ca. 30 nm) were obtained depending upon the solvent used (see experimental section), the minor variations in mobility observed for the HT98 films is evidence that the thickness of the films does not play a vital role in dictating charge transport and is consistent with the presence of an ultrathin accumulation layer.[36] In addition, while GPC data does reveal a substantial difference in MW between HT94 (M_N =19.7 kDa) and HT98 (M_N =12.7 kDa), which could potentially override the influence of RR, given well established reports that mobility increases with M_W,[51,52] and that $\mu_{HT98} > \mu_{HT94}$ (=field effect mobility) in spite of the lower MW of HT98 P3HT, our observations can be isolated to the effect of RR alone.

3.4 Absorption Spectroscopy

The effect of RR is multifaceted. As mentioned earlier, torsions induced along the conjugated backbone because of increased regiorandom character can lead to disruption of intrachain charge transport,[98,99] while the absence of steric twisting leads to improved crystalline quality.[45,96] Distinct features in the electronic absorption spectra of P3HT films are representative of the extent of molecular order, as initially suggested by Sundberg and co-workers[108] and later reaffirmed by Brown et.al.,[83] and thus should, in theory, be able to capture the microstructural differences expected from the above arguments. This view is supported by the absorption spectra obtained

from thin films of HT94 and HT98, as shown in Figures 39(a) and 39(b). The higher RR HT98 films are characterized by the appearance of well resolved fine structure, ascribed to the presence of crystallinity in the films,[108] appearing as "humps" flanking either side of the (0-1) transition-features which are clearly suppressed in the lower RR HT94 films. In addition, the absorption bandwidths are also different, with the narrowing of the absorption band in HT98 films relative to that in HT94 films, obtained from the full width at half maximum of the band, varying between ca. 0.11 eV and ca. 0.26 eV for films obtained from MCB (Figure 39(c)) and BCl respectively. The observed band broadening in HT94 films is likely due to the presence of a multitude of sterically motivated conformers in the lower RR chains resulting in disorder.[109] The intensity of the (0-0) transition, reproducibly observed at ca. 2.08 eV for all films, in particular, appears especially sensitive to the RR of the polymer, and thus represents an index of molecular order in the film.[83] This is consistent with the proposition of Clark et.al. who suggested that the distribution of ordered and disordered phases in P3HT films is actually reflected in low and high energy components of the absorption spectrum respectively.[110] Furthermore, the crystalline regions are thought to be composed of weakly coupled lamellar aggregates in which interchain interactions lead to the formation of an excitonic band, with a bandwidth (W), which according to Spano's model (Equation 17) is directly related to the ratio of the (0-0) and (0-1) peak intensities and the phonon mode coupled to the electronic transition (Ep 0.18 eV).[103]

$$\frac{I_a^{0-0}}{I_a^{0-1}} \approx \frac{(1 - 0.24W/\omega_0)^2}{(1 + 0.073W/\omega_0)^2} \tag{17}$$

I_{0-0} and I_{0-1} are the intensities of the (0-0) and (0-1) transitions respectively. Spano's model is insightful since it provides a quantitative estimate of the free exciton bandwidth, which in turn strongly correlates with the conjugation length of individual polymer chains (and thus intrachain ordering) through the interchain excitonic

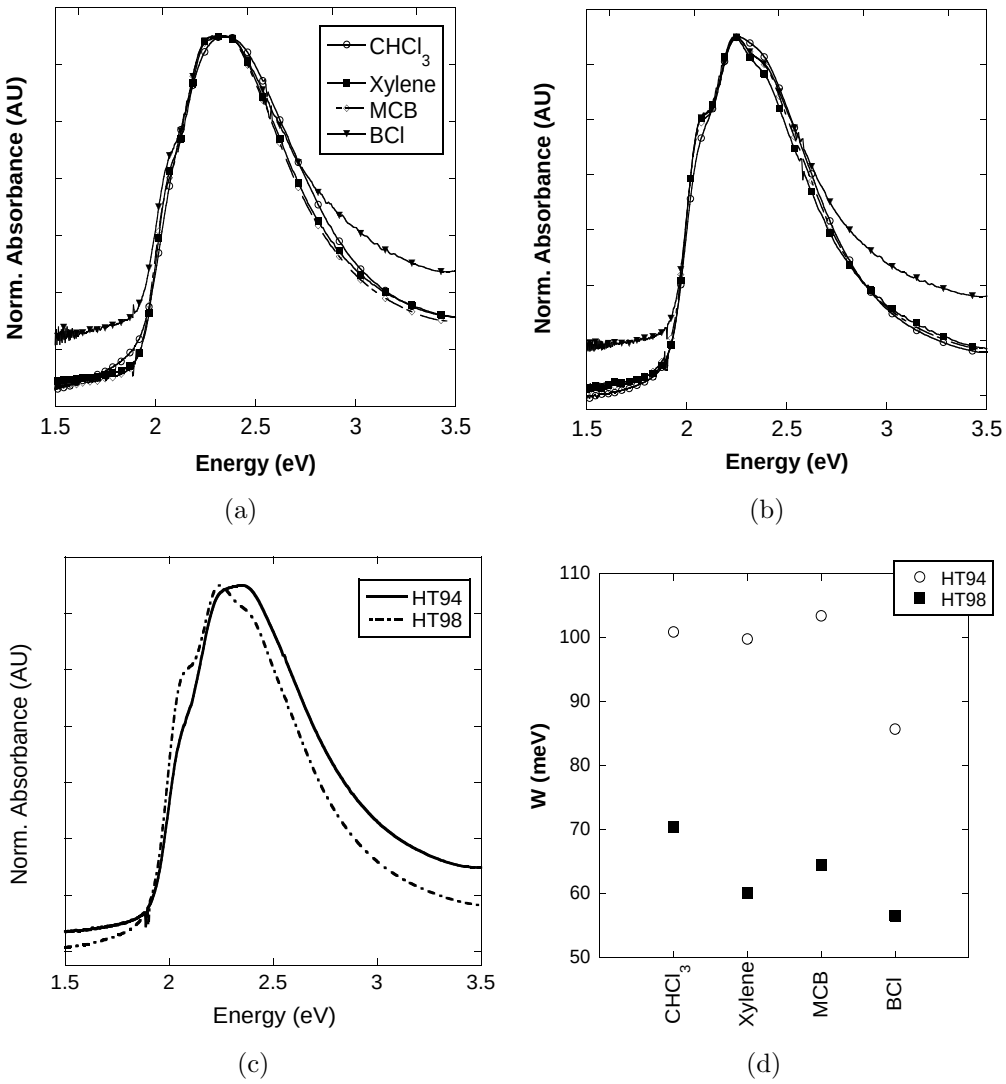

Figure 39: Normalized solid state absorption spectra of P3HT films processed on glass slides from different solvents using (a) HT94 and (b) HT98 P3HT. (c) comparison between the HT94 and HT98 P3HT films obtained from MCB.(d) Free exciton bandwidth (W) calculated using Spano's model.

coupling J (W=4J).[103,111] Applying Spano's model to our experimental absorption data reveals differences in W, Figure 39(d), that are in agreement with enhanced main chain planarization, given that the excitonic coupling decays significantly with extension of π conjugation.[111] The W values calculated represent the average of measurements taken from two different films. Although differences between HT94 and HT98 dominate our observations, W is also found to vary slightly as a function of the

solvent used for a given RR. As with the mobility, the spectroscopic evidence indicates no strict dependence of W (and thus J) on the solvent BP, although it assumes the lowest value for both, HT94 and HT98 films obtained from BCl (BP $\sim$ 179 C). However, we suggest instead that this apparent enhancement of intrachain ordering is borne out of solubility effects and may not be related to the BP of the solvent used (vide infra). Nevertheless, given that the extent of intrachain ordering in HT98 is the least for films obtained from $CHCl_3$, it might be subtle evidence of a competitive mechanism for chain ordering between the effects of BP and RR, the latter strongly influencing the solubility of the polymer as well. It is possible that the lower RR, and thus greater steric barrier, in HT94 might prevent the manifestation of solvent BP effects, explaining the relatively flat profile for W observed in Figure 39(d). Films obtained from BCl are a clear exception, routinely exhibiting the lowest exciton BW for both HT94 and HT98, thus seemingly pointing at a role of solvent BP But this anomaly is addressed by noting that films obtained by spin coating a solution of HT98 in p-xylene (BP$\sim$ 138 C), a relatively poor solvent for P3HT, that has been allowed to cool down to room temperature for several hours prior to spin coating exhibits an exciton BW of 20 meV, a value that is significantly lower than that for films obtained by spin coating the hot solution (W=60 meV), Figure 40. Clark et.al. have reported similar values for the free exciton BW in P3HT films obtained from isodurene (BP$\sim$198 C), also a poor solvent.[110] The role of solubility in the formation of ordered π stacked precursors in P3HT solutions is well documented,[112,113] and it is plausible that the facile $\pi - \pi$ associations are a result of enhanced main chain planarization predicted by the low exciton BW. A similar phenomenon is expected to prevail in BCl solutions as well, explaining the exciton BW minima observed.

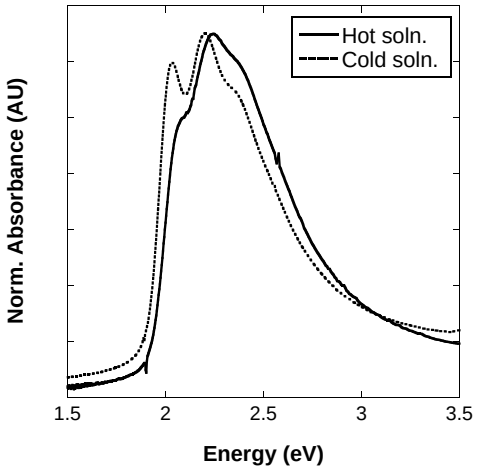

Figure 40: Solid state UV-Vis spectra obtained by spin coating from (i) hot (solid line) and (ii) cooled down (dashed line) solutions of HT98 in xylene on to pre-cleaned glass slides.

3.5 Investigation of morphological changes

The increased conjugation length observed for HT98 is clearly a result of a greater resistance to chain tortuosity and it is conceivable that the morphology of the films would reflect this change in the configurational character of individual polymer chains. In fact, the AFM phase images do indeed reflect the changes associated with an increased RR as shown in Figure 41. As expected,[46] films obtained by spin coating P3HT from $CHCl_3$ solutions are featureless, irrespective of the RR, as shown from representative scans in Figure 41a. Films obtained for both polymer systems from other solvents however, show mesoscale features in the form of nanofibrillar structures that are randomly distributed throughout the scan area.

Closer examination of the images reveals distinct differences in the nanofibril widths of HT94 and HT98 films obtained from xylene, MCB and BCl solution. An analysis of the nanofibril dimensions is revealing, the results of which are summarized in Figure 42(a). The ca. 4% difference in RR leads to nanofibril widths that, surprisingly, vary by as much as 84 $\mathring{A}$ in the case of films obtained from xylene, Figure 41(b). It must however be noted that the nanofibrillar widths are very sensitive to

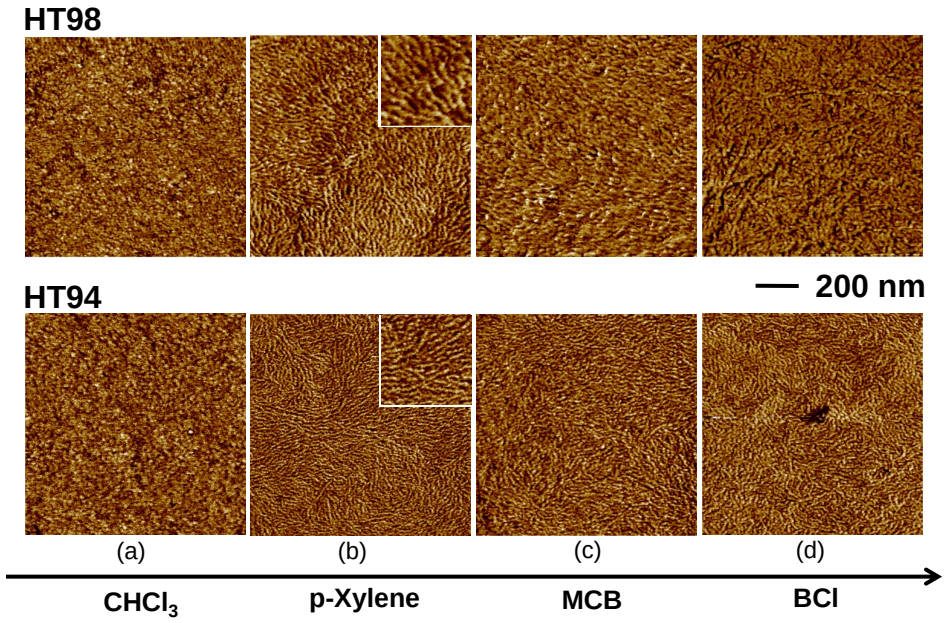

Figure 41: Tapping mode AFM phase images of HT94 and HT98 P3HT films obtained by spin coating from (a) chloroform (b) p-xylene (c) chlorobenzene (d) benzyl chloride. The insets in (b) show the respective magnified images (250 nm × 250 nm)

the processing conditions. This is especially true in the case of BCl and xylene which are relatively poor solvents, and minor variations in both solution concentration and temperature can impact nanofibril width. Nevertheless, differences in the widths between HT94 and HT98 films are observed reproducibly, with the actual value varying between a minimum of ca. 43 $\mathring{A}$ to a maximum of ca. 84 $\mathring{A}$. As before, the effect of solvent is minimal in comparison to that of RR.

3.6 Implications for packing of polymer chains

That the increase in nanofiber width is coincident with the increase in conjugation length when going from HT94 to HT98 is useful for understanding the packing geometry of the P3HT chains within individual nanofibers. Barford's model predicts that for parallel chains with lengths larger than the separation between them, the excitonic coupling J varies as $L^{-1.8}$, where L is the chain length.[114] We can thus obtain an effective conjugation length ($L_{EFF,BARFORD}$), defined as the ratio of conjugation

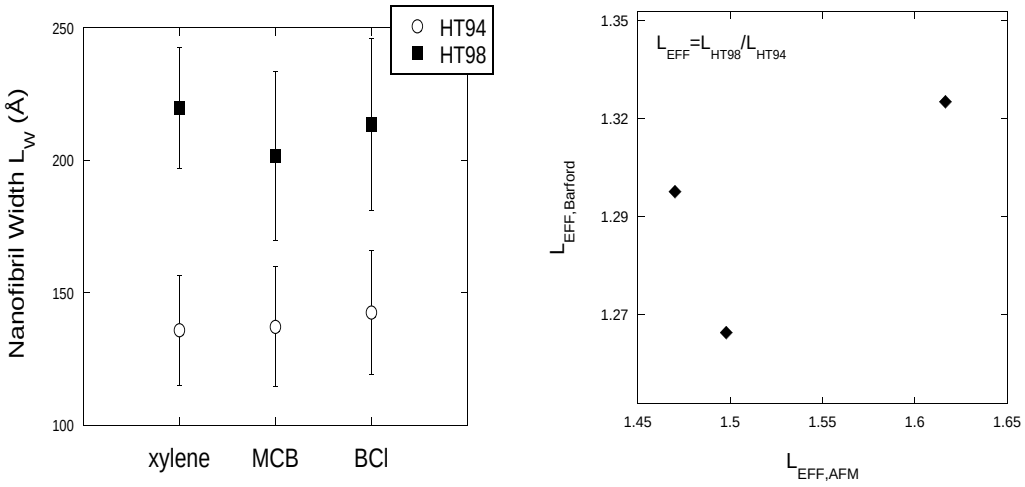

Figure 42: (a) Nanofibril widths obtained from a size analysis of the AFM phase images shown in Figure 41. (b) Comparison of the effective nanofibril width (L_{EFF}) obtained from experiment ($L_{EFF(AFM)}$) and from theory ($L_{EFF(Barford)}$)

lengths in HT98 and HT94, by combining Barford's model with Spano's model, using the exciton coupling integrals obtained from the latter. As shown in Figure 42(b), these values are in close proximity to the effective nanofiber width ($L_{EFF,AFM}$), defined as the ratio of nanofiber widths in HT98 and HT94 films obtained from the AFM phase images, ascribing the increase in conjugation and nanofiber width to a common phenomenon: enhanced main chain planarization in HT98. *Moreover, it proves conclusively that the microstructure of the P3HT films is strongly coupled with features observed in the absorption spectra.* With this information, the packing within each fiber can thus be envisaged as consisting of lamellar stacks of P3HT with the nanofiber axis coincident with the $\pi-\pi$ stacking axis, as has been suggested by others in whiskers of P3HT.[115] Such a packing motif has implications for the conformation of individual polymer chains as well. A comparison with the number average contour lengths of P3HT chains in HT94 and HT98 (ca. 450 $\mathring{A}$ and 280 respectively), estimated from the MW data, hints at the presence of chain folding given that the nanofiber widths are significantly lower than the contour lengths.[115] Moreover, this

marks a substantially larger departure from full extension in the case of HT94 (ca. 300 $\mathring{A}$) than for HT98 (ca. 70 $\mathring{A}$), a result made especially intriguing by the fact that it emanates from a mere 4% difference in RR. However, caution must be exercised in such an analysis since the accuracy of the GPC data hinges on knowledge of the conformational flexibility of P3HT chains in solution, which remains a subject of debate.[116,117]

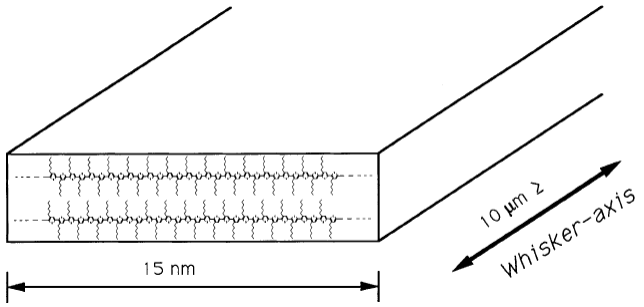

Figure 43: Molecular arrangement of polymer chains within a P3HT nanofiber. Obtained from Ihn et.al.[115]

3.7 Impact on thin film crystallinity[1]

The increased planar assembly of HT98 chains is expected to provide improved opportunities for intermolecular interactions, which in theory, should lead to higher crystallinity of the films.[45] Figure 44, which shows the x-ray diffractograms obtained from GIXD measurements of the P3HT films, appears to support this notion at first glance. The (100) peak appears relatively more intense in all the HT98 films, with the exception of the one obtained from BCl, indicative of better crystal packing within the nanofibers for the higher RR polymer. Although the (100) peaks in both polymer films obtained from $CHCl_3$ solution remain weak, a difference in peak intensities between HT94 and HT98 can be noticed in spite of the kinetically limiting film formation mechanism in the volatile solvent. Subtle differences in RR can thus

[1] ***GIXD scans were performed in collaboration with Dr. Jung-Il Hong, MSE, Georgia Tech***

overcome the barriers to crystallization imposed by the rapid quenching of polymer chains. Increases in the crystallinity of films spin coated from xylene, MCB and BCl are apparent, but as noted earlier, given the sharp increase in (100) peak intensity for HT98-MCB, followed by a dramatic drop in the case in the case of HT98-BCl, the effect cannot be reduced to that of solvent BP. It must be mentioned here that although reproducibility tests conducted to confirm the GIXD results reveal that peak intensities obtained from each film differ across two sets of experiments, a result that is ascribed to the sensitivity of the microstructure to the processing conditions noted earlier, the relative intensities between HT94 and HT98 are preserved. Specifically, the (100) peak intensity is reproducibly the highest for HT98 films obtained from MCB and significantly higher than those obtained from BCl. Surprisingly, although HT98 films appear more crystalline than HT94 films in general, this is clearly not the case for the films obtained from BCl. Based on the AFM results, it can be expected that wider nanofibrils in HT98 would result in a greater areal fraction of ordered structures which is mirrored in the XRD peak intensities, but there appears to be no evidence for the anomalous behavior in the case of BCl. The physical origins of this behavior are not completely understood, but it is possible that solubility effects may be responsible for altering the internal ordering within the nanofibers, without inhibiting their tendency to form in the first place.

3.8 Discussion

In our study, we have shown that a subtle difference in RR can induce changes at the single molecule level (i.e. conjugation); as well as morphological changes associated with assemblies of the polymer chains (i.e. nanofibrils) on the one hand, and in the macroscopic electrical properties on the other. The one to two order of magnitude increase in field effect mobility associated with wider nanofibrils in the higher RR HT98

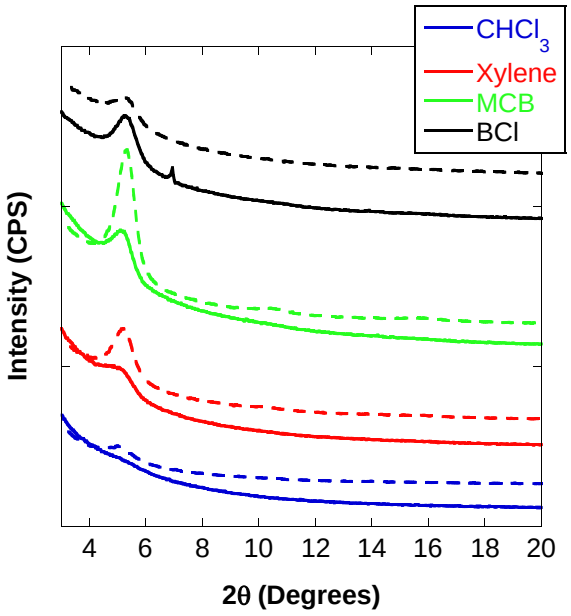

Figure 44: Grazing incidence X-Ray diffraction profiles of HT94 (solid lines) and HT98 (dashed lines) films obtained by spin-coating from different solvents.

films bears a resemblance to the effects of increasing MW, which thus forms an important precedent for our results.[51,52,94,96] Interestingly, the various hypotheses that have so far been proposed to explain the MW dependence of mobility can essentially be reduced to single chain effects,[51,52,94,96] which can also be expected from variations in RR. As pointed out earlier, this is manifested as either elongated chains that bridge ordered domains,[52] an extended conjugated state that may have important consequences for the hopping rate of charge carriers,[94] or simply through improved crystal packing that supports enhanced polaron delocalization between chains.[96] The results discussed here also imply that the origin of the improvement in charge transport properties can be assigned to an improvement in any one (or combinations) of intra-chain, inter-chain and inter-grain charge transport.

Although we concede that given the finite molecular dimensions of the polymer chains, coupled with the fact that the conjugation is actually limited to shorter oligomeric segments (most likely because of conformational disorder), intrachain charge

transport is highly unlikely to *dominate* the movement of carriers over tens of micrometers (i.e. in an OFET geometry), its participation nevertheless, cannot be entirely ruled out. In fact, our coincident observations of enhanced mobility and intrachain order justifies revisiting the role of intrachain charge transport in the determination of macroscopic mobilities. This view is also supported by studies on isolated polythiophene "molecular wires" using pulse radiolysis microwave conductivity (PRMC) measurements (as discussed in the Introduction section), that have yielded mobilities as high as 0.02 $cm^2V^{-1}s^{-1}$,[118] similar to values obtained from "bulk" films from our OFET experiments involving HT98 films. Grozema et.al. have further reported that even higher intrachain mobilities can be observed by reducing the number of torsional defects that impede orbital overlap between neighboring monomeric units.[98] Kline et.al. have argued that even though interchain delocalization maybe the primary mechanism of charge transport, longer chains with lower conjugation defects allow for facile intrachain delocalization, thus providing charge carriers with ample opportunities for hopping between chains.[52] This could, at least in part, account for the differences in mobility observed between HT94 and HT98 films. This observation can also explain why variations in mobility as a function of solvent are relatively minor, since the differences in exciton BW across solvents (for a given RR) is at least half that observed for differences in RR (for a given solvent).

There are further, potentially profound implications to the increased conjugation. It is well known that the process of charge hopping between adjacent polymer chains can be cast into the framework of the Marcus-Hush theory for electron-transfer reactions, with the hopping rate at a given temperature governed by a combination of the internal reorganization energy (λ) that accompanies the charge transfer, and the electronic coupling matrix element, Equation 5.[28,29,119,120] This would imply that in systems with comparable electronic coupling between adjacent segments, a decrease in λ would lead to lower reorganization energy barriers and thus a substantial increase

in the charge hopping rate (assuming self-localized polaron effects are absent[120]). HT98 chains, which show an extension of the conjugation relative to HT94, would represent such a scenario,[120] which could, in theory, contribute to the enhanced mobilities observed in HT98. In addition, because of the exponential dependence of the hopping rate on λ, the latter would exert a dominating influence, superseding the effect of intermolecular electronic coupling.[120] This is verified by the results of Zhang et.al. who have reported an exponential dependence of the mobility on the width of nanofibers with increasing MW, suggesting that extended conjugated states indeed have a dominating influence on macroscopic charge transport.[94] Interestingly, when applying the model derived by Zhang using the maximum difference in nanofiber widths we observed (ca. 84 $\AA$), we obtain calculated mobilities that are very close to the ones determined experimentally for HT98 (ca. 8.2×10^{-3} $cm^2V^{-1}s^{-1}$ compared to an average experimental value of 1.77×10^{-2} $cm^2V^{-1}s^{-1}$). Based on the variations in nanofiber widths we reported earlier, although the model is unlikely to be a foolproof explanation for all our mobility data, it does provide useful insight into the role of conjugation. Importantly, the role of intrachain ordering is not relegated to influencing intrachain transport alone, but it clearly influences the interchain hopping rate as well.

In the absence of tests that probe intrinsic charge transport along a chain (i.e. a molecular wire), it is a substantial challenge to isolate the role of intrachain order. This challenge is compounded by the fact that the improvement in single chain order simultaneously results in supramolecular assemblies with improved crystal quality,[96] which in turn would impact the interchain transfer integral.[22] Our out-of-plane (OOP) GIXD data reflect this apparent improvement in crystalline order in HT98 films, characterized by the higher degree of lamellar packing as well as a narrowing of the absorption bandwidth. However, this result alone cannot form a holistic explanation for the differences in mobility observed between HT94 and HT98 films.

For example, the large difference in (100) peak intensity, along with a concomitant increase in mobility from 5.2±1.79 × 10^{-4} $cm^2V^{-1}s^{-1}$ to 2.3±1.37 × 10^{-2} $cm^2V^{-1}s^{-1}$ for HT94 and HT98 films obtained from MCB would form a strong case for the degree of crystallinity being a dominant influence on the transport of charges. But results from films obtained from other solvents clearly argue against such an assessment, further justifying our use of different solvents in clarifying the microstructure-charge transport correlation. This is apparent in the case of films obtained from $CHCl_3$ (μ_{HT94}=3.3±2.3× 10^{-3} $cm^2V^{-1}s^{-1}$ while μ_{HT98}=1.6±0.7× 10^{-2} $cm^2V^{-1}s^{-1}$) and BCl (μ_{HT94}=4.9±1.9× 10^{-4} $cm^2V^{-1}s^{-1}$ while μ_{HT98}=2.1±0.4× 10^{-2} $cm^2V^{-1}s^{-1}$), where the differences in mobility between HT94 and HT98 OFETs are clearly incommensurate with the changes registered by the respective diffractograms. This is especially apparent for films obtained from BCl, where the difference in (100) peak intensities between HT94 and HT98 films are almost negligible. In addition, the weak and broad peak in the case of HT94 films obtained from $CHCl_3$ would be completely unexpected given that these films routinely exhibit the highest mobility amongst HT94 OFETs. This observation is consistent with results that demonstrate an intense (100) peak in low MW P3HT films compared to a relatively weak peak in the high MW variant, although the latter, remarkably, has a mobility that is four orders of magnitude higher.[52] In a separate study, we identified two distinct regions of charge transport in P3HT films, characterized by an initial sharp increase in the mobility by two orders of magnitude due to an increase in crystallinity up to the percolation limit, followed by a gradual saturation where the mobility becomes independent of the degree of crystallinity.[93] This is further evidence that the film crystallinity is clearly not a dominant factor in dictating charge transport. Other factors, such as structural anisotropy and textural variations are likely to influence charge transport as well.[96] The RR of P3HT has been purported to influence the texture of the corresponding films, with 81% and 96% RR P3HT adopting the so called "face-on" and "edge-on"

orientations respectively, and with the latter configuration being more favorable for in-plane charge transport.[49] Although the AFM phase images do not directly reflect the crystallinity of the films, they do provide contrast between the nanofibrils, which we suggest are the ordered segments, and the amorphous grain boundaries surrounding them. The wider nanofibrils obtained from HT98 films should thus result in fewer grain boundaries that are known to impede charge transport,[121] while simultaneously improving the crystallinity of the film. Macroscopic charge transport would then require charges to travel across regions of low (grain boundaries) and relatively high (nanofibers) conductivity, with the effective mobility a simple harmonic mean of the mobilities within the grains and at the grain boundaries.[121]

The results presented here also raise critical questions about the role of conjugation in macromolecular systems. Although Spano's model predicts, albeit indirectly, improved packing motifs in HT98 P3HT (motivated by enhanced intrachain order) with higher interchain transfer integrals,[103] recent theoretical analysis conducted by Gierschner et.al. has shown that the transfer integrals in polymeric systems are actually near independent of the conjugation length,[122] in apparent contradiction with the above argument. Instead, this might imply that the enhanced interchain hopping is a consequence of reduced reorganization energies afforded by the extended conjugation in HT98 chains. Thus, we suggest that the dramatic difference in field effect mobility observed as a result of the minor increase in RR can be narrowed to two primary effects: (i) an increase in hopping rate due to reduced reorganization energies predicted by Marcus theory and (ii) a reduction in the number of grain boundaries as a result of wider nanofibrils. In essence, both effects are a direct consequence of enhanced conjugation and thus strongly coupled with the RR of the polymer.

3.9 Conclusion

We have demonstrated that the changes in H-T attachments of hexyl side chains to the polythiophene backbone by as little as 4% can have a dramatic impact on the field effect mobility in P3HT thin films. The effect of solvent BP is found to be minimal in comparison to that of RR, which has an overriding influence on the microstructure and the field effect mobility. More importantly, RR provides an effective handle for interrogating single chain effects, which can be multifaceted, on the structural and electronic properties of supramolecular assemblies. Thus, a fundamental understanding of polymer chain conformation will not only provide avenues for maximizing charge transport in polymeric semiconductors, but must also be considered carefully in the design of the next generation of polymeric semiconductors. In addition, the correlations we have reported may be useful in advancing our still evolving understanding of the complex correlations between microstructure and macroscopic charge transport in conjugated polymer systems.

CHAPTER IV

TUNABLE CRYSTALLINITY IN P3HT AND ITS IMPACT ON CHARGE TRANSPORT[1]

4.1 Introduction

It has long been established that the successful technological application of electroactive polymers hinges on the ability to manipulate their π-conjugated architecture.[123,124] This is especially true for solution processable organic semiconductors, such as poly(3-alkylthiophene)s (PATs), which consist of a conjugated aromatic backbone and solubilizing alkyl side chains. The contrasting nature of the backbone and side chains provides avenues to control the properties of solutions of these polymers,[112,125,126] with the opportunity to influence the microstructure of thin films prepared from these solutions.[126,127] Given the importance of microstructure on the intermolecular charge transport in films of conjugated polymers, this suggests the potential to enhance the conducting properties of these thin films through modification of the molecular structure and the way in which the solutions are processed. P3HT has been extensively studied due to its excellent hole transporting properties, resulting in mobilities as high as 0.1 $cm^2V^{-1}s^{-1}$,[6,49] which is close to that of amorphous silicon. This four order of magnitude improvement in mobility over that reported in the first study of PAT-based organic field effect transistors (OFETs)[42] has been achieved through a combination of improved molecular design,[101,128] increasing the polymer molecular weight (MW)[52] and tuning various process parameters such as the solvent boiling point, film deposition method (drop casting versus spin coating), and modifying the semiconductor-dielectric interface,[46,47,53,58,77,129] all of which directly

[1] ***ADV. FUNC. MATER. 2011, 21, 2652.***

impact the self organization of the polymer into ordered supramolecular assemblies.

Solution processable semiconducting polymers generally assemble into polycrystalline thin films in which the charge transport process through the length of the transistor channel requires the charges to move across multiple ordered domains embedded in an amorphous matrix.[33,130] This is especially true of high MW polymers that are formed under rapid film formation conditions such that the long polymer chains are kinetically impeded from organizing into ordered structures.[46] Thus, the coexistence of ordered and disordered domains implies that charge transport would be strongly dependant on the nature of both regions,[33] with the molecular packing structure, film texture, and the degree of crystallinity all contributing to the electronic properties of the polymer film.[49,77,130]

A number of techniques have been explored to manipulate the properties of thin films of PATs, with the regioregularity of the polymers (i.e., the relative placement of side chains along the backbone)[49] and molecular weight[52] being dominant factors in inducing changes in structural and charge transporting properties. Sirringhaus et al. demonstrated a strong influence of the regioregularity of P3HT on the textural anisotropy of spin coated films, with highly regioregular materials yielding mobilities which are two orders of magnitude higher than regiorandom polymers.[49] Increasing the molecular weight of highly regioregular (98% head-tail) polymer results in an increase in mobility: high MW ($M_{\mathrm{W}} = 62$ kDa) P3HT has a mobility that is roughly four orders of magnitude higher than that of the low MW ($M_{\mathrm{W}} = 4.4$ kDa) polymer, in spite of the latter having a higher crystallinity.[52] While Kline et al. have argued that this increase in mobility is due to both, better interconnectivity between isotropic nodules and a longer chain length facilitating intramolecular transport in high MW films,[52] Zen et al. hypothesize that low MW ($M_{\mathrm{W}} = 3.15$ kDa, regioregularity not mentioned) films are characterized by a larger distortion of the conjugated backbone that has a significant impact on interchain interactions, thus lowering the mobility.[51]

Sirringhaus et.al. have explored the role of the degree of crystallinity in high MW P3HT ($M_W = 37$ K, regioregularity 98%) films. The use of high boiling point solvents in spin casting films of these polymers promotes the formation of ordered structures that facilitate facile charge transport.[46] Yang et al. have also shown that the use of different solvents influences the film crystallinity and has a strong impact on the thin film morphology and mobilities, but that there is not a direct correlation with boiling point.[59] Thus, although the structures of P3HT films have been explored in detail, the roles of the degree of crystallinity and morphological factors in controlling charge transport remain unclear, especially in the absence of techniques to tune the thin film microstructure without either changing the MW or the solvent.

In this chapter, we report a strong correlation between the degree of crystallinity and the corresponding charge transport properties of films of a high MW (M_W = ca. 48 kDa) regioregular (92-94%) P3HT by systematically varying its microstructure using ultrasonic irradiation of the polymer solution. A percolation-type mechanism is proposed for charge transport in these materials that are obtained under kinetically limiting, rapid film forming conditions. The spectroscopic evidence supports the ultrasound-induced formation of microcrystallites in solution which are otherwise absent in pristine, non-irradiated solutions. We suggest that the ultrasonication facilitates the assembly of the high MW polymer chains which do not have an inherent tendency to organize into ordered structures either in solution or under rapid film formation conditions. The ultrasound induced crystallinity evolves as a function of irradiation time and leads to an initial sharp increase in the field effect mobility by two orders of magnitude, and eventually saturating at ca. 10^{-2} $cm^2V^{-1}s^{-1}$. The behavior suggests percolation type conductivity. This ultrasonication of polymer solutions prior to film fabrication represents a facile approach to achieving high mobility P3HT OFETs, but also allows for elucidation of the important role of the degree of thin film crystallinity in controlling charge transport. Moreover, keeping the properties of

the polymer (molecular weight and regioregularity) and the solvent fixed, this study leads to an independent analysis of the effects of microcrystallinity.

4.2 Experimental Procedures

4.2.0.1 Materials

The P3HT was purchased from Sigma Aldrich (catalog no. 445703) and used without any further purification. This had a measured M_{N} of 24 kDa and M_{W} of 47.7 kDa (from GPC in tetrahydrofuran calibrated with polystyrene standards using a Waters 1515 Isocratic HPLC system with a Waters 2489 UV/Vis detector, using a Styragel HR 5E column. All data were processed with the Breeze 2 software) and a head to tail regioregularity of 92-94% (as estimated from the ^{1}H NMR spectrum which were recorded using a Bruker DSX 300 in deuterated $CHCl_3$ at 293 K). HPLC grade $CHCl_3$, also purchased from Sigma Aldrich, was used as the primary solvent. Regiorandom P3HT was also purchased from Sigma Aldrich (catalog no. 510823).

4.2.0.2 OFET fabrication and characterization

The FET devices used for electrical characterization consisted of two contact devices where P3HT films are spin coated on 200 nm thick SiO_2 gate dielectric. The highly doped silicon wafer served as the gate electrode while Au/Cr was used for the source and drain contacts. The source and drain contacts were fabricated using a standard photolithography based lift-off process followed by E-beam evaporation of 40 nm Au contacts with 3 nm of Cr as the adhesion layer. Before spin coating P3HT solutions, all the devices were cleaned in piranha solution (4 parts sulfuric acid:1 part hydrogen peroxide) to ensure complete removal of any residual photoresist and other organic contaminants, followed by cleaning with acetone, isopropanol and deionized water in an ultrasound cleaning bath. At the end of the cleaning process, the substrates were hydrophilic. The substrates were then dried on a contact hot plate at 150 °C for about 30 minutes. The solutions used for making field effect transistors were

prepared in air, by dissolving the P3HT in $CHCl_3$ (ca. 4 mg/mL) at ca. 50 °C with stirring. A table top ultrasonic cleaner (Bransonic 2510, 40 kHz, 130 W) was used for ultrasonic irradiation of the solutions. The solutions were prepared and ultrasonicated in sealed glass vials to prevent solvent evaporation. To test for solvent evaporation, an experiment was also conducted using pure $CHCl_3$ without P3HT. Upon heating 3 mL of the solvent for a period of 25-30 mins followed by ultrasonic irradiation for 5 mins, the reduction in solvent volume was ca. 0.1 mL, which included solvent loss when transferring it from the vial into the measuring cylinder. Hence, a significant change in concentration over the 10 min irradiation period is not expected. OFETs were prepared by spin coating the solutions onto the pre-cleaned substrates and tested in air without any further treatment using an Agilent 4155C semiconductor parameter analyzer. The field effect mobility was calculated in the linear region of transistor operation (V_{D}=-3 V) by plotting the drain current (I_{D}) versus the gate voltage (V_{G}) and fitting the data to the following equation[104]

$$I_D = \mu C_{ox} \frac{W}{L} (V_G - V_T) V_D \tag{18}$$

Where V_{T} is the threshold voltage, W and L are the transistor channel width and length respectively and C_{ox} is the capacitance per unit area of the silicon dioxide gate dielectric=$1.72 \times 10^{-8} F\mathrm{cm}^{-2}$. Caution must be exercised when studying the role of irradiation time, since there are variations in ultrasound intensity across the ultrasound bath and therefore between experiments. Although irradiation intensity is a more appropriate index, time is used here in the absence of quantification of the ultrasound intensity. Thus, a single batch of the solution was sequentially irradiated to obtain consistent results within a single set of experiments. The experimental data was fit to a quadratic function for the data up to 3 mins of ultrasonic irradiation. While only an approximate fit, this does provide a visual guideline to depict the trend in the mobility as a function of time, which is reproducible.

4.2.0.3 UV-Vis spectra of P3HT

The solution and solid state UV-Vis spectra were obtained using an Agilent 8510 Spectrophotometer. Films for solid state studies were spin coated onto pre-cleaned glass slides.

4.2.0.4 Dynamic Light Scattering

DLS was carried out on an ALV/DLS/SLS-5022F precision goniometer system with an ALV 5000/E correlator and a He-Ne laser ($\lambda = 632.8$ nm). Cumulant analyses were performed for the measured intensity correlation functions. Apparent hydrodynamic radii, R_{H}, were calculated according to the Stokes-Einstein equation. All measurements were carried out at room temperature. The measurements were performed at a fixed scattering angle of 90°.

4.2.0.5 Grazing Incidence X-Ray diffraction (GIXD)

Out-of-plane grazing incidence X-ray diffraction data were obtained using a Panalytical X'Pert Pro system equipped with a Cu X-ray source operating at 45 kV and 40 mA. Grazing incidence angle was fixed at 1 °and the detector was scanned from 3°to 20°. Peak positions were obtained from the measured profiles by fitting the peaks using the analysis software (MDI JADE). Samples for GIXD measurements were prepared by spin coating P3HT/$CHCl_3$ solutions (with and without ultrasonic irradiation) on hydrophilic silicon substrates with native oxide that were cleaned using the same procedure used for bottom contact FET substrates.

4.2.0.6 Atomic Force Microscopy (AFM) studies of P3HT

The AFM measurements were performed on films spin coated on bare silicon dioxide substrates, with a Veeco Digital Instruments Dimension 3100 scanning probe microscope in tapping mode with a silicon tip. While a different set of solutions was used to prepare samples for AFM, the original UV-Vis spectra were used as a reference

to achieve results similar to solutions used for the OFET studies. Part of the AFM analysis was carried out using the WSxM software.[131]

4.3 Results

4.3.1 Field effect mobility measurements

Bottom contact field effect transistors were fabricated by spin coating films of P3HT from ca. 4 mg/mL chloroform ($CHCl_3$) solution in order to characterize the charge transport properties of films formed from solutions irradiated for various times. 45 shows the increase in the mobility of the films with ultrasonic irradiation time for two sets of experiments (the time scale for the sharp increase in mobility varies slightly between the two sets of data, for reasons noted in the experimental section). In both cases, the trend is characterized by an initial sharp increase in mobility by two orders of magnitude after short irradiation times (ca. 2×10^{-4} $cm^2V^{-1}s^{-1}$ to ca. 2.9×10^{-2} $cm^2V^{-1}s^{-1}$ after 1.5 min irradiation for experiment 1 and ca. 1.6×10^{-4} $cm^2V^{-1}s^{-1}$ to 1.4×10^{-2} $cm^2V^{-1}s^{-1}$ after 1 min irradiation for experiment 2). This is followed by an apparent saturation of the mobility within ca. 1 to 3 mins of ultrasonic irradiation for both experiments, as shown by the shaded region in 45, with slight fluctuations about the average saturated value (ca. 0.03 $cm^2V^{-1}s^{-1}$ and ca. 0.01 $cm^2V^{-1}s^{-1}$ for experiments 1 and 2, respectively). In both experiments an increase in the mobility by almost an order of magnitude is observed for an ultrasonication time of as little as 30 seconds. Such a behavior of the field effect mobility is strong evidence of a percolation type transport mechanism, which is commonly observed in composite materials consisting of carbon nanotubes or carbon black as conductive fillers in insulating polymer matrices.[132,133] Such systems are characterized by a sharp increase in the conductivity at a certain critical filler content known as the percolation threshold, beyond which there is little or no further change in conductivity on further addition of the conductive filler. Vapor deposited organic thin film transistors also exhibit

a sharp increase in charge transport characteristics once a geometric percolation between islands is established.[134] The observation of a similar electrical behavior in spin coated P3HT films, for which the film formation mechanism is significantly different from that involved in vapor deposition, suggests that the percolation behavior might also be due to the presence of multiple phases or regions, each with different charge transport characteristics, and not simply due to a geometric percolation leading to channel formation. Interestingly, the molecular weight dependence of the mobility is also characterized by an initial increase followed by an eventual saturation of the mobility value,[51,52] suggesting that similar mechanisms maybe at play in mediating charge transport in the P3HT thin films investigated.

The similarities in the mobility profiles upon ultrasonication (this work) and the modification of MW[52] supports an ultrasound induced structural change in the spin coated polymer films which has been explored using a number of techniques, as shown below. Although similar ultrasound induced changes have also been recently reported by others,[135,136] their influence on thin film mobility and the use of ultrasound in the context of understanding structure-property relations in OFETs is new to this study.

4.3.2 Visible and UV spectroscopy

46 shows the electronic absorption spectra of $CHCl_3$ solutions of P3HT that have been irradiated with ultrasound (46(a)) and of the corresponding films obtained by spin coating the solutions onto glass slides (46(b)). The solution state absorption maximum, λ_{max}, associated with the π-π^* intraband transition,[137] appears at ca. 450 nm for all solutions, irrespective of the ultrasonic irradiation times and consistent with previous investigations of regioregular head-to-tail P3HT.[138] However, two additional peaks appear at lower energies with increasing irradiation times,[135] suggestive of a vibronic structure with a 0-0 transition at ca. 610 nm and a vibronic side band at

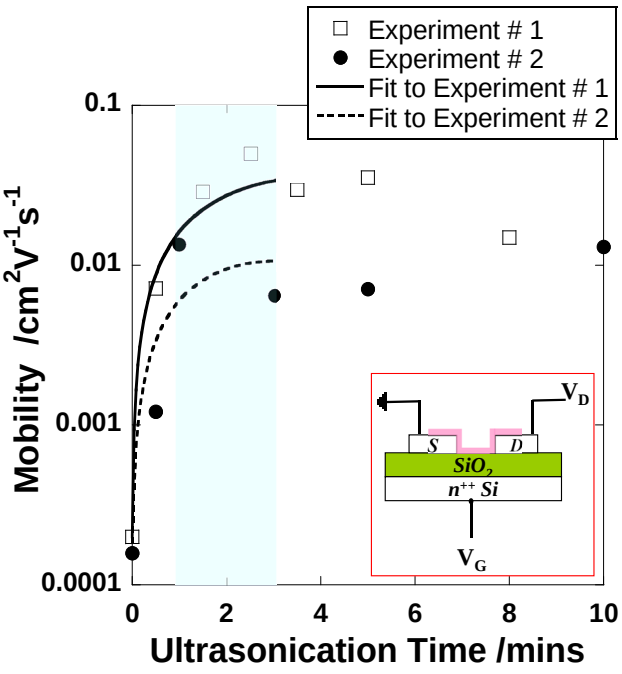

Figure 45: Evolution of field effect mobility as a function of ultrasonication time. Mobilities are calculated in the linear region of transistor operation using V_D = -3 V. Inset shows the OFET geometry used for testing. The fits are shown simply to provide a visual guideline to highlight the saturation of the field effect mobility.

ca. 570 nm respectively.[139] The appearance of these peaks is accompanied by a concomitant change in the color of the solution from bright orange to dark brown. These features are characteristic of aggregates of PATs that are formed upon the addition of a poor solvent (e.g., methanol, hexane) to solutions of the polymers in good solvents (e.g. $CHCl_3$).[112,127,140,141] This is confirmed by dynamic light scattering (DLS) experiments, which register a significant increase in the hydrodynamic radius from ca. 7 nm for pristine solutions to ca. 25 nm for solutions that have been ultrasonicated for one minute (however, reliable hydrodynamic radii could not be obtained for solutions ultrasonicated for longer times due to strong absorbance of the laser used in the DLS studies (He-Ne, 632 nm)). Similar features have also been noted in studies of the thermochromic transitions in solutions of P3HT in a variety of solvents.[139]

In addition, compared to the pristine P3HT solution, the intensity of photoluminescence decreases by 47% and 36% upon ultrasonic irradiation and upon addition of 10 vol.% methanol respectively, consistent with the formation of a π-stacked aggregate that can partially quench the polymer's luminescence, Figure 47.[142,143] Such ultrasound induced changes have been attributed to disorder-order transformations within the individual polymer chains,[135,136]with the spectral evidence consistent with the presence of the solvated (i.e., isolated) conjugated polymer and microcrystallized aggregates of the polymer.[139] The volume of the polymer solution does not change over the time period of ultrasonic irradiation due to evaporation, and hence the suggested aggregation phenomenon is not due to an increased concentration of the polymer in solution (see experimental section). The ultrasound induced spectral changes are thermally reversible, with the time taken for the restoration of the original spectral properties (as well as color of the solution) dependant on the ultrasonic irradiation time applied, Figure 50(a).

Spin coating of the polymer solutions provides thin films with the expected shift of the π-π^* transition with respect to the solution state spectra, due to increased planarity of the conjugated backbone in the solid state.[84] Unlike the spectra of the polymer solutions which have identical values of λ_{max} for the π-π^* transition before and after ultrasonic irradiation, the absorbance maximum in spectra of thin films obtained from ultrasonicated solutions is sequentially red-shifted as a function of solution irradiation time, relative to the film obtained from pristine solutions (e.g. λ_{max} = ca. 544 nm for films obtained from pristine solutions and = ca. 550 nm for films obtained from 10 min irradiated solutions). This suggests a further ultrasound induced planarization of the main chain. In addition, a weak peak begins to develop at ca. 605 nm in the spectrum of the thin films prepared from solutions that had been irradiated for at least ca. 1 min. This peak become more pronounced in the spectra of thin films that were prepared from solutions that had been ultrasonicated for longer

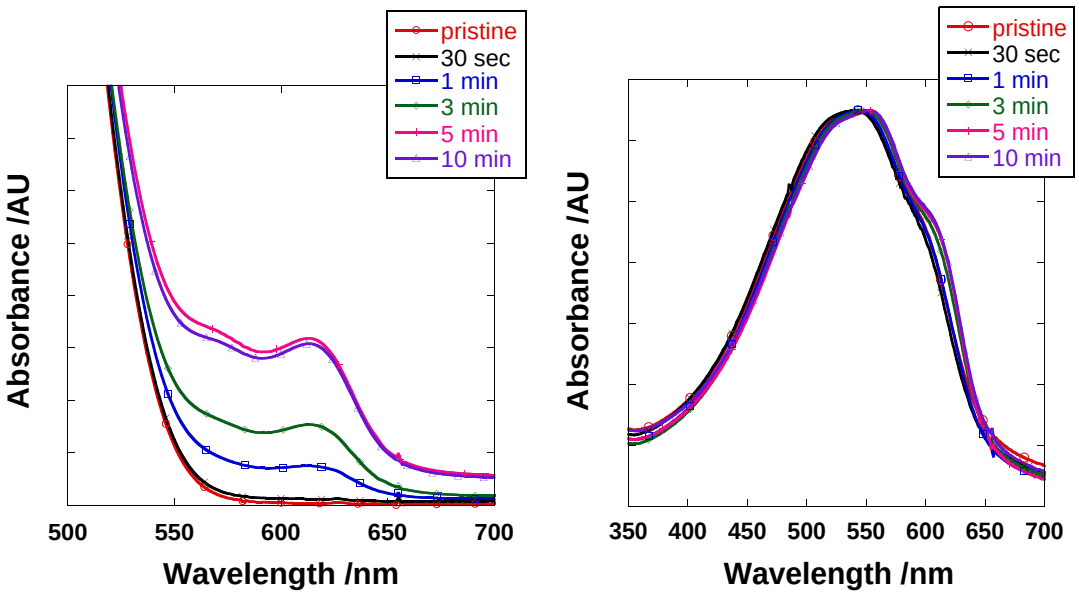

Figure 46: Normalized UV-Vis absorption spectra of (a) P3HT/$CHCl_3$ solutions as a function of solution irradiation time and (b) corresponding P3HT films obtained by spin coating. For better clarity in the solution state spectra, only the section from 500-700 nm is shown.

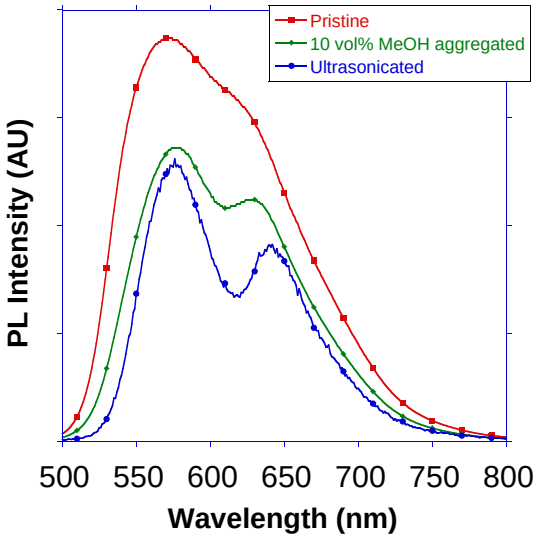

Figure 47: Photoluminescence spectra of pristine, 5 min ultrasonicated and 10 vol% MeOH aggregated P3HT/$CHCl_3$ solutions.

times. This fine structure has been attributed to an interchain absorption whose intensity is a measure of the degree of molecular order in the polymer film.[83] Thus,

it appears that the increased main chain planarization leads to improved cofacial π stacking and improved order. The close correspondence between the irradiation time dependant development of vibronic structures in the solution and the solid state is clear evidence of the formation of ordered precursors in the polymer solution that are preserved through the film-forming process.

4.3.3 Crystallinity and microstructure of thin films[2]

Out of plane grazing incidence X-ray diffraction (GIXD) of thin films of P3HT (48) reveal the dramatic effect of ultrasonic irradiation of solutions on the crystallinity of the films. An increase in irradiation time leads to a gradual increase in the intensity of the (100) peak, associated with the lamellar packing of polymer chains along the crystallographic direction perpendicular to the backbone.[123] This dramatic increase could be a result of either an increase in the size of individual crystallites, the number of crystallites, or both. Debye-Scherrer analysis of the peaks reveals that the coherence length corresponding to the interlayer packing along the ¡100¿ direction varies from 70 to 80 for films obtained from pristine and irradiated solutions (10 min), respectively. This is consistent with an increase in number of crystallites with a narrow size distribution leading to an increase in the overall crystallinity of the thin film.[46] The effect is apparent from Figure 48(b), in which a short time (ca. 1 min) irradiation of the solution leads to a quadrupling of the intensity of (100) peak, with no further increase in crystallite formation beyond 5 mins of irradiation. The microstructural change is also characterized by a simultaneous decrease in the d-spacing in the direction along the side chains, from ca. 17.6 to ca. 16.8 after 10 min of irradiation, which suggests either an increase in the overlap between side chains from neighboring lamellae or a change in the side chain tilt.[77] In agreement with the thermal reversibility of the irradiation induced changes to the UV-Vis spectra described above, thermal

[2] ***GIXD scans were performed in collaboration with Dr. Jung-Il Hong, MSE, Georgia Tech***

treatment of the ultrasonicated solutions also leads to a loss of crystallinity of the films, Figure 50(b).

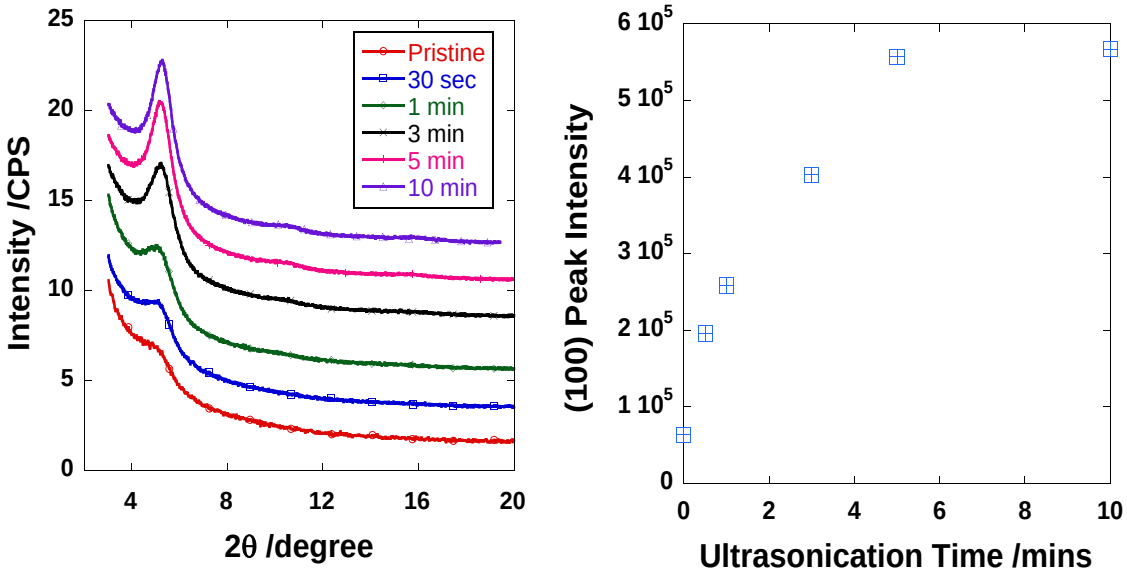

(a) (b)

Figure 48: (a). Grazing incidence X-Ray diffraction profiles and (b) (100) peak intensity of films spin-coated from P3HT/$CHCl_3$ solutions that have been ultrasonicated for sequentially longer times.

Atomic force microscopy (AFM) micrographs of P3HT films obtained from pristine and ultrasonically irradiated P3HT solutions are shown in Figure 49(a). This shows the clear evolution of a nanofibrillar morphology with increased irradiation times. In the absence of irradiation, the films show no significant signs of mesoscale structures, consistent with reports where the short time scales during spin coating from volatile solvents hinder the formation of well ordered structures,[46] although a closer examination reveals the presence of short nanofibrils embedded within a largely amorphous and featureless phase, as shown in Figure 49(b). Applying a short time (ca. 1 min) ultrasonic irradiation to the solutions leads to the formation of more distinct nanofiber-like structures that are ca. 30 nm wide with lengths ranging from 150-200 nm, with the short nanofibrillar structures and amorphous regions present

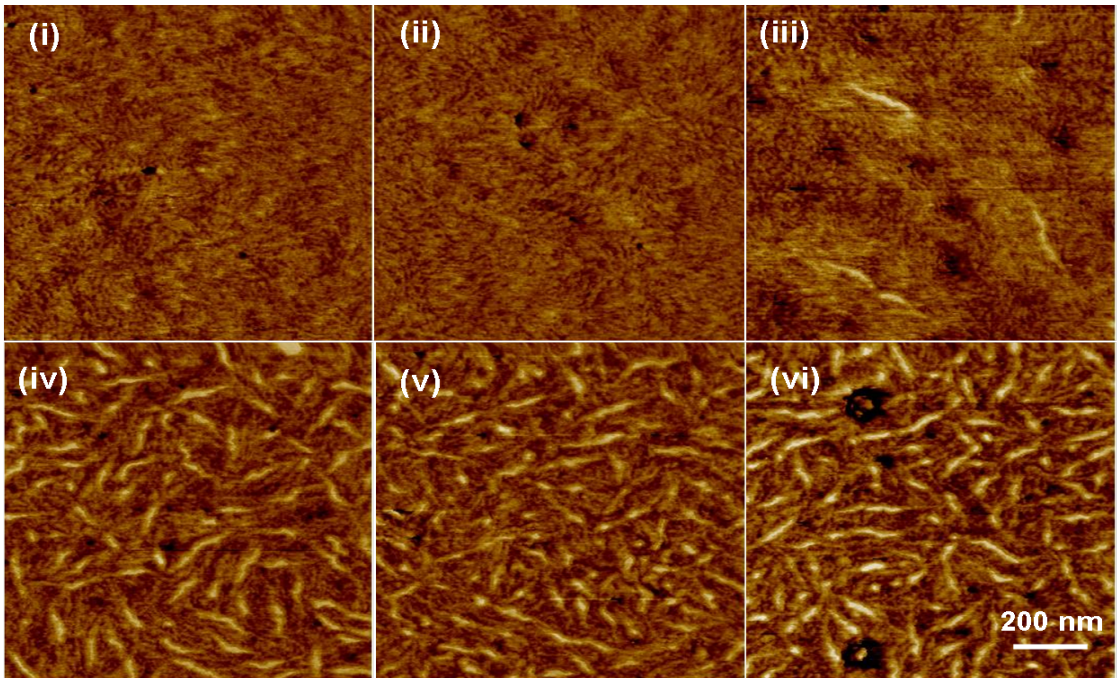

(a)

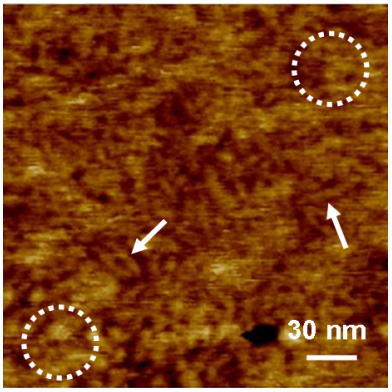

(b)

Figure 49: (a). Tapping mode AFM phase images of P3HT films obtained by spin coating from $CHCl_3$ solutions which are sequentially ultrasonically irradiated for (i) 0 mins (ii) 30 secs (iii) 1 min (iv) 3 mins (v) 5 mins and (vi) 10 mins. (b) Figure 49(a)(i) magnified. The arrows and the dotted circles indicate the presence of short nanofibrillar structures and amorphous regions respectively.

in all films irrespective of the ultrasonication time. Increasing the irradiation time leads to an increased number of nanofibers detected within the scan area, without any substantial increase in their size. Irradiation beyond 3 mins leads to no further significant changes. The presence of three phases in films obtained upon irradiation

for at least 1 min must be noted: distinct large nanofibers, smaller less distinct ones and an amorphous phase. This is in agreement with the XRD results, suggesting that the increase in the degree of crystallinity of the thin films is a direct consequence of increase in microcrystallites distributed across the films. Reports by others on ultrasonic irradiation of P3HT solutions have shown the formation of nanowires,[135,136] although, we suggest that the process is aided by the use of relatively poor solvent systems, which are conducive to the formation of the nanofibrilar morphology[127,144] even in the absence of any ultrasonic irradiation.

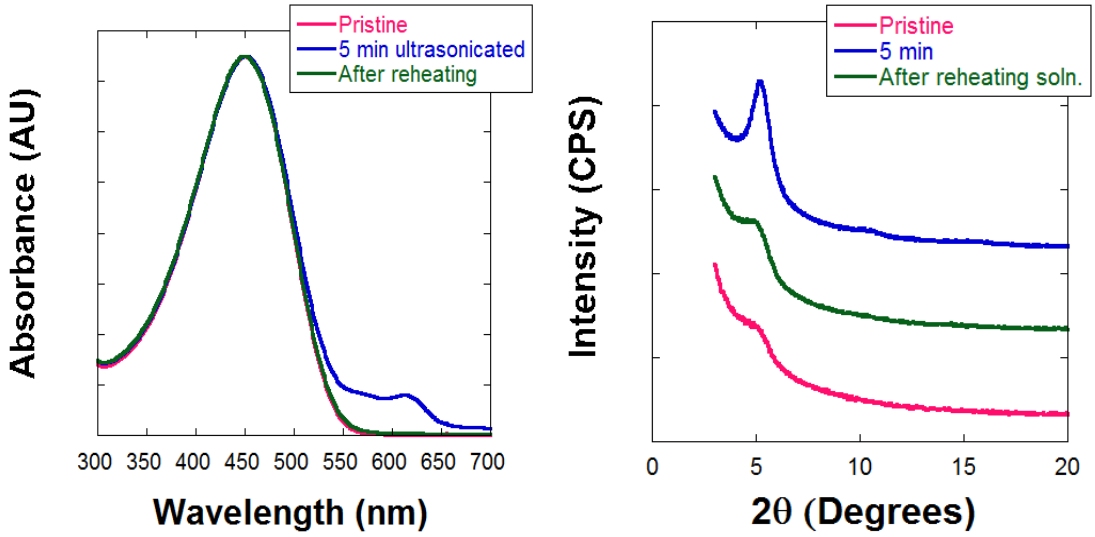

Figure 50: (a)Solution state UV-Vis spectra of P3HT/$CHCl_3$ solutions after 5 min ultrasonication and reheating for a period of 16 hours at 55 °C (b) XRD profiles obtained by spin coating the pristine, irradiated and thermally reversed solutions.

4.3.4 Discussion

The demonstration of an ultrasound induced disorder-order transition in solutions of P3HT[135,136] and enhanced charge transport in thin films prepared from these solutions highlights the intricate dependence of electrical properties on microstructural changes in the the solid state of these materials. The crystallinity of thin films of

the polymer can be varied over a wide range through the application of ultrasonic irradiation of the solutions. The increase in mobility is consistent with the spectroscopic evidence, which is suggestive of considerable conjugation of the polymer main chain, leading to intermolecular ordering in films prepared from irradiated solutions.[75,83,127,135,136,145] It is interesting to note that the ultrasound induced spectral behavior is analogous to temperature dependent studies on both solutions and films of P3HT, where an increase in temperature leads to considerable main chain disorder, as evidenced by the hypsochromic shifts in the UV absorption spectra.[85,137,139] Although thermotropic-like transitions are observed in the solid state UV-Vis spectra, they lack a distinct isosbestic point indicating the presence of a multiphase morphology in the films,[85] which is confirmed by the AFM images. As suggested by Rughooputh et.al., the increasing intensity of the vibronic structure in the solution state spectra with irradiation can be ascribed to increased generation of microcrystallites.[139] The observation of strong mesoscale features in the film, in spite of an inherent kinetically limited film formation mechanism, supports the UV-Vis data and suggests the formation of microcrystallites in solution.

The low mobility in pristine films is in agreement with the low crystallinity of the film, which is confirmed by the relatively featureless morphology detected by the AFM. The (100) peak intensity in the X-ray diffractogram almost quadruples after just a minute of ultrasonic irradiation, with the mobility sharply increasing by two orders of magnitude within a comparable time scale. The (100) peak intensity continues to develop beyond a minute of irradiation, finally leveling off beyond 5 mins of ultrasonication. This is strongly supported by the development of mesoscale crystallites, 49(a)(iii-vi), which clearly indicates that the number of crystallites sharply increases between 1 and 3 min of irradiation, with a relative invariance beyond 3-5 mins. The charge transport properties are sensitive even to short irradiation times,

with the mobility increasing by an order of magnitude within 30 seconds, suggesting a rapid initial increase in the ordered assembly of polymer chains followed by a more gradual attainment of saturation between 1-3 minutes irradiation, although the film crystallinity continues to develop beyond 3 mins. This is strong evidence of a percolation type transport mechanism characterized by a threshold crystallinity, with any further increase in the degree of crystallinity beyond 3 mins having little or no impact on the mobility of carriers, akin to a percolation threshold in carbon black/polymer systems.[133] We suggest that the percolation pathway in the P3HT thin films is formed by regions of varying conductivity, attributed to the presence of three distinct phases, possibly varying in their crystalline order. Based on the analysis of Holdcroft et.al.[85] we suggest that ultrasonic irradiation of solutions leads to a continuous transition from a disordered (for films obtained from pristine solutions) to an ordered state, with both incorporating fractions of an intermediate quasi-ordered phase. Short irradiation times lead to formation of π stacked polymer aggregates that act as nucleation centers for nanofiber formation, with short nanofibrils constituting the quasi-ordered phase discussed above. The percolation pathway between 1-3 mins of irradiation is established by facile charge transport through the large nanofibers (constituting the ordered phase), with the disordered and quasi-ordered phases acting as charge transport conduits between the ordered domains. Prior to percolation, the increase in mobility by an order of magnitude can be attributed to an increased fraction of the quasi-ordered phase, evidenced by the three fold increase in the (100) peak intensity. It is possible that the wider and more distinct nanofibrils consist of polymer chains in extended conjugated states reflected in the ca. 6 nm bathochromic shift in the solid state absorption spectrum,[94] while the disordered or quasi ordered phases are formed by chains with a twisted and disordered conformation,[51] resulting in the proposed differences in conductivities between the phases. Moreover, previous work by Ihn et al. using electron diffraction and X-ray has shown that nanofibers of

P3HT consist of polymer macromolecule stacks that are oriented normal to the fiber axis, conducive to facile charge transport.[49,115] Inspite of an increase in the number density of ordered domains beyond the percolation threshold (ca. 3 mins), the AFM images register significant disordered and quasi-ordered regions in the film as well, which in turn are the bottlenecks for charge transport, thus accounting for only minor variations in the mobility beyond percolation. The existence of an upper limit for the mobility, ca. 0.03 and 0.01 $cm^2V^{-1}s^{-1}$ (for Experiments 1 and 2 respectively), in conjunction with the relative invariance of the domain size shown by AFM, may be an indication that beyond the percolation threshold, the maximum mobility is limited either by the intrinsic charge transport within the ordered domains (and thus the degree of order within the nanofibers) or by the interaction between them.[77]

That the experimental data indicates an enhanced supramolecular π stacking in the P3HT solution through the application of ultrasound is surprising, especially given the disaggregation effects of ultrasound on polymers that are commonly reported.[146] However, it is important to note that a great degree of control can be exercised on the acoustic cavitation process by manipulating the experimental conditions. Suslick et.al. have suggested that the cavitational collapse of the bubbles created during ultrasonic irradiation is strongly dependent on the solution concentration, temperature and volatility of the solvent used. The use of a volatile solvent such as $CHCl_3$ increases the vapor pressure inside the bubble, cushioning its collapse and thus making it less violent.[147]

To discount the possibility that ultrasonic irradiation of the P3HT solution causes chemical changes, a solution of 3,3"- dioctyl-2,2':5',2"- terthiophene was used as a model for the polymer. The ^1H NMR spectra of both P3HT and the model oligomer were unchanged by this treatment. In addition, the gel-permeation chromatograms (GPC) of P3HT remain unchanged before and after irradiation as well, indicating no change in molecular weight. Moreover, the ultrasonic irradiation intensity and times

(ca. 0.4 Wcm^{-2}, 40 kHz for ca. 10 mins) used in our experiments is relatively mild compared to those used in systems that can cause polymer degradation (6.8 Wcm^{-2}, 960 kHz for 2 hours).[148] Instead, we suggest that the flow fields created by ultrasonic irradiation results in a shear induced conformational change of the individual polymer chains, significantly reducing interchain entanglement and promoting facile π-π associations, as suggested in Figure51. Similar ultrasound induced disentanglement of chains in low density polyethylene and polystyrene have been reported by other researchers,[149,150] where individual polymer chains are "activated" by the shock waves created during acoustic cavitation.[150] Shear exposure can lead to fibril formation in proteins due to the improved orientational order that facilitates association[151]-a result that has also been reproduced in peptides through the application of ultrasound to solutions in trifluoroethanol.[152]

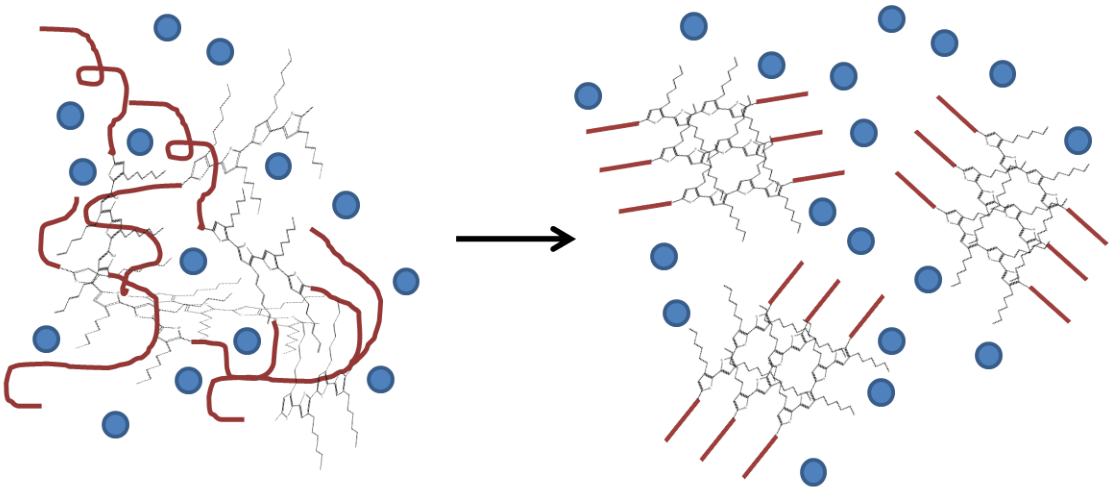

Figure 51: Suggested model for the ultrasound induced aggregation process.

Interestingly, solutions of regiorandom P3HT in $CHCl_3$ showed none of the spectroscopic changes reported in the regioregular polymer, even when exposed to relatively long irradiation times (ca. 20 mins) (data not shown). This suggests that the ultrasound-induced aggregation is possibly linked to the interaction of side chains and to solute-solvent interactions, which are expected to be significantly enhanced in

the regiorandom polymer. The polymer molecular weight also has an effect on the crystallinity of the P3HT films,[52] and might be expected to influence the aggregation in solution. Low molecular weight P3HT chains have a smaller degree of entanglement and are generally more soluble.[153] However, this effect was not evaluated in this study because of the poor charge transport properties of low molecular weight P3HT.[52]

In addition, the relative invariance of the crystallite size in thin films is indication of a dynamic equilibrium between aggregation and disaggregation[146] effects being established during the process of irradiation. A more detailed understanding of this novel ultrasound mediated supramolecular stacking phenomenon would require further experiments possibly elucidating any micro-rheological changes induced by changes in the polymer conformation.[154]

4.4 Conclusion

The results presented here establish a critical relationship between the degree of crystallinity and charge transport in high MW P3HT films. Ultrasonication of solutions of conjugated polymers provides a unique and facile approach to achieve "tunable" crystallinity and allows for the development of a more thorough understanding of structure-property correlations. Charge transport in conjugated polymer thin films is distributed between disordered, quasi-ordered and ordered phases. The field effect mobility is strongly dependent on the degree of crystallanity up to the percolation threshold, beyond which additional crystallite formation does not further aid charge transport. Further experiments to also achieve a tunable domain size would provide vital information to enhance our understanding of the complex structure-property relations in organic semiconductor thin films. Such a solution phase control of the solid state properties of polymer films could lead to the development of facile methods to manipulate charge transport and thereby eliminate the need for dielectric surface

modifications or additional processing steps such as thermal annealing of the thin films themselves.

CHAPTER V

ULTRASOUND INDUCED ORDERING IN POLY(3-HEXYLTHIOPHENE): THE ROLE OF MOLECULAR PARAMETERS AND PROCESS CONDITIONS ON MORPHOLOGY AND CHARGE TRANSPORT

5.1 Introduction

In the previous chapter, we demonstrated the utility of ultrasonic irradiation of P3HT in chloroform ($CHCl_3$) solution in creating ordered precursors that survive the spin casting process, and are manifest in the solid state as ordered nanofibrillar structures which effect a dramatic two order of magnitude increase in the field effect mobility.[93] Ultrasonic irradiation was an effective tool for inducing tunable crystallinity in the π-conjugated polymer thin film that also proved invaluable in identifying a percolation type charge transport mechanism operating in the P3HT films. The effects of ultrasonic irradiation discussed in detail in the previous chapter are summarized in Figure 52.

Alternate processes have also been explored that primarily take advantage of processes that predominantly prevail in the solution state before the formation of the solidified film. For eg., Bao et.al. were one of the first researchers to demonstrate that the choice of solvents when processing P3HT films can have a strong impact on the subsequent field effect mobility.[41] This was followed by studies of Chang et.al., who demonstrated that the use of high boiling solvents can lead to relatively crystalline films (compared to those obtained from volatile solvents) that routinely

demonstrate higher mobilities.[46] They argued that in volatile solvents, the polymer chains are kinetically trapped in to a disordered morphology because of the rapid evaporation of the solvent. In contrast, Yang et.al. showed that the effect of varying the solvent environment around the polymer chains may not necessarily be one of solvent boiling point, but instead the differences in crystallinity and mobility result from variations in morphology between well dispersed nanofibrils and spherulites.[59] Surin et.al. showed that variations in the morphology of the films can also be obtained by altering the film deposition method used such as drop casting, dip coating and spin coating.[47]

The primary goal in this chapter is to probe the role of processing conditions such as film deposition method, molecular properties of the polymer such as regioregularity (RR) and the solvent used in controlling the morphology of P3HT films obtained from both pristine and ultrasonically irradiated solutions. We demonstrate that in spite of the creation of micro-crystallites prior to thin film formation, extrinsic factors such as the film deposition method can have a large impact on the final microstructure of the polymer films. Moreover, the ultrasound induced aggregation process itself is sensitive to the regioregularity of both the polymer and solvent used. The field effect mobilities obtained from polymers with two different regioregularities (ca. 94% and ¿98%) from a variety of processing conditions vary by one order of magnitude and interestingly, are not commensurate with the variations in the corresponding thin film morphologies. The dependence of the solidified P3HT morphology on different stages of the deposition process provides insight into factors that must be carefully considered in order to ultimately realize an optimized morphology that supports facile charge transport in π-conjugated organic semiconductors.

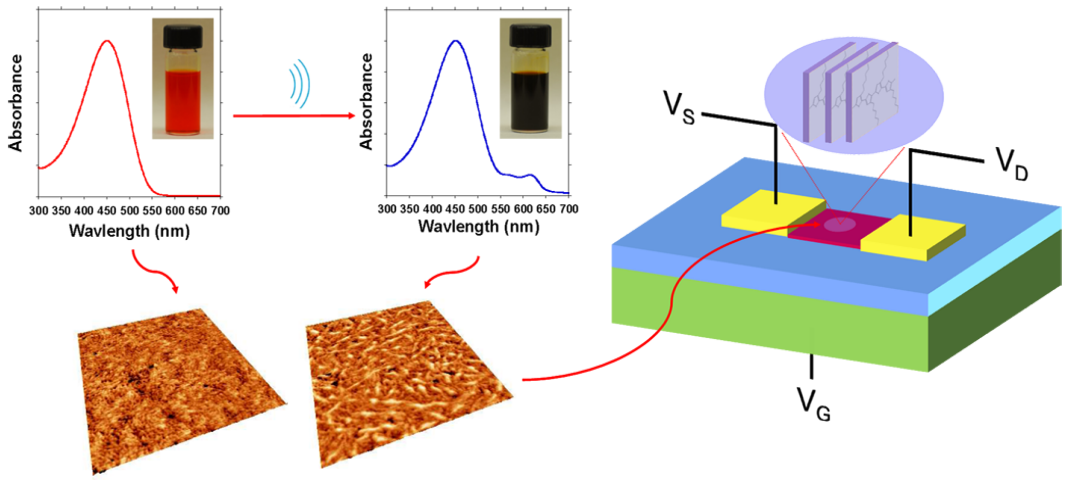

Figure 52: Summary of the ultrasound induced molecular aggregation process that was introduced in Chapter 4

5.2 Experimental Methods

Materials: Regioregular P3HT (referred to as HT94 and HT98 henceforth) used for the study was purchased from Sigma Aldrich (Catalog no. catalog no. 445703) and Rieke Metals, Inc. respectively and used without further purification. The molecular weight (MW) and regioregularity (RR) of both samples are summarized in Table 2. All the solvents used in the study were purchased from Sigma Aldrich and used without any further purification. Trichloro(octadecyl)silane (OTS) and Hexamethyldisilazane (HMDS) were also purchased from Sigma-Aldrich and used without any further purification.

Table 2: Molecular weight and regioregularity of the P3HT samples used

P3HT Sample	**Molecular Weight (kDa)**		**Regioregularity**
	M_N	M_W	%H-T
P100 (HT94)	24	47.7	94
P200 (HT98)	12.7	23	98

The MW data were obtained through gel permeation chromatography (GPC) of the polymer samples in tetrahydrofuran solution. A Waters 1515 Isocratic high performance liquid chromatography system with a Waters 2489 UV/Vis detector,

fitted with a Styragel HR 5E column was used. MW data were determined using polystyrene standards. Polymer regioregularity was estimated from the ^{1}H NMR spectra obtained from deuterated chloroform solution at 293 K using a Bruker DSX 300.

Organic FET (OFET) fabrication and characterization The FET devices used for electrical characterization consisted of two contact devices where P3HT films were prepared via spin coating the relevant polymer solution onto either a 200 or 300 nm thick SiO2 gate dielectric. The highly doped silicon wafer served as the gate electrode while Au/Cr was used for the source and drain contacts. The source and drain contacts were fabricated using a standard photolithography based lift-off process, followed by E-beam evaporation (CVC Inc.) of 50 nm Au contacts with 5 nm of Cr as the adhesion layer. Before spin coating P3HT solutions, the dielectric surface was cleaned using one of two processes (i) cleaning the substrates in piranha solution (4 parts sulfuric acid:1 part hydrogen peroxide) followed by cleaning with acetone, isopropanol and deionized water in an ultrasound cleaning bath (ii) placing the devices in a UV-Ozone cleaner (Novascan PSD-UV) (15 minutes). Both (i) and (ii) allow for complete removal of any residual photoresist and other organic contaminants from the oxide surface. The substrates were rendered hydrophilic at the end of either treatment, although UV-Ozone cleaning appears to result in a lower contact angle as determined by a visual examination.

Solutions of P3HT were prepared at a concentration of ca. 3-4 mgs/mL by heating the solution on a contact hot-plate at a temperature close to the boiling point of the solvent used (for e.g. at 55 C for chloroform ($CHCl_3$) as the solvent). A table top ultrasonic cleaner (Bransonic 2510, 40 kHz, 130 W) was used for ultrasonic irradiation of the solutions. The solutions were prepared and ultrasonicated in sealed glass vials to prevent solvent evaporation. Ultrasonic irradiation was performed by first sealing the glass vials with paraffin paper and temporarily removing them from the

glove-box; the solutions were then ultrasonicated and replaced inside the box. For spin coating, the substrates were spun at a speed of 1500 rpm affording ca. 25-30 nm thick P3HT films (as determined by spectroscopic ellipsometry). Dip coating was performed manually by lowering the substrates vertically into a stock solution of the polymer in $CHCl_3$, where it remained (vertically) for a period of 1 minute before slowly withdrawing the substrate vertically. Because the entire operation was conducted manually, some variations in the morphology and possibly related charge transport characteristics are expected as will be discussed below. Dip coated films had thicknesses that typically ranged from 16-20 nm as measured by ellipsometry. Both spin and dip coated films were then thermally annealed at 110 C for 10 hours on a contact hot plate inside a nitrogen glove-box. The OFETs prepared by either dip coating or spin coating were tested using an Agilent 4155C semiconductor parameter analyzer. The field effect mobility was calculated in the linear region of transistor operation (V_{D}=-3 V) by plotting the drain current (I_{D}) versus the gate voltage (V_{G}) and fitting the data to the following equation[104]:

$$I_D \;=\; \mu\, C_{ox} \frac{W}{L} \left(V_G \;-\; V_T\right) V_D \tag{19}$$

Where V_{T} is the threshold voltage, W and L are the transistor channel width and length respectively and C_{ox} is the capacitance per unit area of the silicon dioxide gate dielectric=1.15 or $1.78 \times 10^{-8} F\mathrm{cm}^{-2}$ depending on the thickness of the dielectric used. It must be noted that there are variations in ultrasound intensity across the ultrasound bath and therefore between experiments which may complicate the results, especially in the absence of quantification of the ultrasound intensity. However, such variations have been accounted for as mentioned later in the text. Unless otherwise mentioned, all experiments were performed in a nitrogen glove-box with less than 1 ppm of oxygen and moisture.

UV-Vis spectra of P3HT: The solid state UV-Vis spectra were obtained using

an Agilent 8510 Spectrophotometer by spin coating the P3HT solutions onto pre-cleaned glass slides under conditions equivalent to those for OFET fabrication.

Grazing Incidence X-Ray diffractions: Out-of-plane (OOP) grazing incidence X-ray diffraction data were obtained using a Panalytical X'Pert Pro system equipped with a Cu X-ray source operating at 45 kV and 40 mA. Grazing incidence angle was fixed at 1 and the detector was scanned from 3 to 20. Peak positions were obtained from the measured profiles by fitting the peaks using XRD analysis software (MDI JADE). Samples for GIXD measurements were prepared by spin and dip coating P3HT solutions onto hydrophilic silicon substrates having a native oxide that were cleaned using the same procedure used for bottom contact FET structures. These solutions used for the GIXD measurements were the same as those used for the OFET measurements.

Atomic Force Microscopy (AFM) studies of P3HT: AFM measurements were performed by scanning the channel region of the bottom contact OFET substrates used for the mobility measurements, with a Veeco Digital Instruments Dimension 3100 scanning probe microscope in tapping mode using a silicon tip (NSC 14, Mikromasch).

5.3 Results and Discussion

Figure 53 shows the field effect mobilities obtained from HT94 and HT98 P3HT OFETs fabricated by spin casting and dip coating the π-conjugated polymer from pristine as well as ultrasonicated solutions in $CHCl_3$. The measured mobility values are also summarized in Table 3.

It must be noted that in this experiment the HT94 P3HT solutions were irradiated for ca. 10 mins, while the HT98 solutions were irradiated for ca. 5 mins, because of a difference in "sensitivity" of the two samples to ultrasonication, *vide infra*. The mobility of HT94 P3HT varies from $1.16 \pm 0.67 \times 10^{-3}$ $cm^2V^{-1}s^{-1}$ for spin coated

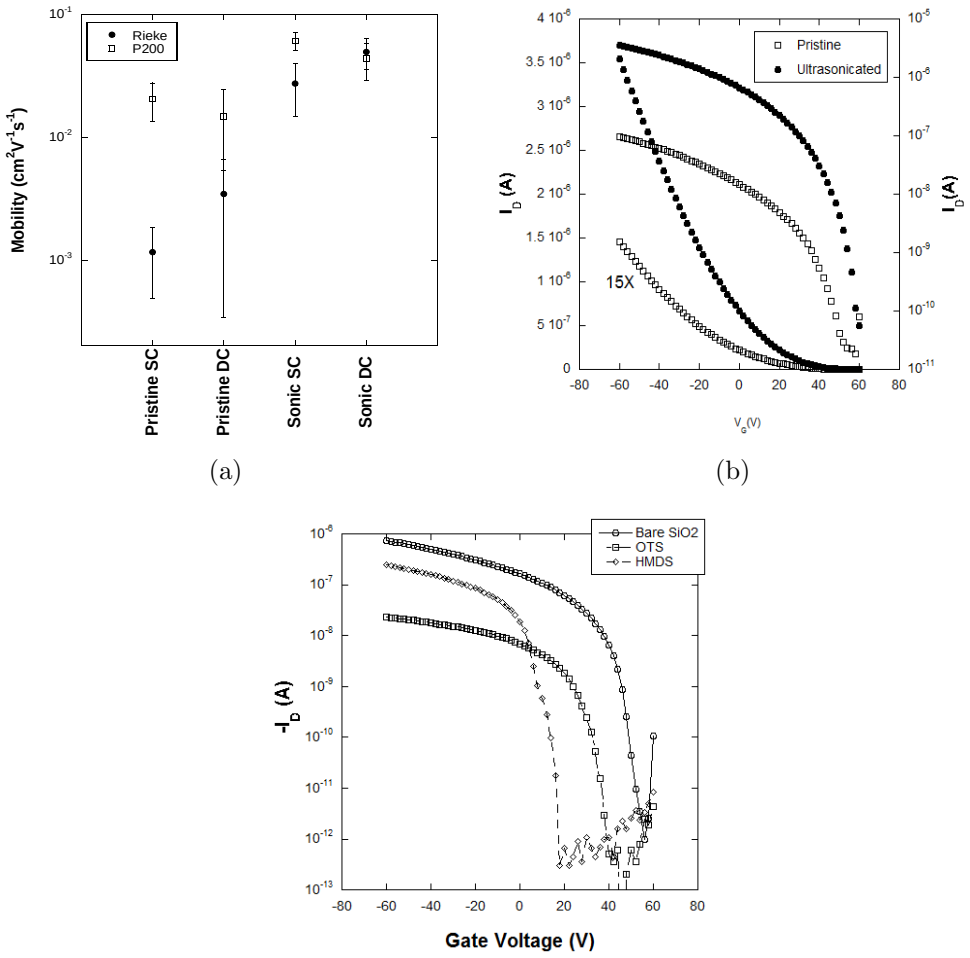

Figure 53: (a) Effect of processing conditions on mobility of films obtained by ultrasonic irradiation of P3HT solutions. All experiments conducted inside a glove-box. (b) Representative transfer characteristics obtained from HT94 P3HT films spin coated from pristine as well as ultrasonicated solutions in $CHCl_3$. (c) Transfer characteristics of HT98 P3HT OFETs obtained by spin coating from solutions in chloroform on substrates with (i) no modification and (ii) modified with OTS and HMDS. All the devices were thermally annealed in a nitrogen glove-box for a period of ca. 10 hrs.

films obtained from pristine solutions to $4.94\pm1.41 \times 10^{-2}$ $cm^2V^{-1}s^{-1}$ for dip coated films of the ultrasonicated solutions, a difference of over one order of magnitude. In contrast, the mobility of the higher RR polymer, HT98 P3HT, varied only by a factor of 4 from $2.05\pm0.71 \times 10^{-2}$ $cm^2V^{-1}s^{-1}$ to $6.08\pm1.01 \times 10^{-2}$ $cm^2V^{-1}s^{-1}$ for films obtained by spin coating from pristine and ultrasonicated solutions in $CHCl_3$,

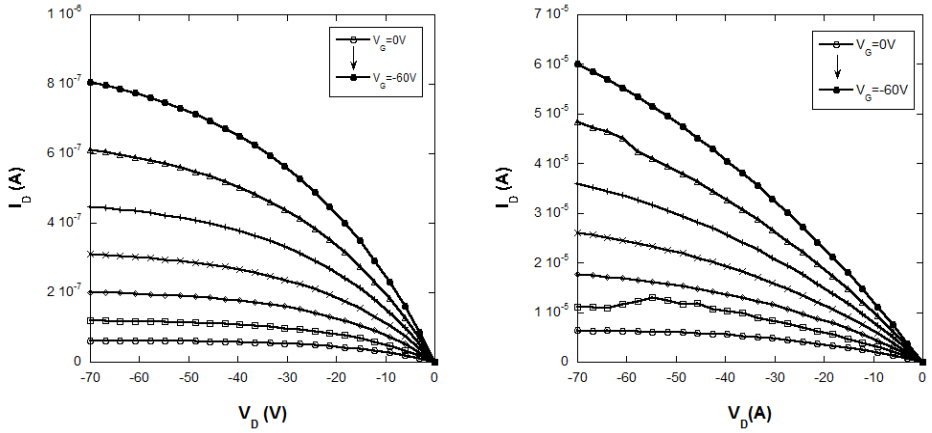

(a) (b)

Figure 54: Representative output characteristics obtained from HT94 P3HT films obtained by spin coating from (a) pristine and (b) ultrasonicated solutions in $CHCl_3$. All the devices were thermally annealed in a nitrogen glove-box for a period of ca. 10 hrs.

Table 3: Summary of field effect mobilities (in $cm^2V^{-1}s^{-1}$) obtained by spin coating (SC) and dip coating (DC) of HT94 and HT98 P3HT solutions with and without ultrasonic irradiation.

Condition	HT94 P3HT	HT98 P3HT
Pristine SC	$1.16\pm0.67\times10^{-3}$	$2.05\pm0.71\times10^{-2}$
Pristine DC	$3.45\pm3.11\times10^{-3}$	$1.48\pm0.95\times10^{-2}$
Sonicated SC	$2.73\pm1.25\times10^{-2}$	$6.08\pm1.01\times10^{-2}$
Sonicated DC	$4.94\pm1.41\times10^{-2}$	$4.36\pm1.46\times10^{-2}$

respectively. The differences in the mobility values noted in Figure 53 (both within a particular P3HT sample as well as across samples) clearly result from both differences in polymer regioregularity as well processing conditions; both are known to affect the microstructure of the resultant films, and thus charge transport.[22,47,49,119,155] Figures 53(b), 54(a) and 54(b) show representative transfer and output characteristics of HT94 P3HT OFETs respectively, obtained from pristine and ultrasonicated solutions in $CHCl_3$, which are typical of p-channel OFET operation in the accumulation mode. The high turn-on voltages (V_{ON}) obtained, as seen from the semi-log plot in Figure 53(b), are attributed to the effects of residual doping and/or acceptor-like traps at

the P3HT-oxide interface.[105,106] This is especially likely given the absence of passivation of hydroxyl groups (generated due to the piranha/UV-ozone treatment of the substrates) that can act as charge traps.[107] Additional experiments show that there is indeed a large reduction in (V_{ON}) when using semiconductor-dielectric modifications, as shown in Figure 53(c). Concomitant with the reduction of (V_{ON}) however, is a decrease in the field effect mobility, with the values of OFETs by spin coating from pristine HT98 solutions dropping to ca. $2.6\times\ 10^{-3}$ $cm^2V^{-1}s^{-1}$ and ca. $2\times\ 10^{-4}$ $cm^2V^{-1}s^{-1}$ in the case of HMDS and OTS treated substrates, respectively. The observed decrease in mobility is likely a result of poor wettability of the P3HT solutions on the hydrophobic surfaces generated by the OTS/HMDS treatment, possibly leading to inhomogeneous, amorphous films.[156,157] In a prior study using spin coated pristine HT94 P3HT/$CHCl_3$ solutions on piranha-cleaned bottom contact substrates (see experimental section for details), average mobilities of ca. $2\times\ 10^{-4}$ $cm^2V^{-1}s^{-1}$, an order of magnitude lower than those obtained here, were observed.[93] While it is apparent that even a slight variation in the hydrophobicity of the critical polymer-dielectric interface is sufficient to drastically alter the charge transport properties of the material, a detailed study of the effects of semiconductor-dielectric interface modification on the morphology and the charge transport in P3HT was not conducted in this work.

The effect of processing conditions on carrier transport is more pronounced in the case of HT94 P3HT films, where dip coated films routinely exhibit higher mobilities compared to the spin coated counterparts ($3.45\pm\ 3.11\ \times\ 10^{-3}$ $cm^2V^{-1}s^{-1}$ (DC) vs $1.16\pm\ 0.67\ \times\ 10^{-3}$ $cm^2V^{-1}s^{-1}$ (SC) for films obtained from pristine solutions and $4.94\pm\ 1.41\ \times\ 10^{-2}$ $cm^2V^{-1}s^{-1}$ (DC) vs $2.73\pm\ 1.25\ \times\ 10^{-2}$ $cm^2V^{-1}s^{-1}$ (SC) for films obtained from ultrasonicated solutions. This is not surprising given that dip coating is believed to yield films with near-equilibrium structures having higher crystallinity.[158,159] In contrast, for the higher RR HT98 films, the correlation

is reversed, i.e. spin coated films (=2.05± 0.71× 10^{-2} $cm^2V^{-1}s^{-1}$ and 6.08± 1.01× 10^{-2} $cm^2V^{-1}s^{-1}$ respectively for films obtained from pristine and ultrasonicated solutions) exhibit higher mobilities relative to dip coated ones (=1.48± 0.951× 10^{-2} $cm^2V^{-1}s^{-1}$ and 4.36± 1.46× 10^{-2} $cm^2V^{-1}s^{-1}$ respectively for films obtained from pristine and ultrasonicated solutions). Thus a notable inter-play between the effects of the molecular properties of the polymer and the processing conditions, both of which are expected to play crucial roles in determining the final morphology of the film, is apparent.[49] The subtle effects of RR on the morphology as well as charge transport in spin coated P3HT films have been reported elsewhere,[160] and the results presented here are further confirmation of the subtlety of the effect. Given that the charge transport in field effect transistors is dominated by an accumulation layer that only spans a few mono-layers from the polymer-dielectric interface,[161] the ordering of the macromolecules at that interface is expected to exert a dominating influence on charge carrier mobility. Thus, it is likely that the differences in mobility noted between both dip coated and spin coated films, as well as between HT94 and HT98 films originate with the microstructure.

Spectral features in the UV-visible absorption spectrum of a π-conjugated system strongly correlate with the state of micro-structural order in the film.[83,103,110] The spectroscopic changes associated with ultrasonic irradiation of the materials discussed here are summarized in Figure 55(a), where we associate the development of the low energy features in the solution (at ca. 570 and 620 nm) and solid state spectra (at ca. 605 nm) with the presence of micro-crystalline aggregates in solution, that in turn provide a film having increased molecular order.citeaiyar:ultrasound Moreover, compared to the pristine P3HT solution, the intensity of photoluminescence (inset of Figure 55(a)) decreases by 47% and 36% upon ultrasonic irradiation and upon addition of 10 vol.% methanol (MeOH) respectively, consistent with the formation of a π-stacked aggregate that can partially quench the polymer's luminescence.[142,143]

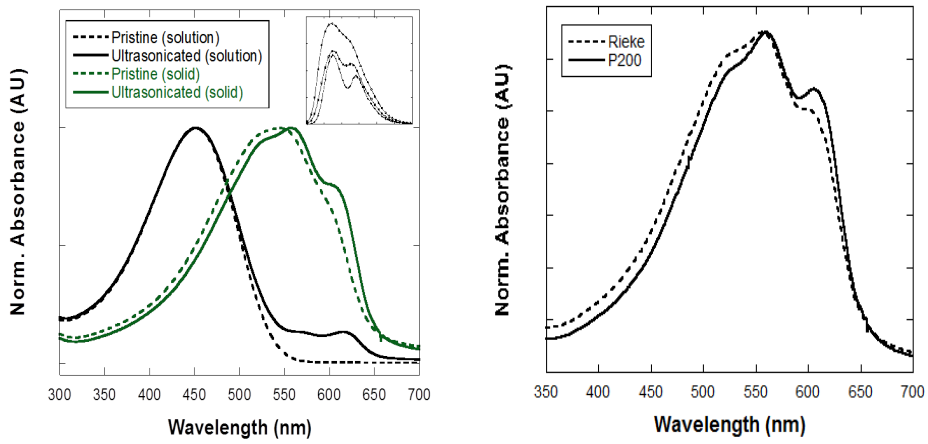

Figure 55: (a) Normalized solution and solid state UV-Vis plots for pristine and ultrasonicated HT94 P3HT/$CHCl_3$ solutions. Inset shows the solution photoluminescence spectra of pristine, 5 min ultrasonicated and 10 vol.% MeOH aggregated P3HT/CHCl3 solutions (b) Comparison of absorption spectra of HT94 P3HT and HT98 P3HT films obtained from ultrasonicated solutions. All solutions ultrasonicated for ca. 5 mins in air.

Zhao et.al. have suggested that the primary effect of ultrasonic irradiation of P3HT solutions is a dramatic increase in interaction between the solute (individual polymer chains) and the solvent, resulting in decreased chain entanglement, which in turn promotes polymer-polymer associations.[135] Thus, it is anticipated that the disorder-order transformation will be influenced by the conformation of the individual polymer chains and thus molecular parameters such as the RR may be expected to alter the effects/impact of ultrasonic irradiation. Figure 55(b) shows the solid state absorption spectra of HT94 and HT98 P3HT films obtained from the respective ultrasonically irradiated solutions which indicate a bathochromic shift of the absorption maximum λ_{max} from 556 nm for the HT94 film to 561 nm for HT98 film, with the latter also showing a more pronounced shoulder at ca. 602 nm. The increased intensity of the (0-0) transition (at ca. 602 nm) (and thus of the intensity ratio of the (0-0) and (0-1) transitions) in the HT98 film is indicative of increased intermolecular ordering in the higher regioregularity film, probably resulting from an extended main chain

conformation afforded by fewer steric distortions.[83,110] This is also reflected in the higher free exciton bandwidth in the HT94 P3HT film compared to the HT98 film (ca. 120 meV in HT94 vs ca. 90 meV in HT98).[103] This is clear evidence of the dependence of the ultrasound induced aggregation process on the RR of the polymer. This observation is also consistent with the extent of intra-chain order being particularly sensitive to subtle changes in the head-tail (HT) attachments of the hexyl side chains as demonstrated elsewhere.[160] Based on the results of Wang et.al., similar differences in the absorption spectra are also expected between spin coated and dip coated films, with the latter yielding films having higher molecular order.[162] The increased intermolecular ordering present in the HT98 films can thus explain the higher mobility observed for OFET structures prepared with HT98. Furthermore, ultrasonic irradiation of P3HT solutions (irrespective of regioregularity) results in changes that bear similarities to the effect of RR and thus the increase in mobility with solution irradiation also shares a common origin with that of RR-increased molecular order.

The tapping mode AFM phase images shown in Figure 56 show dramatic variations in the morphology of the P3HT films. Notably, spin coated films of both HT94 as well as HT98 P3HT obtained from pristine solutions are relatively featureless and apparently lacking texture, consistent with the rapid drying times encountered in spin coating from volatile solvents such as $CHCl_3$, resulting in a kinetically limited process that suppresses the formation of ordered structures.[46] The absence of ordered structures in the AFM phase images is mirrored in the x-ray diffractograms, Figure 57, where no discernible peak was detected for either sample obtained from spin coated pristine solutions. Thus, it is not surprising that spin coated films (at least in the case of HT94 P3HT) routinely exhibit mobilities that are the lowest in magnitude ($=1.16\pm0.67\times\ 10^{-3}$ $cm^2V^{-1}s^{-1}$). By the same token, the mobilities obtained from HT98 P3HT OFETs spin coated from pristine solutions are also expected to be low, especially given that the film morphology does not display any obvious signs of order.

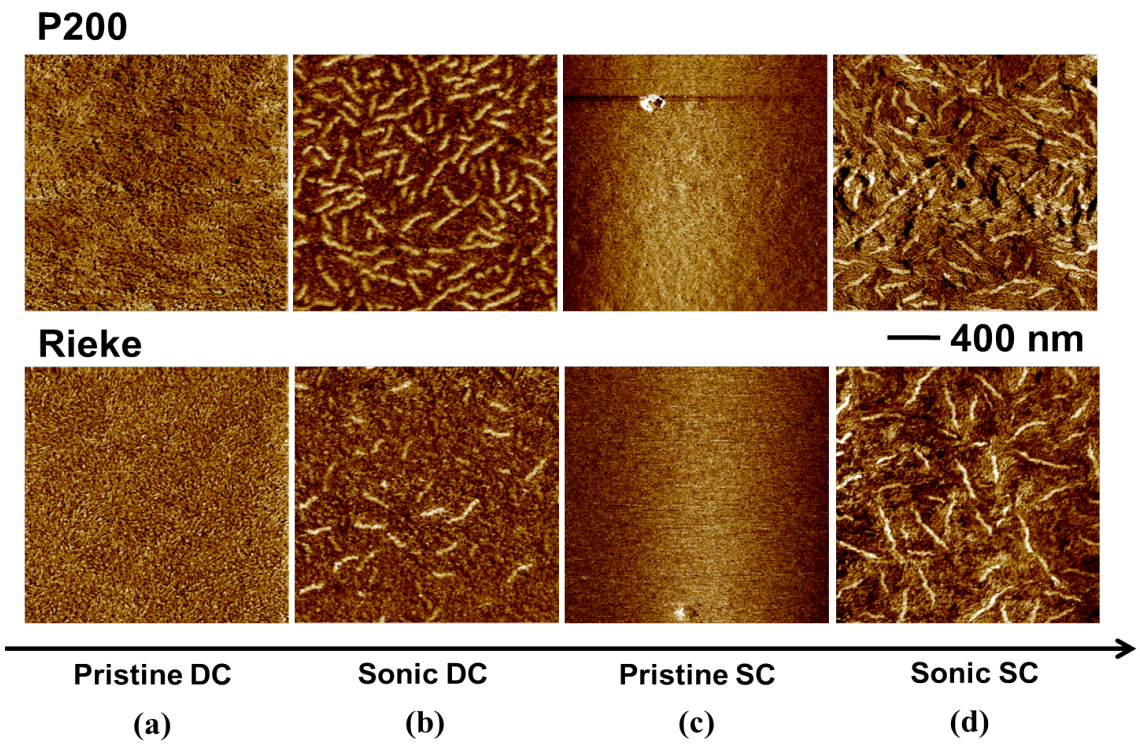

Figure 56: Tapping mode AFM phase images of HT94 and HT98 P3HT films obtained by spin as well dip coating from pristine as well ultrasonicated chloroform solutions.

However, this is clearly not the case; OFET mobilities obtained for these HT98 films are $2.05\pm0.71\times\ 10^{-2}$ $cm^2V^{-1}s^{-1}$ even though the film morphology remains relatively featureless. However, the absorption spectra of P3HT films, where subtle variations in the RR result in increased molecular order in the films,[160] could contain a potential explanation for the difference in mobility observed between HT94 and HT98 OFETs.

Interestingly, changing from a spin coating to a dip coating process results in morphologies that clearly incorporate nanofibrillar structures within both the higher and lower P3HT films, Figure 56(a). The subsequently higher mobility of dip coated films of HT94 P3HT obtained from pristine solutions (μ=$3.45\pm3.11\times\ 10^{-3}$ $cm^2V^{-1}s^{-1}$) clearly demonstrates that the presence of the nanofibrillar network is representative of increased structural order which in turn promotes facile charge transport. Although

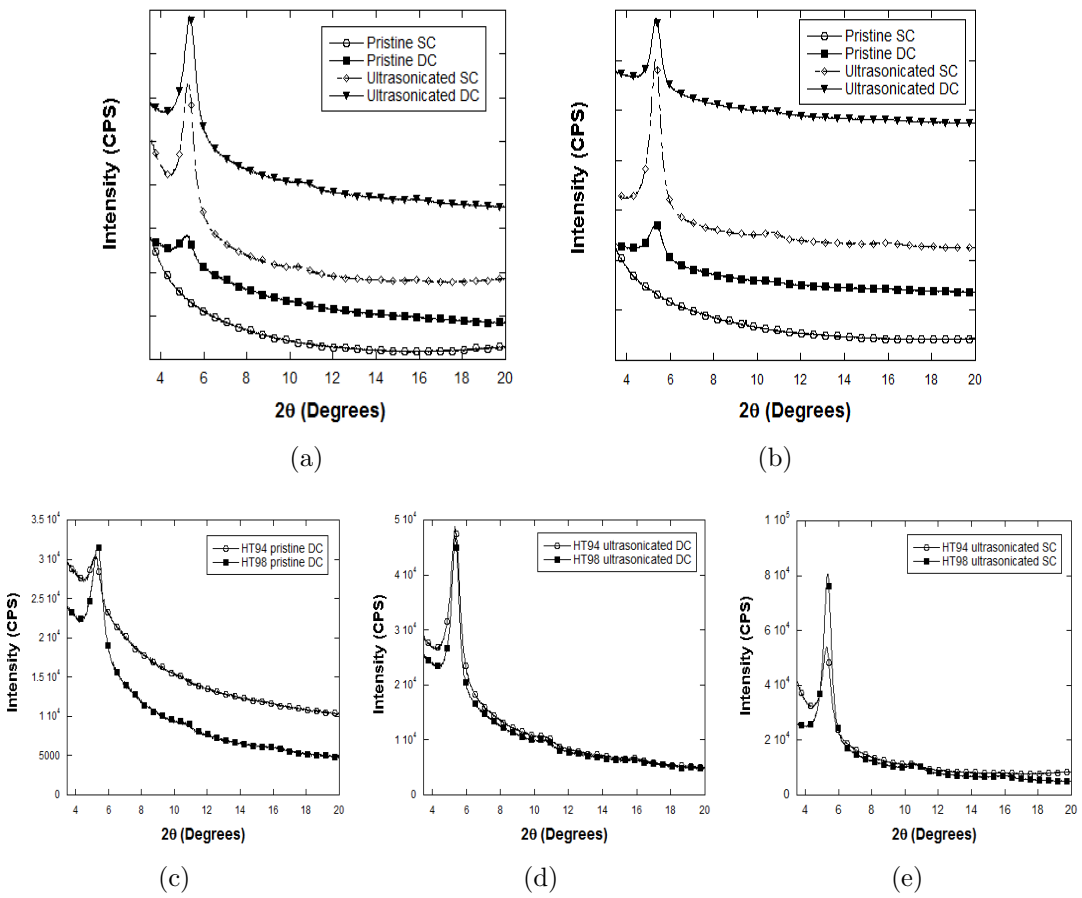

Figure 57: Grazing incidence X-Ray diffraction profiles of (a) HT94 and (b) HT98 P3HT films obtained by spin-coating and dip coating from pristine and ultrasonically irradiation solutions in CHCl3. Comparison of the XRD profiles of HT94 and HT98 films obtained by (c) dip coating from pristine solutions (d) dip coating from irradiated solutions and (e) spin coating from irradiated solutions.

not direct evidence for the presence of structural order, the nanofibrils strongly indicate the existence of $\pi - \pi$ associations between adjacent polymer chains that result in the formation of the nanofibers themselves.[115] A similar nanofibrillar network is visible in HT98 P3HT films obtained from dip coated pristine solutions, even though, surprisingly, the mobilities (μ=1.48±0.95× 10^{-2} $cm^2V^{-1}s^{-1}$) are slightly lower than those obtained from the spin coated films where nanofiber formation appears significantly suppressed relative to the dip coated samples. Even more surprising is the fact that spin coated films of HT98 (μ=2.05±0.71× 10^{-2} $cm^2V^{-1}s^{-1}$) have a mobility that is almost an order of magnitude higher than that obtained for devices prepared

from dip coated HT94 (μ=3.45±3.11× 10^{-3} $cm^2V^{-1}s^{-1}$), in spite of HT94 films consisting of a distinct nanofibrillar network. Our results are reaffirmed by the molecular weight dependence of charge transport in P3HT, that has clearly demonstrated that a highly ordered microstructure may not always result in high charge carrier mobilities.[52] The (100) peak in the x-ray diffractograms, associated with the lamellar packing of polymer chains along the crystallographic direction perpendicular to the backbone,[123] which was clearly absent in the spin coated films, is well-developed in both dip-coated films, although the peak appears to be more intense for the HT98 film. The development of the (100) peak in the dip-coated films is reflective of the formation of near-equilibrium structures through dip coating, which are otherwise quenched during the spin coating process.[158,159] The x-ray peak intensities are consistent with the improvement in the mobility observed for the dip coated HT94 films and to a certain extent could also form a basis to explain the difference in mobility noted between HT94 and HT98 dip coated films, but it fails to account for the mobility difference between the spin coated films for which the (100) peak is clearly absent. Instead it is possible that the higher degree of intra-chain ordering afforded by the higher RR in HT98 compensates for the kinetically hindered structures that arise from spin coating preventing the mobility values from being compromised as a result of the disordered morphology observed via AFM and confirmed by XRD. In line with an earlier hypothesis, the higher macroscopic mobility observed for the spin coated HT98 film results from a reduction in the reorganization energy, allowing for facile inter-chain hopping in spite of the absence of nanofibrillar structures.[160] Ultrasonic irradiation of the P3HT solutions results in dramatic changes to the morphology as well as the (100) peak intensities, confirming our original observation of the effect of ultrasound on microstructure. The morphology of both spin coated as well as dip coated films of HT94 and HT98 P3HT obtained from irradiated solutions are characterized by the presence of distinct nanofibrillar structures embedded in a

matrix that is composed of both disordered as well as quasi-ordered structures.[93] Interestingly, although the ordered precursors are thought to be generated in solution, the film deposition method and the polymer RR clearly influence their manifestation in the solid state, Figures 56(b) and 56(d). For example, a comparison of films obtained by dip vs spin coating reveals subtle differences in the physical appearance of the nanofibrillar structures incorporated in both films. The effect of RR is also clearly apparent in the case of the dip coated films, with the HT94 film containing a significantly lower fraction of the nanofibrillar structures compared to the HT98 film. It should be noted that the same solutions were used for both the spin coating as well as dip coating experiments to avoid ambiguities associated with changes in irradiation intensities (see experimental section). However, different irradiation times were required for HT94 and HT98 solutions, since the former was routinely less sensitive to ultrasound induced changes in comparison with the higher RR HT98 counterpart (vide infra). In sharp contrast to the dip coated films, a significantly smaller difference is noted from a comparison of the morphologies obtained from spin coated films, Figure 56(d), suggesting that the differences noted in the dip coated films arise predominantly from the deposition method itself, rather than a difference in ultrasonication time. The dramatic increase in the (100) peak intensity in the x-ray diffractograms for both spin coated as well as dip coated films is consistent with the appearance of ordered nanofibrillar structures in the film as a result of ultrasonic irradiation of the respective solutions. The slightly higher (100) peak intensity in the case of the HT98 film mirrors the AFM phase image, which detects the presence of a greater number of the ordered nanofibrils relative to the HT94 films, 56(d). However, there appears to be no such correspondence for the dip coated films, where in spite of the sparse distribution of ordered nanofibrils in the HT94 film relative to the HT98 film, Figure 56(b), the (100) x-ray peak intensities in both cases are nearly identical. The origin of this behavior is not completely understood, however, the identical

crystallinity between the two samples may result from an equal overall distribution of disordered, quasi-ordered and ordered phases. In the absence of any appreciable thickness difference between the two films (ca. 19 nm and ca. 21 nm for HT94 and HT98 dip coated films respectively), the near identical (100) peak intensities indicate the presence of equal volume fractions of ordered crystallites in both films. Thus, the lower fraction of ordered crystallites in the HT94 film may be compensated by a higher areal fraction of the quasi-ordered phase resulting in a net degree of crystallinity which is similar to that obtained from the HT98 film where the effect of the greater number of nanofibrillar structures is offset by a higher disordered amorphous content. Moreover, the different morphologies of dip coated HT94 and HT98 films once again highlight the inter-play between the effects of polymer RR and the *dynamics of film formation*. We have suggested elsewhere that the formation of the ordered nanofibrils involves sequential nucleation of the π stacked polymer aggregates into an intermediate quasi-ordered phase and eventually into the ordered phase.[93] This coupled with the fact that HT98 P3HT is far more sensitive to ultrasonic irradiation would suggest a greater conversion of the intermediate quasi-ordered phase into the ordered phase resulting in films that incorporate greater numbers of the nanofibrillar structures embedded in a largely disordered phase. In contrast, the weaker response to ultrasonic irradiation in the lower RR polymers results in fewer ordered nanofibrils, but conceivably a greater conversion of the disordered phase into a quasi-ordered phase. Thus the facile charge transport within the ordered nanofibrils in the HT98 dip coated films would be offset by poor transport within the amorphous matrix resulting in a mobility of $4.36\pm1.46\times\ 10^{-2}$ $cm^2V^{-1}s^{-1}$, that is within experimental error identical to that obtained from HT94 dip coated films (μ=$4.94\pm1.41\times\ 10^{-2}$ $cm^2V^{-1}s^{-1}$), where the lower fraction of ordered nanofibrils is possibly offset by a higher areal fraction of the quasi-ordered phase. However, the variations in film crystallinity and morphology noted in Figures 56 and 57 are insufficient to justify the differences in

mobility observed in Figure 53. For example, the dramatic difference in the degree of crystallinity and the film morphology between HT94 films obtained by spin coating from pristine versus ultrasonicated solutions would explain the increase in mobility from $1.16\pm0.67\times 10^{-3}$ $cm^2V^{-1}s^{-1}$ to $2.73\pm1.25\times 10^{-2}$ $cm^2V^{-1}s^{-1}$ obtained from the corresponding films, but for similar variations in the microstructural properties in the case of HT98 films, the mobility variations are clearly incommensurate, varying by as little as a factor of 3. This once again raises the importance of intra-chain vs inter-chain effects in dominating macroscopic charge transport. The inherently higher intra-chain order in HT98 films obtained from pristine solutions, evidenced by solid state absorption spectrum, could explain why only minor differences in mobility are obtained through ultrasonic irradiation in spite of a large increase in the degree of inter-chain ordering. This observation is consistent with a percolation type charge transport mechanism, where any increase in the microstructural quality of the film beyond a percolation threshold does not necessarily result in further improvements in macroscopic charge transport, especially when the charges encounter large amorphous or quasi-ordered regions.[93]

In spite of the role played by film deposition conditions, it is evident that intrinsic molecular properties such as the RR are crucial to the manifestation of the ultrasound induced phenomena reported here and elsewhere.[93,135] As hypothesized by Zhao et.al., changes observed upon ultrasonic irradiation are fundamentally one of disorder-order transitions.[135] The acoustic cavitation process likely leads to chain disentanglement, followed a shear induced change of the polymer chain conformation maximizing opportunities for cofacial stacking between the individual chains.[93] This would also mean that the nature of the molecular aggregate thus formed would depend crucially on the solvent environment the disentangled polymer chains find themselves in before $\pi - \pi$ associations are formed. In addition, elucidation of the role of solvent-solute interactions in general is expected to clarify understanding of

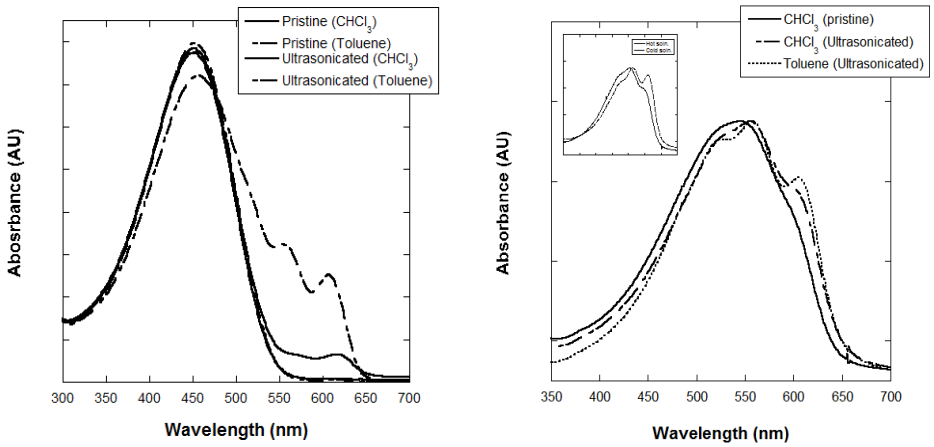

Figure 58: Solution state (a) and solid state (b) absorption spectra of HT94 P3HT solutions in $CHCl_3$ and toluene and the corresponding films obtained by spin coating them on to pre-cleaned glass slides. Inset in Figure 58(b) shows the solid state absorption spectra of HT98 P3HT films obtained by spin coating from cold and hold pristine solutions in p-xylene.

the molecular aggregation process suggested by results from ultrasonic irradiation of the polymer solutions. Through experiments with P3HT of varying molecular weights (M_W=11, 30-40 and 87 kDa), Zhao et.al. have suggested that the effects of ultrasonic irradiation are reduced to that of solubility of the polymer in the solvent system. In their experiments, the disorder-order transformations in high molecular weight P3HT solutions in xylene were significantly more favorable relative to medium and low RR solutions. This was mirrored not only in the steeper transitions observed in the corresponding absorption spectra of the solutions upon irradiation, but also confirmed by the reported thermochromic transitions.[135] Interestingly, similar experiments performed using "marginal" solvents such as toluene or p-xylene, Figure 58(a), revealed that the molecular aggregation process is dramatically accelerated resulting in spectroscopic changes that bear a close resemblance to those obtained by Zhao et.al. from their high MW P3HT solutions. In addition, the spectroscopic changes noted in Figure 58(a) are significantly different from the results obtained from irradiation of the corresponding P3HT/$CHCl_3$ solutions, Figure 55(a), clearly highlighting the role of

the solvent system. Two essential differences must be noted in the case ultrasonic irradiation of HT94 P3HT solutions in toluene-(i) the absorption maximum, λ_{max}, is clearly red-shifted by ca. 8 nm and (ii) the low energy transitions at ca. 555 nm and 603 nm are more intense for the same irradiation time (2 mins). These results clearly suggest that solubility effects have some part to play in the ultrasound induced ordering phenomenon. In fact, upon irradiation for longer times (¿ 2mins) and then allowing the P3HT/toluene (or xylene) solution to rest for a few minutes, a gel-like substance was obtained, consistent with the reports of Malik et.al. who have previously demonstrated thermo-reversible gel formation in P3HT/xylene systems.[144] Based on the spectral features observed in Figure 58(a), it is plausible that ultrasonic irradiation drives a random coil to rod transformation, evidenced by the bathochromic shift of the absorption maximum, followed by aggregation of the rods or fibrillar crystallization.[113,144] Furthermore, there are distinct similarities in the spectral features of the irradiated toluene solutions in Figure 58 and thermochromic transitions in P3HT solution observed by Rughooputh et.al., supporting the idea of an ultrasound induced coil-rod transformation driving the crystallization process.[113] Kiriy et.al. have suggested that the addition of non-solvents to well dissolved P3HT solutions results in solvophobic interactions that lead to main chain collapse into a helical conformation followed by a concentration dependent association of individual helices into one dimensional aggregates.[125] However, as noted above, the significant differences in the spectral features between irradiated $CHCl_3$ and toluene solutions indicate that the development of micro-crystalline aggregates might be fundamentally different in the two systems. Figure 58(b) shows the solid state spectra obtained by spin coating the HT94 P3HT solutions in toluene and $CHCl_3$. Based on arguments made earlier, it would appear that ultrasonic irradiation of solutions of P3HT in marginal solvents results in increased molecular order in the solid state. Surprisingly, this is not mirrored in the corresponding field effect mobilities, with values of ca. 2×

10^{-3} $cm^2V^{-1}s^{-1}$ and $2\times$ 10^{-2} $cm^2V^{-1}s^{-1}$ for OFETs obtained by spin coating irradiated solutions of HT94 P3HT from toluene and $CHCl_3$ respectively. This is further evidence that the *physical conformation* of the aggregates generated by ultrasonic irradiation is dependent on the nature of the interactions between the polymer and the solvent. We note that the same solutions were used for both the spectroscopic as well as OFET measurements. The inset in Figure 58(b) showing the solid state spectra of HT98 P3HT obtained by spin coating from both, a hot solution in p-xylene and a solution that has been allowed to cool to room temperature. Like toluene, p-xylene is a marginal solvent for P3HT and the reduced solubility clearly results in increased aggregation between the polymer chains, as evidenced by difference in the absorption spectra.

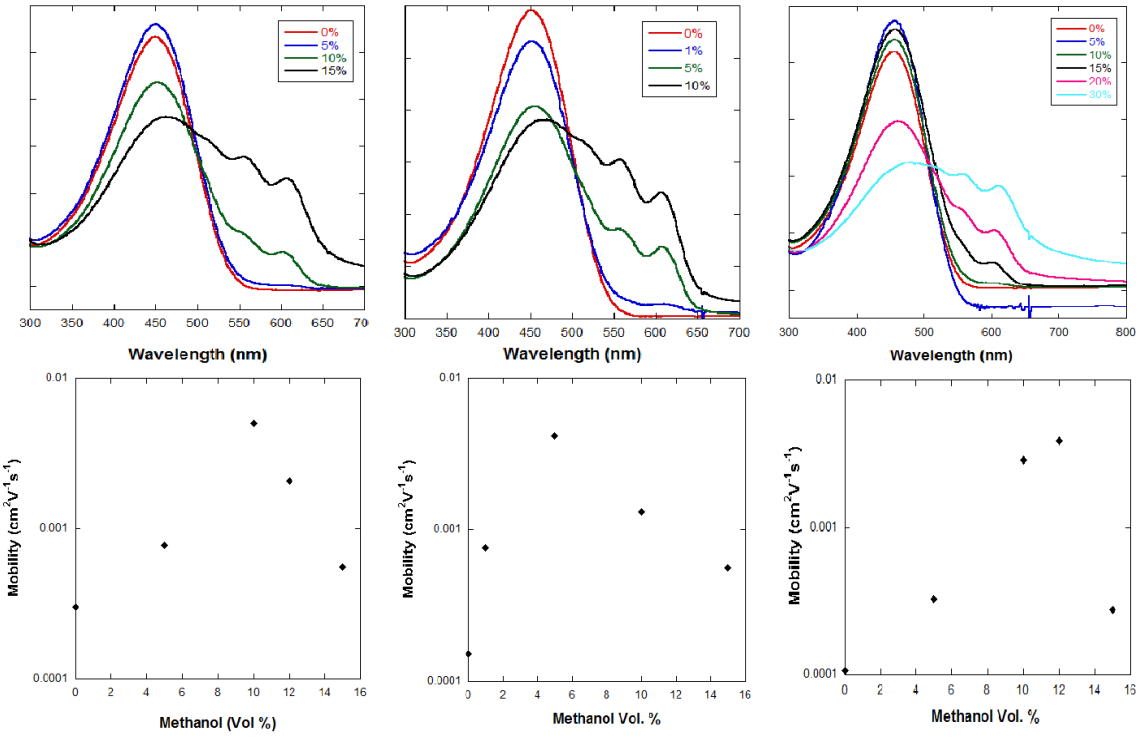

(a) (b) (c)

Figure 59: Aggregation of HT94 P3HT solutions in various solvents by the addition of methanol as a non solvent-solution state absorption spectra and field effect mobility as a function of methanol volume percentage in (a) $CHCl_3$ (b) toluene and (c) MCB solutions.

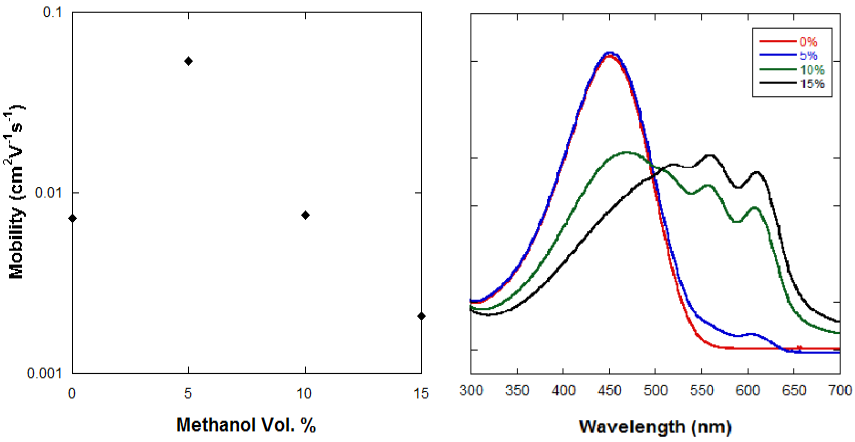

(a) (b)

Figure 60: Aggregation of HT98 P3HT solutions in various solvents by the addition of methanol as a non solvent-solution state absorption spectra and field effect mobility as a function of methanol volume percentage in $CHCl_3$ solutions.

Experiments performed by the addition of a non-solvent (MeOH) to solutions of HT94 P3HT in various solvents including $CHCl_3$, toluene and MCB contains further clues as to the role of the solvent in modulating the aggregation process encountered through ultrasonic irradiation, Figure 59. It is clear from the absorption spectra that the addition of increased amounts of MeOH drives the solution system towards precipitation, but the amount of MeOH required to precipitate the P3HT solution is strongly dependent on the primary solvent (i.e. $CHCl_3$, MCB etc.) used. For e.g., ca. 30 vol.% MeOH is required to completely precipitate a solution of the P3HT in MCB, while significantly lower amounts are required to precipitate solutions in $CHCl_3$ and toluene (ca. 15 vol.% and 10 vol. % respectively). Based on the MeOH aggregation experiments, we suggest that the solubility of P3HT in MCB¿$CHCl_3$¿Toluene. Interestingly, ultrasonic irradiation of solutions of HT94 P3HT in MCB show none of the spectroscopic changes observed in $CHCl_3$ and toluene even upon irradiation for 20 minutes, confirming the role of solubility effects in the ultrasound induced changes. The fact that HT98 P3HT solutions are routinely more sensitive to ultrasonic irradiation in spite of the lower molecular weight of HT98 compared to HT94 (see Table

1), suggests that RR has a dominant influence on the solubility of the polymer. The corresponding mobility profiles of the P3HT films as a function of MeOH vol.% added to the pristine solutions used for spin coating the films, are instructive. The onset of molecular aggregation clearly results in an improvement of charge transport, but the existence of a peak mobility is a clear indication of the sensitivity of the charge transport to the nature of the aggregate that is formed in the solution. Moreover, the peak mobilities obtained from all the three experiments in Figure 59 are not only very close in their values, but are incidentally obtained from films spin coated from solutions that display very similar absorption spectra. Note that the mobility starts to decrease well before complete precipitation of the solution (detected by the spectra as well as visual observation of macroscopic particles in the solution), hence the decrease in mobility cannot simply be attributed to the formation of an inhomogeneous film alone as suggested by others.[127] Also, note that the peak mobilities obtained here may not represent the maximum obtainable as the MeOH dilution experiments were performed to determine the mobility profile rather than to estimate peak mobility.

The effect of RR can also be understood in light of the solubility effects discussed above. The more planar and rigid chain conformation in HT98 P3HT, afforded by fewer steric distortions imposed by the hexyl side chains, is expected to lead to a lower solubility in a given solvent relative to HT94 P3HT. This is apparent from Figure 60, which shows that the aggregation process for HT98 P3HT solutions (in $CHCl_3$) is significantly more sensitive to the MeOH vol.% in comparison to HT94 solutions, with 10 vol.% MeOH sufficient to induce precipitation of the P3HT. This would explain why the ultrasound induced aggregation phenomenon is clearly accelerated in HT98 solutions, as shown in Figure 61. However, it must be noted that the time dependence of the intensity of the low energy transitions reported in Figure 61 can be misleading, especially given the variations in intensity within the ultrasound bath. Thus, both

experiments (in Figure 61) were conducted back to back in order to minimize extrinsic causes of the differences in the spectra. Nevertheless, irrespective of the solution irradiation time used in the case of HT94 solutions, the (0-0) peak intensity of the corresponding films is consistently lower than that recorded from HT98 films, suggesting that differences in kinetics of the aggregation process (due to a difference in solubility of the two P3HT samples and/or variations in ultrasound intensity) alone cannot account for the effect of RR. In addition, the significantly higher mobilities obtained from the MeOH dilution experiments (μ=ca. 0.05 $cm^2V^{-1}s^{-1}$ for HT98 P3HT vs. $5\times$ 10^{-3} $cm^2V^{-1}s^{-1}$ for HT94 P3HT), Figure 60(b), is further evidence that subtle differences in RR have a significant impact on aggregate formation, which in turn influences charge transport. This is also indicative of the fact that the ultrasonic irradiation process is strongly influenced by single chain effects. The disentanglement of the polymer chain that results from ultrasonic irradiation, in turn results in molecular aggregates, the nature of which depends on the solvent environment around the disentangled chains and the polymer RR, both of which explain the differences noted above in the absorption spectra. Additionally, we note that regiorandom P3HT with a H-T content of ca. 50% is unresponsive to ultrasonic irradiation. The decrease in sensitivity of the polymer to ultrasonic irradiation with decreasing RR suggests that our ultrasonication conditions (40 kHz, 130 W) may be too mild to surmount the large steric barrier in less regioregular polymers, preventing effec co-facial π stacking.

Although the suggested propensity of the π-conjugated polymer to form ultrasound induced molecular aggregates is strongly dependent on the solubility of the polymer in the solvent, other factors must also be considered. Since the manifestation of the effects of ultrasound are through acoustic cavitation, physical properties of the solvent such as its viscosity, and solution properties such as dilution, are expected to participate in the process as well. The results of Briggs et.al. have shown that an increase in viscosity of the liquid would result in an increased power demand to induce

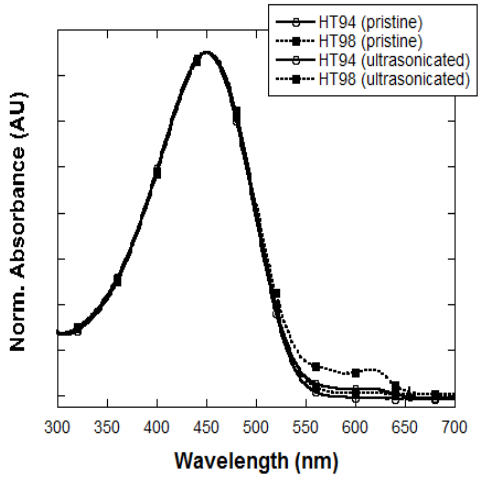

Figure 61: Solution state absorption spectra of pristine and ultrasonicated HT94 and HT98 P3HT solutions in $CHCl_3$. Both solutions were ultrasonicated for a period of 5 mins.

cavitation in that system.[163] Thus it is conceivable that the insensitivity of solvents such as MCB, with a viscosity of 0.8 cP, is due to an increase in viscosity relative to $CHCl_3$, which has a viscosity of 0.58 cP. This is also supported by experiments with 1,2,4-trichlorobezene (TCB), a system which is also unresponsive to the irradiation, consistent with its higher viscosity (ca. 2.08 cP) preventing acoustic cavitation from setting in at the applied power. However, given that a transition from $CHCl_3$ to MCB results in changes in not just the viscosity, but also polymer solubility, further experiments to explore the impact of ultrasonic irradiation intensity and frequency are required to identify solvent parameters that are crucial to the process.

Interestingly, the process is found to be significantly accelerated for both HT94 as well as HT98 solutions when the experiment is performed in an ambient vs. an inert atmosphere. This phenomenon is confirmed through a visual observation of the color change that typically accompanies the ultrasound induced aggregation process, which starts to occur within ca. 1 minute in air for both P3HT samples. This result is in contrast to solutions prepared in the glove-box, which display a significantly delayed response to the irradiation, an effect that is more noticeable in the case of HT94

solutions, where an irradiation time as high as ca. 5-6 mins is required to observe the first signs of color change. Kim et.al. have reported a similar acceleration of the color change process under the influence of ambient light in ultrasonically treated solutions of P3HT in mixtures of chlorobenzene and acetonitrile, which they attribute to an increase in chain planarity due to photo-oxidation.[136] P3HT is known to form a reversible charge transfer complex with oxygen,[71] and hence a sono-chemically motivated association with ambient or dissolved oxygen in the solvent is not entirely unexpected, especially given the retardation of the changes in an inert atmosphere. Moreover, the experiments performed here were conducted under ambient light, so photo-oxidation effects may be observed. However, it is not currently understood if and how photo-oxidation influences the molecular aggregation process as several anomalies exist. The absence of any color change upon ultrasonic irradiation under ambient conditions in regio-random P3HT or P3HT dissolved in MCB and TCB are inconsistent with photo-oxidation being the driving force for the molecular aggregation process. Furthermore, the retardation of the color change is less apparent for HT98 solutions, with the first signs of color change occurring within the first one to two minutes.

Nevertheless, the output characteristics of transistors obtained from P3HT solutions in $CHCl_3$ that have been ultrasonically irradiated in air bear a remarkable resemblance to those obtained in the presence of an oxygen atmosphere, Figure 62.[71] In fact, a similar output characteristic is also obtained from the OFETs prepared from irradiated solutions inside the glove-box, which have not been subjected to thermal annealing, Figure 62. This result raises the possibility that the increase in mobility observed upon ultrasonic irradiation is one of doping by molecular oxygen rather than one associated with structural changes. However, "de-doping" experiments performed either by thermal annealing (Figure 54(b) or by placing and testing the samples under high vacuum (ca. 10^{-8} Torr) resulted in output characteristics curves that no longer

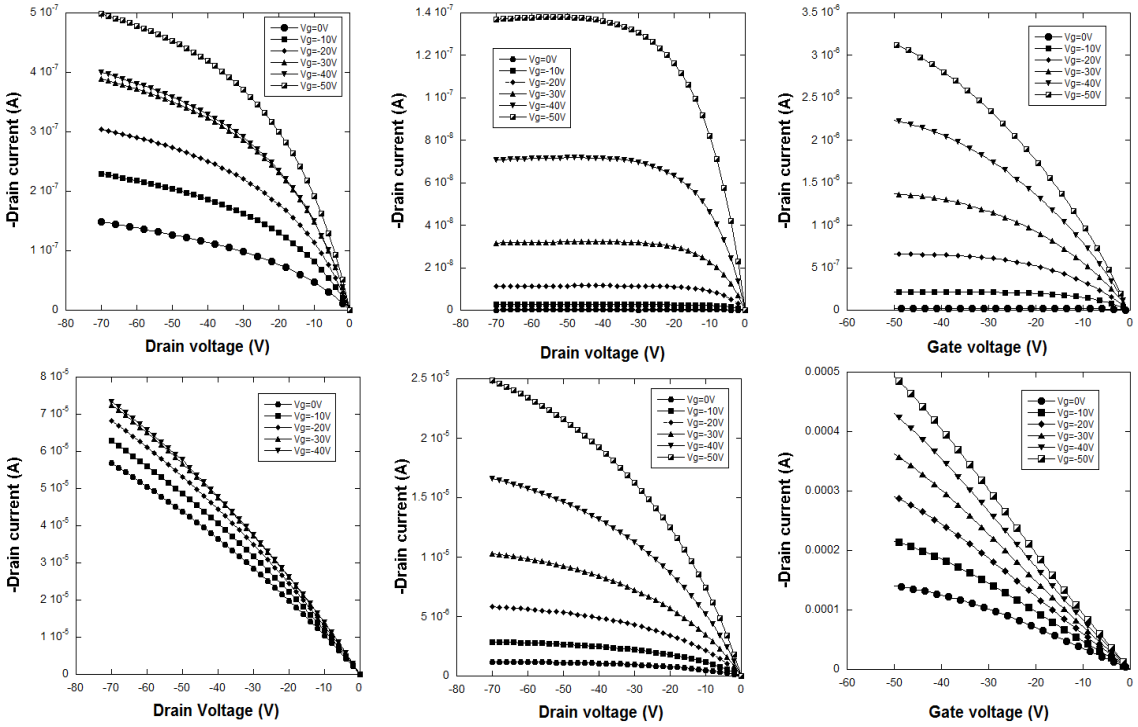

Figure 62: Output characteristics of HT94 based OFETs prepared by spin coating from P3HT solutions without (top row) and with (bottom row) ultrasonic irradiation. (a) Prepared and tested in air (b) Prepared in air, but tested under a dynamic vacuum of 10^{-8} Torr and (c) prepared and tested in a nitrogen glove-box. All samples tested without any thermal annealing.

bore resemblance to the effects of oxygen exposure, without a significant reduction of the original increase in field effect mobility. This observation gives credence to our original hypothesis that the improvement in P3HT charge transport characteristics are a direct result of improved thin film microstructural quality, although the role of oxidation effects in mediating the formation of the ordered structures cannot be ruled out.

5.4 Conclusion

The results presented in this section highlight an interesting inter-play between the individual roles of ultrasound induced pre-assembled aggregates in solution, molecular parameters such as regioregularity and the dynamics of the film formation process

itself. An order of magnitude increase in field effect mobility is routinely observed upon ultrasonication of the lower regioregularity (ca. 94% H-T) polymer, irrespective of the deposition method used. Whilst the changes in thin film morphology and crystallinity observed upon ultrasonication of 98% H-T P3HT are similar to those obtained from the lower regioregularity polymer, the enhancement of mobility is far less dramatic. Dip coating of P3HT films obtained from pristine solutions clearly result in the formation of ordered nanofibrillar structures which are clearly absent in the featureless spin coated counterparts, with its impact on the mobility dependent on the regioregularity of the polymer used. Thus, we suggest that although the dynamics of film formation process clearly influence the morphology and charge transport, it is the polymer regioregularity which has a dominant influence. The dependencies we have reported not only identifies the competition between process parameters and molecular parameters, but also provide a stimulus for further investigations into the role of intra-chain effects in controlling macroscopic charge transport.

CHAPTER VI

CONCLUSIONS

The primary objective of this thesis was to elucidate the complex correlations between thin film microstructure and the corresponding macroscopic charge transport properties in OFETs made from these films. Our goal was oriented towards addressing some of the questions raised in Figure 63.

We started our investigation in Chapter 2 by understanding how the microstructure evolves when going from the solution state to the solid state, especially since the polymer chain conformations in the solution form an important precedent to solid state microstructure. We identified a lyotropic liquid crystalline phase as an intermediate between the isotropic solution state and the final solidified microstructure. The structural changes were found to correspond well with the evolution of drain current in an evaporating P3HT/TCB solution, raising the possibility that the presence of long range order possibly induces enhanced charge transport. This was also corroborated by the the time evolution of the field effect mobility in an evaporating droplet of P3HT in $CHCl_3$ (Section2.1), which shows a sharp peak, before eventually decreasing, once again hinting at correlations with the structural evolution in the evaporating droplet. Our joint *in situ* investigation of the evolution of drain current and structure in Section 2.3 revealed that there is a close correspondence between the evolution of single chain conformation (conjugation) and the sharp increase of the drain current in the evaporating P3HT/TCB droplet. More importantly, the sharp onset of the current is observed even though a significant amount of solvent remains in the film creating an isotropic solution phase. This study is important on several

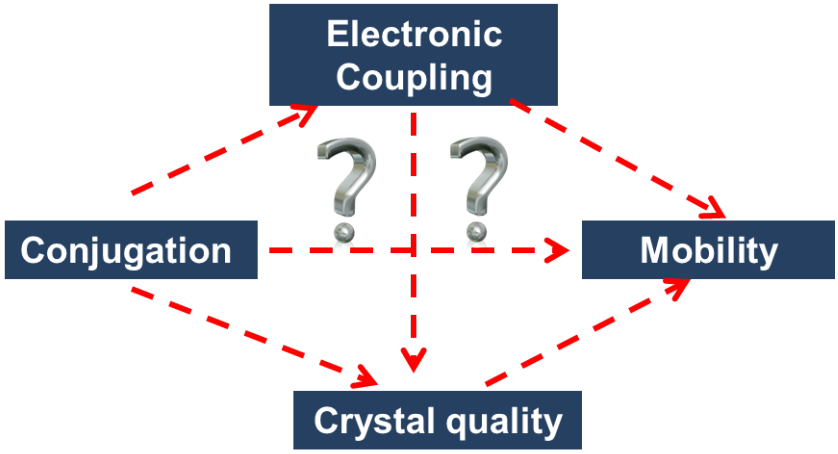

Figure 63: The role of microscopic factors in macroscopic charge transport

counts.The presence of a lyotropic liquid crystalline phase can have important implications for enhanced charge transport motivated by long range order. The fact that the liquid crystallinity is observed through a simple self-assembly route mediated through solvent evaporation suggests that macroscopic morphology control can be achieved through simple means for conjugated polymers. The concurrent evolution of structure and current provides a fundamental insight into how the development of drain current corresponds with the development of single chain conformation and eventually supramolecular assemblies into crystallites.

Chapter 3 then investigates single chain effects in P3HT, using regioregularity as an effective "handle" to manipulate the thin film morphology. We demonstrate that subtle variations in the regioregularity as small as ca. 4% is sufficient to dramatically alter the field effect mobility by as much as two orders of magnitude. The concurrent variations noted in the absorption spectra of HT94 and HT98 P3HT films suggest that effects at the single molecule level, i.e. conjugation, may be responsible for both the changes in morphology (nanofibrillar width) as well as enhanced interchain polaron delocalization due to a reduced reorganization energy. The increase in intrachain order is also accompanied by variations in nanofibrillar widths, which then result in a reduced areal fraction of grain boundaries and thus could be a secondary

mechanism for rationalizing the dramatic improvement in mobility. The results presented in this chapter clearly point at the dominant role of single chain effects. It follows how changes of polymer chain conformation can severely impact assembly into supramolecular structures with subsequent changes to macroscopic charge transport. It also highlights the importance of *intra*-chain effects relative to *inter*-chain effects.

Chapter 4 explores novel methods of creating supramolecular order through the generation of ultrasound induced microcrystallized aggregates in solution. The resulting films display a multiphase morphology consisting of disordered, quasi-ordered and ordered phases that result in a percolation type charge transport mechanism, where the mobility becomes independent of the microstructure beyond a "threshold" crystallinity. Not only is ultrasonic irradiation a facile method for enhancing charge transport in polymeric semiconductors, but it is also a useful tool for clarifying the complex correlations between microstructure and charge transport. Chapter 5 extends the work in Chapter 4 to explore the impact of molecular parameters such as polymer regioregularity and processing parameters such as the solvent and film deposition method on the ultrasound induced aggregation process. We demonstrated that the molecular aggregation process itself is strongly dependent on factors such as solubility of the polymer in the solvent. More importantly, although we suggested that the ordered precursors are formed in the solution state, the deposition method used (dip coating vs spin coating) clearly impacts the morphology as well, hinting at the dual role of solvent-solute as well solute-solvent-substrate interactions in creating the ordered morphology. However, as noted in Chapter 4, in spite of the significant differences noted in the morphology, the differences in mobility are far less dramatic, reaffirming our suggestion that the disorder clearly dominates the charge transport mechanism.

In summary, this thesis explores microstructure-charge transport correlations using P3HT as a model system and demonstrates that the structural heterogeneity of

conjugated polymer thin films results in a percolation type charge transport mechanism, characterized by the saturation of the mobility beyond a "threshold crystallinity". Moreover, new approaches have been presented to not only provide understanding of these correlations, but also the very process of film formation in solution processable organic semiconductors, which could in turn hold the key to approaching the mobility benchmark represented by single crystals.

6.1 Future work

Although the results presented here lead to a significant clarification of the role of microstructure in influencing charge transport, further experiments must be conducted to elucidate the fundamental nature of carrier transport.

In order to accomplish these goals, experiments must be conducted at all length scales starting from the nano-scale all the way to the macro-scale, as depicted in Figure 64. Experimental techniques such as microwave conductivity (PRMC) described in Chapter 1, which can probe the movement of charge carriers across single polymer chains could be invaluable in further understanding the single chain effects described in Chapter 3 and coupled with OFET measurements could provide a holistic picture of charge transport in organic semiconductors that accounts for *intra*- as well as *inter*-chain effects.

Liquid crystallinity is an attractive route towards achievement of high macroscopic mobilities and further experiments on "quenching" the intermediate anisotropically ordered phase in the course of evaporative self-assembly of the P3HT chains, could prove a facile approach to achieving the macroscopic alignment necessary. This could potentially be achieved by replacing 1,2,4-Trichlorobenzene with 1,3,5-Trichlorobenzene, the latter being a solid at room temperature (melting point 63-63°C). Thus, conducting the experiment described in Section 2.2 at temperatures above the melting point of 1,3,5-TCB would enable the liquid crystalline phase (when

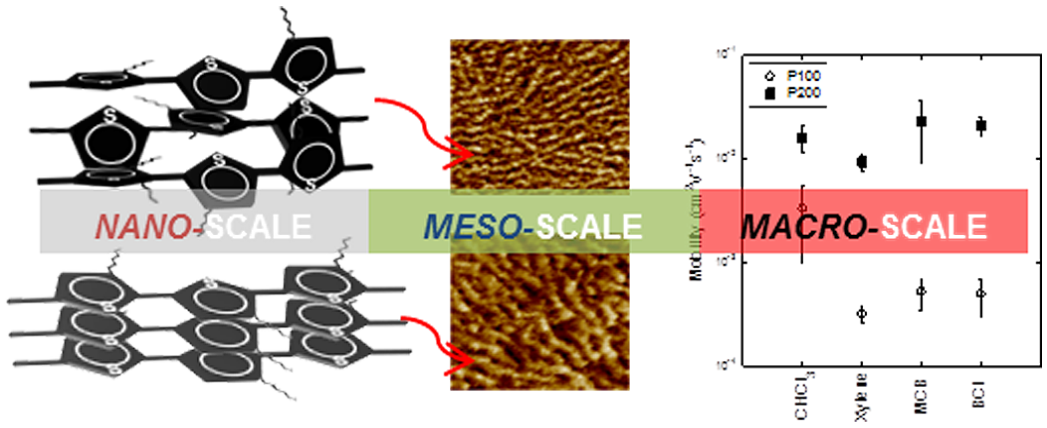

Figure 64: Probing charge transport across length scales: Nano-scale to the macro-scale

observed) to be quenched by cooling the solution down to room temperature.

In-situ optical spectroscopy experiments on an electrostatically doped organic semiconductor, such as those performed by Kaake et.al.[164], could prove escpecially useful in further understanding the percolation mechanism reported in Chapter 4. Kaake et.al. are able to identify the presence of hole polarons in P3HT in two distinct environments: amorphous and crystalline. Applying similar measurements to multiphase systems generated by ultrasonic irradiation might provide fundamental insights into how the presence of order and disorder impacts the delocalization of hole polarons. Varying the gate dielectric by incorporating polymeric insulators would yield further information on the impact of dielectric constant on the carrier delocalization.

Finally, other molecular designs must be investigated as well in order to create charge transport mechanisms and models that are universally applicable to polymeric semiconductors at large. Such an understanding would truly enable us to realize the potential shown by organic semiconductors.

References

[1] Wikipedia. Stephen Gray, 2011. URL `http://en.wikipedia.org/wiki/Stephen_Gray_(scientist)`. [Online; accessed August-2011].

[2] Wikipedia. Cat's Whisker Diode, 2011. URL `http://en.wikipedia.org/wiki/Cat%27s_whisker_diode`. [Online; accessed August-2011].

[3] J.A. Rogers, Z. Bao, K. Baldwin, A. Dodabalapur, B. Crone, V.R. Raju, V. Kuck, H. Katz, K. Amundson, and J. Ewing. Paper-like electronic displays: Large-area rubber-stamped plastic sheets of electronics and microencapsulated electrophoretic inks. *P. Natl. Acad. Sci.*, 98(9):4835, 2001.

[4] Y. Sun and J.A. Rogers. Inorganic semiconductors for flexible electronics. *Adv. Mater.*, 19(15):1897–1916, 2007.

[5] Wikipedia. Printed Electronics, 2011. URL `http://en.wikipedia.org/wiki/Printed_electronics`. [Online; accessed August-2011].

[6] H. Sirringhaus, N. Tessler, and R. H. Friend. Integrated optoelectronic devices based on conjugated polymers. *Science*, 280(5370):1741–1744, 1998.

[7] C. Wang, H. Dong, W. Hu, Y. Liu, and D. Zhu. Semiconducting π-conjugated systems in field-effect transistors: A material odyssey of organic electronics. *Chem. Rev.*, 2011.

[8] N.C. Greenham and R. H. Friend. *Semiconductor Device Physics of Conjugated Polymers*, volume Volume 49. Academic Press, 1996.

[9] R.H. Friend, R.W. Gymer, A.B. Holmes, J.H. Burroughes, R.N. Marks, C. Taliani, D.D.C. Bradley, D.A. Santos, J.L. Bredas, and M. Logdlund. Electroluminescence in conjugated polymers. *Nature*, 397(6715):121–128, 1999.

[10] C.J. Brabec, N.S. Sariciftci, and J.C. Hummelen. Plastic solar cells. *Adv. Func. Mater.*, 11(1):15–26, 2001.

[11] J.R. Sheats. Manufacturing and commercialization issues in organic electronics. *J. Mater. Res.*, 19(07):1974–1989, 2004.

[12] Z. Bao, J. A. Rogers, and H. E. Katz. Printable organic and polymeric semiconducting materials and devices. *J. Mater. Chem.*, 9(9):1895–1904, 1999.

[13] Organic Electronics Association (OE-A). Organic and printed electronics, 2011. URL `http://www.vdma.org/oe-a`. [Online; accessed August-2011].

[14] T.N. Jackson. Organic semiconductors: Beyond moore's law. *Nat. Mater.*, 4 (8):581–582, 2005.

[15] LG Electronics. Oled tv by lg, 2011. URL http://www.lg.com/ae/home-entertainment/buyer-guide/what-is-oled-tv-is-it-a-new-generational-type-of-tv.jsp. [Online; accessed August-2011].

[16] W. R. Salaneck, R. H. Friend, and J. L. Bredas. Electronic structure of conjugated polymers: consequences of electron-lattice coupling. *Phys. Rep.*, 319(6): 231–251, 1999.

[17] J. L. Bredas and G. B. Street. Polarons, bipolarons, and solitons in conducting polymers. *Accounts Chem. Res.*, 18(10):309–315, 1985.

[18] R.G. Kepler. Charge carrier production and mobility in anthracene crystals. *Phys. Rev.*, 119(4):1226, 1960.

[19] C. K. Chiang, C. R. Fincher, Y. W. Park, A. J. Heeger, H. Shirakawa, E. J. Louis, S. C. Gau, and Alan G. MacDiarmid. Electrical conductivity in doped polyacetylene. *Phys. Rev. Lett.*, 39(17):1098, 1977.

[20] Z. Bao and J.J. Locklin. *Organic Field-Effect Transistors*, volume 128. CRC, 2007.

[21] J. Bredas, J. Cornil, and A.J. Heeger. The exciton binding energy in luminescent conjugated polymers. *Adv. Mater.*, 8(5):447–452, 1996.

[22] V. Coropceanu, J. Cornil, D. A. da Silva Filho, Y. Olivier, R. Silbey, and J. L. Bredas. Charge transport in organic semiconductors. *Chem. Rev.*, 107(4):926–952, 2007.

[23] J.L. Bredas, D. Beljonne, V. Coropceanu, and J. Cornil. Charge-transfer and energy-transfer processes in π-conjugated oligomers and polymers:a molecular picture. *Chem. Rev.*, 104(11):4971–5004, 2004.

[24] V. Podzorov, E. Menard, A. Borissov, V. Kiryukhin, J. A. Rogers, and M. E. Gershenson. Intrinsic charge transport on the surface of organic semiconductors. *Phys. Rev. Lett.*, 93(8):086602, 2004.

[25] J. M. Shaw and P. F. Seidler. Organic electronics: Introduction. *IBM J. Res. Dev.*, 45(1):3–9, 2001.

[26] C.B. Duke and L. B. Schein. Organic solids: is energy-band theory enough? *Phys. Today*, 33(2):42–48, 1980.

[27] H. Sirringhaus. Device physics of solution-processed organic field-effect transistors. *Adv. Mater.*, 17(20):2411–2425, 2005.

[28] N.S. Hush. Adiabatic rate processes at electrodes. i. energy charge relationships. *J. Chem. Phys.*, 28:962, 1958.

[29] R.A. Marcus. On the theory of oxidation reduction reactions involving electron transfer. i. *J. Chem. Phys.*, 24:966, 1956.

[30] H. Bassler. Charge transport in disordered organic photoconductors a monte carlo simulation study. *Phys. Status Solidi B*, 175(1):15–56, 1993.

[31] S.S. Sun and N.S. Sariciftci. *Organic photovoltaics: mechanism, materials, and devices*, volume 99. CRC, 2005.

[32] PN Murgatroyd. Theory of space-charge-limited current enhanced by frenkel effect. *Journal of Physics D: Applied Physics*, 3:151, 1970.

[33] R.A. Street. Thin-film transistors. *Adv. Mater.*, 21(20):2007–2022, 2009.

[34] G. Horowitz. Organic field-effect transistors. *Adv. Mater.*, 10(5):365–377, 1998.

[35] Antonio Facchetti. Semiconductors for organic transistors. *Mater. Today*, 10 (3):28–37, 2007.

[36] G. Horowitz, R. Hajlaoui, R. Bourguiga, and M. Hajlaoui. Theory of the organic field-effect transistor. *Synthetic Met.*, 101(1-3):401–404, 1999.

[37] G. Horowitz, R. Hajlaoui, D. Fichou, and A. El Kassmi. Gate voltage dependent mobility of oligothiophene field-effect transistors. *J. Appl. Phys.*, 85(6):3202–3206, 1999.

[38] A.L. Briseno, S.C.B. Mannsfeld, M.M. Ling, S. Liu, R.J. Tseng, C. Reese, M.E. Roberts, Y. Yang, F. Wudl, and Z. Bao. Patterning organic single-crystal transistor arrays. *Nature*, 444(7121):913–917, 2006.

[39] A.L. Appleton, S. M. Brombosz, S. Barlow, J.S. Sears, J.L. Bredas, S.R. Marder, and U.H. F. Bunz. Effects of electronegative substitution on the optical and electronic properties of acenes and diazaacenes. *Nat. Commun.*, 1(7):91, 2011.

[40] I. McCulloch. Thin films: Rolling out organic electronics. *Nat. Mater.*, 4(8): 583–584, 2005. 10.1038/nmat1443.

[41] Z. Bao, A. Dodabalapur, and A.J. Lovinger. Soluble and processable regioregular poly(3-hexylthiophene) for thin film field-effect transistor applications with high mobility. *Appl. Phys. Lett.*, 69(26):4108–4110, 1996.

[42] A. Tsumura, H. Koezuka, and T. Ando. Macromolecular electronic device: Field-effect transistor with a polythiophene thin film. *Appl. Phys. Lett.*, 49(18): 1210–1212, 1986.

[43] R. L. Elsenbaumer, K. Y. Jen, G. G. Miller, and L. W. Shacklette. Processible, environmentally stable, highly conductive forms of polythiophene. *Synthetic Met.*, 18(1-3):277–282, 1987.

[44] Richard D. McCullough, Renae D. Lowe, Manikandan Jayaraman, and Deborah L. Anderson. Design, synthesis, and control of conducting polymer architectures: structurally homogeneous poly(3-alkylthiophenes). *J. Org. Chem.*, 58 (4):904–912, 1993.

[45] I. McCulloch, M. Heeney, C. Bailey, K. Genevicius, I. MacDonald, M. Shkunov, D. Sparrowe, S. Tierney, R. Wagner, and W. Zhang. Liquid-crystalline semiconducting polymers with high charge-carrier mobility. *Nat. Mater.*, 5(4):328–333, 2006.

[46] J. F. Chang, B. Sun, D. W. Breiby, M. M. Nielsen, T. I. Solling, M. Giles, I. McCulloch, and H. Sirringhaus. Enhanced mobility of poly(3-hexylthiophene) transistors by spin-coating from high-boiling-point solvents. *Chem. Mater.*, 16 (23):4772–4776, 2004.

[47] M. Surin, Ph. Leclere, R. Lazzaroni, J. D. Yuen, G. Wang, D. Moses, A. J. Heeger, S. Cho, and K. Lee. Relationship between the microscopic morphology and the charge transport properties in poly(3-hexylthiophene) field-effect transistors. *J. Appl. Phys.*, 100(3):033712–1–033712–6, 2006.

[48] A. Babel and S. A. Jenekhe. Alkyl chain length dependence of the field-effect carrier mobility in regioregular poly(3-alkylthiophene)s. *Synthetic Met.*, 148(2): 169–173, 2005.

[49] H. Sirringhaus, P. J. Brown, R. H. Friend, M. M. Nielsen, K. Bechgaard, B. M. W. Langeveld-Voss, A. J. H. Spiering, R. A. J. Janssen, E. W. Meijer, and P. Herwig. Two-dimensional charge transport in self-organized, high-mobility conjugated polymers. *Nature*, 401(6754):685–688, 1999.

[50] I. Osaka and R.D. McCullough. Advances in molecular design and synthesis of regioregular polythiophenes. *Accounts Chem. Res.*, 41(9):1202–1214, 2008.

[51] A. Zen, J. Pflaum, S. Hirschmann, W. Zhuang, F. Jaiser, U. Asawapirom, J. P. Rabe, U. Scherf, and D. Neher. Effect of molecular weight and annealing of poly (3-hexylthiophene) s on the performance of organic field-effect transistors. *Adv. Funct. Mater.*, 14(8):757–764, 2004.

[52] R. J. Kline, M. D. McGehee, E. N. Kadnikova, J. Liu, and J. M. J. Frchet. Controlling the field-effect mobility of regioregular polythiophene by changing the molecular weight. *Adv. Mater.*, 15(18):1519–1522, 2003.

[53] D. H Kim, Y. D Park, Y. Jang, H. Yang, Y. H Kim, J. I Han, D. G Moon, S. Park, T. Chang, C. Chang, M. Joo, C. Y Ryu, and K. Cho. Enhancement of field-effect mobility due to surface-mediated molecular ordering in regioregular polythiophene thin film transistors. *Adv. Func. Mater.*, 15(1):77–82, 2005.

[54] Y.D. Park, J.H. Cho, D.H. Kim, Y. Jang, H.S. Lee, K. Ihm, T.H. Kang, and K. Cho. Energy-level alignment at interfaces between gold and poly(3-hexylthiophene) films with two different molecular structures. *Electrochemical and Solid-State Letters*, 9(11):G317–G319, 2006.

[55] Brian A. Mattis, Paul C. Chang, and Vivek Subramanian. Performance recovery and optimization of poly(3-hexylthiophene) transistors by thermal cycling. *Synthetic Met.*, 156(18-20):1241–1248, 2006.

[56] M. Muthukumar. *Shifting Paradigms in Polymer Crystallization*, volume 714 of *Lecture Notes in Physics*, pages 1–18. Springer Berlin / Heidelberg, 2007.

[57] R. J. Kline and M. D. McGehee. Morphology and charge transport in conjugated polymers. *Polymer Rev.*, 46(1):27–45, 2006.

[58] D.M. DeLongchamp, B.M. Vogel, Y. Jung, M.C. Gurau, C. A. Richter, O.A. Kirillov, J. Obrzut, D.A. Fischer, S. Sambasivan, L.J. Richter, and E.K. Lin. Variations in semiconducting polymer microstructure and hole mobility with spin-coating speed. *Chem. Mater.*, 17(23):5610–5612, 2005.

[59] H. Yang, T. J. Shin, L. Yang, K. Cho, C. Y. Ryu, and Z. Bao. Effect of mesoscale crystalline structure on the field-effect mobility of regioregular poly (3-hexyl thiophene) in thin-film transistors. *Adv. Funct. Mater.*, 15(4):671–676, 2005.

[60] H. Yang, T. Joo Shin, Z. Bao, and C. Y. Ryu. Structural transitions of nanocrystalline domains in regioregular poly(3-hexyl thiophene) thin films. *J. Polym. Sci. Pol. Phys.*, 45(11):1303–1312, 2007.

[61] T. Q. Nguyen, V. Doan, and B. J. Schwartz. Conjugated polymer aggregates in solution: Control of interchain interactions. *J. Chem. Phys.*, 110:4068, 1999.

[62] M.S. Park, A. Aiyar, J.O. Park, E. Reichmanis, and M. Srinivasarao. Solvent evaporation induced liquid crystalline phase in poly(3-hexylthiophene). *J. Am. Chem. Soc.*, 133(19):7244–7247, 2011.

[63] B. N. Park and et al. Channel formation in single-monolayer pentacene thin film transistors. *J. Phys. D Appl. Phys.*, 40(11):3506, 2007.

[64] M. Tsige and G.S. Grest. Solvent evaporation and interdiffusion in polymer films. *J. Phys.: Condens. Matter*, 17:S4119, 2005.

[65] R.D. Deegan, O. Bakajin, T.F. Dupont, G. Huber, S.R. Nagel, and T.A. Witten. Capillary flow as the cause of ring stains from dried liquid drops. *Nature*, 389 (6653):827–828, 1997.

[66] H. Richardson, C. Carelli, J.L. Keddie, and M. Sferrazza. Structural relaxation of spin-cast glassy polymer thin films as a possible factor in dewetting. *Eur. Phys. J. E Soft Matter*, 12(3):437–441, 2003.

[67] M. Ercken, P. Adriaensens, D. Vanderzande, and J. Gelan. Study of solvent diffusion in polymeric materials using magnetic resonance imaging. *Macromolecules*, 28(25):8541–8547, 1995.

[68] G.D. Cody and R.E. Botto. In-situ analysis and quantification of swelling kinetics in glassy and rubbery networks using 1h and 19f magnetic resonance microscopies. *Macromolecules*, 27(9):2607–2614, 1994.

[69] J. Garcia-Turiel and B. Jerome. Solvent retention in thin polymer films studied by gas chromatography. *Colloid Polym. Sci.*, 285(14):1617–1623, 2007.

[70] S. Hoshino, M. Yoshida, S. Uemura, T. Kodzasa, N. Takada, T. Kamata, and K. Yase. Influence of moisture on device characteristics of polythiophene-based field-effect transistors. *J. Appl. Phys.*, 95:5088, 2004.

[71] M. S. A. Abdou, F. P. Orfino, Y. Son, and S. Holdcroft. Interaction of oxygen with conjugated polymers: Charge transfer complex formation with poly(3-alkylthiophenes). *J. Am. Chem. Soc.*, 119(19):4518–4524, 1997.

[72] M.L. Chabinyc, F. Endicott, B.D. Vogt, D.M. DeLongchamp, E.K. Lin, Y. Wu, P. Liu, and B.S. Ong. Effects of humidity on unencapsulated poly (thiophene) thin-film transistors. *Appl. Phys. Lett.*, 88:113514, 2006.

[73] M. Baibarac, M. Lapkowski, A. Pron, S. Lefrant, and I. Baltog. Sers spectra of poly(3-hexylthiophene) in oxidized and unoxidized states. *J. Raman Spectrosc.*, 29(9):825–832, 1998.

[74] G. Louarn, M. Trznadel, J. P. Buisson, J. Laska, A. Pron, M. Lapkowski, and S. Lefrant. Raman spectroscopic studies of regioregular poly(3-alkylthiophenes). *J. Phys. Chem.*, 100(30):12532–12539, 1996.

[75] Y. Furukawa, M. Akimoto, and I. Harada. Vibrational key bands and electrical conductivity of polythiophene. *Synthetic Met.*, 18(1-3):151–156, 1987.

[76] J. R. Scherer and J. C. Evans. Vibrational spectra and assignments for 16 chlorobenzenes. *Spectrochimica Acta*, 19(11):1739–1775, 1963.

[77] R. J. Kline, M.D. McGehee, and M.F. Toney. Highly oriented crystals at the buried interface in polythiophene thin-film transistors. *Nat. Mater.*, 5(3):222–228, 2006.

[78] J. T. L. Navarrete and G. Zerbi. Lattice-dynamics and vibrational-spectra of polythiophene .1. oligomers and polymers. *J. Chem. Phys.*, 94(2):957–964, 1991.

[79] R. D. Deegan, O. Bakajin, T. F. Dupont, G. Huber, S. R. Nagel, and T. A. Witten. Capillary flow as the cause of ring stains from dried liquid drops. *Nature*, 389(6653):827–829, 1997.

[80] Y. O. Popov and T. A. Witten. Characteristic angles in the wetting of an angular region: Surface shape. *European Physical Journal E*, 6(3):211–220, 2001.

[81] V. Sharma, K. Park, and M. Srinivasarao. Colloidal dispersion of gold nanorods: Historical background, optical properties, seed-mediated synthesis, shape separation and self-assembly. *Materials Science & Engineering R-Reports*, 65(1-3): 1–38, 2009.

[82] S. Laschat, A. Baro, N. Steinke, F. Giesselmann, C. Hagele, G. Scalia, R. Judele, E. Kapatsina, S. Sauer, A. Schreivogel, and M. Tosoni. Discotic liquid crystals: From tailor-made synthesis to plastic electronics. *Angew. Chem. Int. Edit.*, 46 (26):4832–4887, 2007.

[83] P.J. Brown, S.D. Thomas, A. Kohler, J.S. Wilson, J.S. Kim, C.M. Ramsdale, H. Sirringhaus, and R.H. Friend. Effect of interchain interactions on the absorption and emission of poly(3-hexylthiophene). *Phys. Rev. B*, 67(6):064203–1–064203–16, 2003.

[84] S. Hotta, S. D. D. V. Rughooputh, A. J. Heeger, and F. Wudl. Spectroscopic studies of soluble poly(3-alkylthienylenes). *Macromolecules*, 20(1):212–215, 1987.

[85] C. Yang, F. P. Orfino, and S. Holdcroft. A phenomenological model for predicting thermochromism of regioregular and nonregioregular poly(3-alkylthiophenes). *Macromolecules*, 29(20):6510–6517, 1996.

[86] G. Zerbi, B. Chierichetti, and O. Inganas. Thermochromism in polyalkylthiophenes - molecular aspects from vibrational spectroscopy. *J. Chem. Phys.*, 94 (6):4646–4658, 1991.

[87] K. Tashiro, Y. Minagawa, M. Kobayashi, S. Morita, T. Kawai, and K. Yoshino. Structure and thermochromic solid-state phase-transition of poly(3-alkylthiophene) - 3 effects of alkyl side-chain length on the phase transitional behavior. *Synthetic Met.*, 55(1):321–328, 1993.

[88] W. C. Tsoi, D. T. James, J. S. Kim, P. G. Nicholson, Nurphy C. E., D. D. C. Bradley, J. Nelson, and J-S. Kim. The nature of in-plane skeleton raman modes of p3ht and their correlation to the degree of molecular order in p3ht:pcbm blend thin films. *J. Am. Chem. Soc.*, 133(25):9834–9843, 2011.

[89] Y. Q. Gao and J. K. Grey. Resonance chemical imaging of polythiophene/fullerene photovoltaic thin films: Mapping morphology-dependent aggregated and unaggregated c=c species. *J. Am. Chem. Soc.*, 131(28):9654–9662, 2009.

[90] R. A. Street, J. E. Northrup, and A. Salleo. Transport in polycrystalline polymer thin-film transistors. *Physical Review B*, 71(16):165202, 2005.

[91] F. Garnier, G. Horowitz, X. Z. Peng, and D. Fichou. Structural basis for high carrier mobility in conjugated oligomers. *Synthetic Metals*, 45(2):163–171, 1991.

[92] R.D. McCullough, R.D. Lowe, M. Jayaraman, and D.L. Anderson. Design, synthesis, and control of conducting polymer architectures: structurally homogeneous poly(3-alkylthiophenes). *J. Org. Chem.*, 58(4):904–912, 1993.

[93] A.R. Aiyar, J.I. Hong, R. Nambiar, D.M. Collard, and E. Reichmanis. Tunable crystallinity in regioregular poly(3-hexylthiophene) thin films and its impact on field effect mobility. *Adv. Func. Mater.*, 21(14):2652, 2011.

[94] R. Zhang, B. Li, M. C. Iovu, M. Jeffries-El, G. Sauve, J. Cooper, S. Jia, S. Tristram-Nagle, D. M. Smilgies, and D. N. Lambeth. Nanostructure dependence of field-effect mobility in regioregular poly (3-hexylthiophene) thin film field effect transistors. *J. Am. Chem. Soc.*, 128(11):3480–3481, 2006.

[95] Y. Kim, S. Cook, S.M. Tuladhar, S.A. Choulis, J. Nelson, J.R. Durrant, D. D. C. Bradley, M. Giles, I. McCulloch, C.S. Ha, and M. Ree. A strong regioregularity effect in self-organizing conjugated polymer films and high-efficiency polythiophene:fullerene solar cells. *Nat. Mater.*, 5(3):197–203, 2006.

[96] J.F. Chang, J. Clark, N. Zhao, H. Sirringhaus, D.W. Breiby, J.W. Andreasen, M.M. Nielsen, M. Giles, M. Heeney, and I. McCulloch. Molecular-weight dependence of interchain polaron delocalization and exciton bandwidth in high-mobility conjugated polymers. *Phys. Rev. B*, 74(11):115318, 2006.

[97] R. J. Kline, M. D. McGehee, E. N. Kadnikova, J. Liu, J. M. J. Frechet, and M. F. Toney. Dependence of regioregular poly (3-hexylthiophene) film morphology and field-effect mobility on molecular weight. *Macromolecules*, 38(8):3312–3319, 2005.

[98] F. C. Grozema, P. T. Van Duijnen, Y. A. Berlin, M. A. Ratner, and L. D. A. Siebbeles. Intramolecular charge transport along isolated chains of conjugated polymers: effect of torsional disorder and polymerization defects. *J. Phys. Chem. B*, 106(32):7791–7795, 2002.

[99] J. L. Bredas, G. B. Street, B. Themans, and J. M. Andre. Organic polymers based on aromatic rings (polyparaphenylene, polypyrrole, polythiophene): Evolution of the electronic properties as a function of the torsion angle between adjacent rings. *J. Chem. Phys.*, 83(3):1323–1329, 1985.

[100] S.S. Zade and M. Bendikov. Twisting of conjugated oligomers and polymers: Case study of oligo- and polythiophene. *Chem.-European J.*, 13(13):3688–3700, 2007.

[101] R. D. McCullough. The chemistry of conducting polythiophenes. *Adv. Mater.*, 10(2):93–116, 1998.

[102] C. Roux and M. Leclerc. Thermochromic properties of polythiophene derivatives: Formation of localized and delocalized conformational defects. *Chem. Mater.*, 6(5):620–624, 1994.

[103] F.C. Spano. Absorption in regio-regular poly(3-hexyl)thiophene thin films: Fermi resonances, interband coupling and disorder. *Chem. Phys.*, 325(1):22–35, 2006.

[104] R. F. Pierret. *Field Effect Devices*. Prentice Hall, 1990.

[105] A.R. Volkel, R. A. Street, and D. Knipp. Carrier transport and density of state distributions in pentacene transistors. *Physical Review B*, 66(19):195336, 2002.

[106] H. Sirringhaus, N. Tessler, D. Thomas, P. Brown, and R. Friend. *High-mobility conjugated polymer field-effect transistors*, volume 39 of *Advances in Solid State Physics*, pages 101–110. Springer Berlin / Heidelberg, 1999.

[107] L.L. Chua, J. Zaumseil, J. F. Chang, E.C.W. Ou, P.K.H. Ho, H. Sirringhaus, and R. H. Friend. General observation of n-type field-effect behaviour in organic semiconductors. *Nature*, 434(7030):194, 2005.

[108] M. Sundberg, O. Inganas, S. Stafstrom, G. Gustafsson, and B. Sjogren. Optical-absorption of poly(3-alkylthiophenes) at low-temperatures. *Solid State Communications*, 71(6):435–439, 1989.

[109] M. Belletete, L. Mazerolle, N. Desrosiers, M. Leclerc, and G. Durocher. Spectroscopy and photophysics of some oligomers and polymers derived from thiophenes. *Macromolecules*, 28(25):8587–8597, 1995.

[110] J. Clark, C. Silva, R.H. Friend, and F.C. Spano. Role of intermolecular coupling in the photophysics of disordered organic semiconductors: Aggregate emission in regioregular polythiophene. *Phys. Rev. Lett.*, 98(20):206406, 2007.

[111] D. Beljonne, J. Cornil, R. Silbey, P. Millie, and J. L. Bredas. Interchain interactions in conjugated materials: The exciton model versus the supermolecular approach. *J. Chem. Phys.*, 112(10):4749–4758, 2000.

[112] T. Yamamoto, D. Komarudin, M. Arai, B. L. Lee, H. Suganuma, N. Asakawa, Y. Inoue, K. Kubota, S. Sasaki, and T. Fukuda. Extensive studies on [pi]-stacking of poly (3-alkylthiophene-2, 5-diyl) s and poly (4-alkylthiazole-2, 5-diyl) s by optical spectroscopy, nmr analysis, light scattering analysis, and x-ray crystallography. *J. Am. Chem. Soc.*, 120(9):2047–2058, 1998.

[113] S. Rughooputh, S. Hotta, A. J. Heeger, and F. Wudl. Chromism of soluble polythienylenes. *J. Polym. Sci. Pol. Phys.*, 25(5):1071–1078, 1987.

[114] W. Barford. Exciton transfer integrals between polymer chains. *J. Chem. Phys.*, 126(13):134905, 2007.

[115] K.J. Ihn, J. Moulton, and P. Smith. Whiskers of poly(3-alkylthiophene)s. *J. Polym. Sci. Pol. Phys.*, 31(6):735–742, 1993.

[116] G.W. Heffner and D.S. Pearson. Molecular characterization of poly(3-hexylthiophene). *Macromolecules*, 24(23):6295–6299, 1991.

[117] J. Liu, R.S. Loewe, and R.D. McCullough. Employing maldi-ms on poly(alkylthiophenes):analysis of molecular weights, molecular weight distributions, end-group structures, and end-group modifications. *Macromolecules*, 32(18):5777–5785, 1999.

[118] F. C. Grozema, L. D. A. Siebbeles, J. M. Warman, S. Seki, S. Tagawa, and U. Scherf. Hole conduction along molecular wires: ?-bonded silicon versus ?-bond-conjugated carbon. *Adv. Mater.*, 14(3):228–231, 2002.

[119] J.L. Bredas, D. Beljonne, V. Coropceanu, and J. Cornil. Charge-transfer and energy-transfer processes in π-conjugated oligomers and polymers: A molecular picture. *Chem. Rev.*, 104(11):4971–5004, 2004.

[120] G.R. Hutchison, M.A. Ratner, and T.J. Marks. Hopping transport in conductive heterocyclic oligomers:? reorganization energies and substituent effects. *J. Am. Chem. Soc.*, 127(7):2339–2350, 2005.

[121] G. Horowitz and M. E. Hajlaoui. Mobility in polycrystalline oligothiophene field-effect transistors dependent on grain size. *Adv. Mater.*, 12(14):1046–1050, 2000.

[122] J. Gierschner, Y.S. Huang, B. Van Averbeke, J. Cornil, R.H. Friend, and D. Beljonne. Excitonic versus electronic couplings in molecular assemblies: The importance of non-nearest neighbor interactions. *J. Chem. Phys.*, 130(4): 044105, 2009.

[123] T. J. Prosa, M. J. Winokur, J. Moulton, P. Smith, and A. J. Heeger. X-ray structural studies of poly (3-alkylthiophenes): an example of an inverse comb. *Macromolecules*, 25(17):4364–4372, 1992.

[124] R. D. McCullough, R. D. Lowe, M. Jayaraman, and D. L. Anderson. Design, synthesis, and control of conducting polymer architectures: structurally homogeneous poly (3-alkylthiophenes). *J. Org. Chem.*, 58(4):904–912, 1993.

[125] N. Kiriy, E. Jhne, H. J. Adler, M. Schneider, A. Kiriy, G. Gorodyska, S. Minko, D. Jehnichen, P. Simon, and A. A. Fokin. One-dimensional aggregation of regioregular polyalkylthiophenes. *Nano Lett.*, 3(6):707–712, 2003.

[126] S. Berson, R. De Bettignies, S. Bailly, and S. Guillerez. Poly(3-hexylthiophene) fibers for photovoltaic applications. *Adv. Funct. Mater.*, 17(8):1377–1384, 2007.

[127] Y. D. Park, H.S. Lee, Y.J. Choi, D. Kwak, J.H. Cho, S. Lee, and K. Cho. Solubility-induced ordered polythiophene precursors for high-performance organic thin-film transistors. *Adv. Funct. Mater.*, 19(8):1200–1206, 2009.

[128] T.A. Chen, X. Wu, and R.D. Rieke. Regiocontrolled synthesis of poly(3-alkylthiophenes) mediated by rieke zinc: Their characterization and solid-state properties. *J. Am. Chem. Soc.*, 117(1):233–244, 1995.

[129] H. Yang, S.W. LeFevre, C.Y. Ryu, and Z. Bao. Solubility-driven thin film structures of regioregular poly(3-hexyl thiophene) using volatile solvents. *Appl. Phys. Lett.*, 90(17):172116–1–172116–3, 2007.

[130] M.L. Chabinyc. X-ray scattering from films of semiconducting polymers. *Polym. Rev.*, 48(3):463–492, 2008.

[131] I. Horcas, R. Fernandez, J. M. Gomez-Rodriguez, J. Colchero, J. Gomez-Herrero, and A. M. Baro. Wsxm: A software for scanning probe microscopy and a tool for nanotechnology. *Rev. Sci. Instrum.*, 78(1):013705–1–013705–8, 2007.

[132] J. N. Coleman, S. Curran, A. B. Dalton, A. P. Davey, B. McCarthy, W. Blau, and R. C. Barklie. Percolation-dominated conductivity in a conjugated-polymer-carbon-nanotube composite. *Phys. Rev. B*, 58(12):R7492–R7495, 1998.

[133] M. Zhang, J. Xu, H. Zeng, Q. Huo, Z. Zhang, F. Yun, and K. Friedrich. Fractal approach to the critical filler volume fraction of an electrically conductive polymer composite. *J. Mater. Sci.*, 30(17):4226–4232, 1995.

[134] F. Dinelli, M. Murgia, P. Levy, M. Cavallini, F. Biscarini, and D. M. de Leeuw. Spatially correlated charge transport in organic thin film transistors. *Phys. Rev. Lett.*, 92(11):116802–1–116802–4, 2004.

[135] K. Zhao, L. Xue, J. Liu, X. Gao, S. Wu, Y. Han, and Y. Geng. A new method to improve poly(3-hexyl thiophene) (p3ht) crystalline behavior: Decreasing chains entanglement to promote orderdisorder transformation in solution. *Langmuir*, 26(1):471–477, 2009.

[136] B.G. Kim, M.S. Kim, and J. Kim. Ultrasonic-assisted nanodimensional self-assembly of poly-3-hexylthiophene for organic photovoltaic cells. *ACS Nano*, 4 (4):2160–2166, 2010.

[137] M. J. Winokur, D. Spiegel, Y. Kim, S. Hotta, and A. J. Heeger. Structural and absorption studies of the thermochromic transition in poly(3-hexylthiophene). *Synthetic Met.*, 28(1-2):419–426, 1989.

[138] M. C. Gurau, D. M. Delongchamp, B. M. Vogel, E. K. Lin, D. A. Fischer, S. Sambasivan, and L. J. Richter. Measuring molecular order in poly (3-alkylthiophene) thin films with polarizing spectroscopies. *Langmuir*, 23(2): 834–842, 2007.

[139] S. Rughooputh, S. Hotta, A. J. Heeger, and F. Wudl. Chromism of soluble polythienylenes. *J. Polym. Sci. Pol. Phys.*, 25(5):1071–1078, 1987.

[140] G. Lu and X. Yang. Improving performance of polymer photovoltaic devices using an annealing-free approach via construction of ordered aggregates in solution. *J. Mater. Chem.*, 18(17):1984–1990, 2008.

[141] A. J. Moul and K. Meerholz. Controlling morphology in polymer-fullerene mixtures. *Adv. Mater.*, 20(2):240–245, 2008.

[142] S.R. Amrutha and M. Jayakannan. Control of π-stacking for highly emissive poly (p-phenylenevinylene) s: Synthesis and photoluminescence of new tricyclodecane substituted bulky poly (p-phenylenevinylene) s and its copolymers. *J. Phys. Chem. B*, 110(9):4083–4091, 2006.

[143] T. Q. Nguyen, R. Y. Yee, and B. J. Schwartz. Solution processing of conjugated polymers: the effects of polymer solubility on the morphology and electronic properties of semiconducting polymer films. *J. Photoch. Photobio. A*, 144(1): 21–30, 2001.

[144] S. Malik, T. Jana, and A.K. Nandi. Thermoreversible gelation of regioregular poly(3-hexylthiophene) in xylene. *Macromolecules*, 34(2):275–282, 2000.

[145] V. Hernandez, J. Casado, F. J. Ramirez, G. Zotti, Hotta Shu, and J. T. Lopez Navarrete. Efficient pi electrons delocalization in alpha,alpha [prime]-dimethyl end-capped oligothiophenes: A vibrational spectroscopic study. *J. Chem. Phys.*, 104(23):9271–9282, 1996.

[146] M. Angelopoulos, R.A. DiPietro, and J.M. Shaw. Vibrational methods of deaggregation of electrically conductive polymers and precursors thereof. *US Patent 6139778,*, 2000.

[147] K. S. Suslick and G. J. Price. Applications of ultrasound to materials chemistry. *Annu. Rev. Mater. Sci.*, 29(1):295–326, 1999.

[148] D. Peters. Ultrasound in materials chemistry. *J. Mater. Chem.*, 6(10):1605–1618, 1996.

[149] S. Guo, Y. Li, G. Chen, and H. Li. Ultrasonic improvement of rheological and processing behaviour of lldpe during extrusion. *Polym. Int.*, 52(1):68–73, 2003.

[150] Y. Chen and H. Li. Mechanism for effect of ultrasound on polymer melt in extrusion. *J. Polym. Sci. Pol. Phys.*, 45(10):1226–1233, 2007.

[151] E.K. Hill, B. Krebs, D.G. Goodall, G.J. Howlett, and D.E. Dunstan. Shear flow induces amyloid fibril formation. *Biomacromolecules*, 7(1):10–13, 2005.

[152] A.V. Filippov, G. Grobner, and O.N. Antzutkin. Aggregation of amyloid aβ(140) peptide in perdeuterated 2,2,2-trifluoroethanol caused by ultrasound sonication. *Magn. Reson. Chem.*, 48(6):427–434, 2010.

[153] S. Samitsu, T. Shimomura, S.i Heike, T. Hashizume, and K. Ito. Effective production of poly(3-alkylthiophene) nanofibers by means of whisker method using anisole solvent: Structural, optical, and electrical properties. *Macromolecules*, 41(21):8000–8010, 2008.

[154] R.S. Tu and V. Breedveld. Microrheological detection of protein unfolding. *Phys. Rev. E*, 72(4):041914–1–041914–5, 2005.

[155] G. Wang, T. Hirasa, D. Moses, and A. J. Heeger. Fabrication of regioregular poly(3-hexylthiophene) field-effect transistors by dip-coating. *Synthetic Met.*, 146(2):127–132, 2004.

[156] D. Janssen, R. De Palma, S. Verlaak, P. Heremans, and W. Dehaen. Static solvent contact angle measurements, surface free energy and wettability determination of various self-assembled monolayers on silicon dioxide. *Thin Solid Films*, 515(4):1433–1438, 2006.

[157] R. Rawcliffe, M. Shkunov, M. Heeney, S. Tierney, I. McCulloch, and A. Campbell. Organic field-effect transistors of poly(2,5-bis(3-dodecylthiophen-2-yl)thieno[2,3-b]thiophene) deposited on five different silane self-assembled monolayers. *Chem. Comm.*, (7):871–873, 2008.

[158] X. T. Hao, T. Hosokai, N. Mitsuo, S. Kera, K. K. Okudaira, K. Mase, and N. Ueno. Control of the interchain $\pi?\pi$ interaction and electron density distribution at the surface of conjugated poly(3-hexylthiophene) thin films. *J. Phys. Chem. B*, 111(35):10365–10372, 2007.

[159] H. G. O. Sandberg, G. L. Frey, M. N. Shkunov, H. Sirringhaus, R. H. Friend, M. M. Nielsen, and C. Kumpf. Ultrathin regioregular poly(3-hexyl thiophene) field-effect transistors. *Langmuir*, 18(26):10176–10182, 2002.

[160] A.R. Aiyar, J.I. Hong, J. Izumi, and E. Reichmanis. A dramatic effect of regioregularity on the nanostructure and charge transport in two dimensional supramolecular assemblies of polythiophenes. *Chem. Mater.*, Under review, 2011.

[161] A. Dodabalapur, L. Torsi, and H. E. Katz. Organic transistors: Two-dimensional transport and improved electrical characteristics. *Science*, 268 (5208):270, 1995.

[162] G. Wang, J. Swensen, D. Moses, and A.J. Heeger. Increased mobility from regioregular poly (3-hexylthiophene) field-effect transistors. *J. Appl. Phys.*, 93 (10):6137–6141, 2003.

[163] H. B. Briggs, J. B. Johnson, and W. P. Mason. Properties of liquids at high sound pressure. *J. Acoust. Soc. Am.*, 19(4):664–677, 1947.

[164] L. G. Kaake and X. Y. Zhu. Charge transport, nanostructure, and the mott insulator-to-metal transition in poly(3-hexylthiophene). *J. Phys. Chem. C*, 112 (42):16174–16177, 2008.

VITA

Avishek Aiyar was born and raised in Calcutta, West Bengal, India. He received his B.Tech in Chemical Engineering from the AC College of Technology, Anna University, Chennai in 2005, upon completion of which he enrolled in the graduate program in Chemical Engineering at Georgia Tech. He completed his MS in Chemical Engineering working with Prof. Mark G. Allen, focusing on microfabrication of polymer MEMS based flow sensors for detection of trapped vorticity. He then joined the research group of Prof. Elsa Reichmanis in Summer 2008 to pursue his PhD in Chemical Engineering. In his free time, Avi enjoys photography, reading, writing and playing racquetball.